PREDATOR-PREY MODELS WITH DISTRIBUTED TIME DELAY

PREDATOR-PREY MODELS WITH TIME DISTRIBUTED DELAY

By

ALEXANDRA TESLYA, M.SC.

A Thesis

Submitted to the School oif Graduate Studies

in Partial Fulfillment of the Requirements

for the Degree

Doctor of Philosophy

McMaster University

Doctor of Philosophy (2015) McMaster University
(Mathematics) Hamilton, Ontario

TITLE:	Predator-prey models with distributed time delay
AUTHOR:	Alexandra Teslya, M.Sc. (Ryerson University)
SUPERVISOR:	Dr. Gail S.K. Wolkowicz
NUMBER OF PAGES:	ix, 174

To My Family

Abstract

Rich dynamics have been demonstrated when a discrete time delay is introduced in a simple predator-prey system. For example, Hopf bifurcations and a sequence of period doubling bifurcations that appear to lead to chaotic dynamics have been observed. In this thesis we consider two different predator-prey models: the classical Gause-type predator-prey model and the chemostat predator-prey model. In both cases, we explore how different ways of modeling the time between the first contact of the predator with the prey and its eventual conversion to predator biomass affects the possible range of dynamics predicted by the models. The models we explore are systems of integro-differential equations with delay kernels from various distributions including the gamma distribution of different orders, the uniform distribution, and the Dirac delta distribution. We study the models using bifurcation theory taking the mean delay as the main bifurcation parameter. We use both an analytical approach and a computational approach using the numerical continuation software XPPAUT and DDE-BIFTOOL. First, general results common to all the models are established. Then, the differences due to the selection of particular delay kernels are considered. In particular, the differences in regions of stability of the coexistence equilibrium are investigated. Finally, the effects on the predicted range of dynamics between the classical Gause-type and the chemostat predator-prey models are compared.

Acknowledgments

First, I would like thank my supervisor Dr. Gail Wolkowicz, for her guidance, encouragement, kindness and dedication and for setting an example of academic excellence.

I also would like to thank the members of my committee Dr. Ben Bolker and Dr. David Earn, for their insights on our research and mentorship they provided me with. I have enjoyed learning from them immensely.

Additionally, I would like to express my gratitude to Dr. Tony Humphries for sharing his expertise and for the extremely helpful discussions that helped to advance this thesis.

In addition, thank you to my external examiners, Dr. Xinzhi Liu and Dr. Dmitry Pelinovsky for reading this thesis and supplying me with comments and extremely useful feedback.

Finally, I would like to thank my parents Nataliya and Igor, sister Yaroslava, and fiance Nikolay who believed in and supported me throughout the experience and were always by my side through the ups and downs of this journey.

Contents

List of Figures

Chapter 1

Introduction

In this thesis we consider two different predator-prey models that include a distributed delay to model the time between the capture of the prey by the predator and its conversion to predator biomass. The first model is a classical Gause-type model, and the second model is a predator-prey model in the chemostat. In both models we select the functional response of prey to the nutrient concentration and predator to prey density to be Holling type I (see [1], [2]), as shown in (1.1a). In the absence of the delay both models exhibit asymptotic convergence to an equilibrium. Therefore, any non-equilibrium dynamics in the model when delay is included can be solely attributed to the inclusion of the delay. We assume that the delay is distributed and model the delay using integro-differential equations with various kernels, including the gamma distribution, the uniform distribution, and the Dirac delta distribution.

In this chapter, we first give an overview of the relevant work in the field of predator-prey models with distributed delay, including the methods used to describe the local dynamics for such models. We discuss the motivation and work completed for various discrete delay and distributed delay predator-prey models. We contrast the main difference observed in the local dynamics among models with various delay distributions.

The following is the structure of this thesis. For each model we start by establishing well-posedness and basic properties of solutions of models with non-specified delay, such as boundedness, existence of equilibria, and uniform persistence of the populations. We compare these to their well studied counterparts with discrete delay (see [3], [4]). We then consider the local dynamics as the mean delay varies. We show that, in both models, if the coexistence equilibrium loses its stability, as the delay increases, then it first does so through a Hopf bifurcation. Using numerical analysis, we observe and compare bifurcation dynamics across various distributions such as the gamma, the uniform and the Dirac delta distributions.

1.1 Predator-prey model

The Gause-type predator-prey model is a well known simple mathematical model describing the interaction between species. Its variations and extensions are studied in modern day population dynamics theory (see, for example, [5], [6], [7]). This model is based on the assumption that in real world eco-systems prey populations do not grow exponentially in the absence of predator, but rather their size is eventually limited by the absence of resources. To account for this, the model has a population regulation term.

Field data from observing the dynamics of real ecosystems shows that species dynamics often display sustained oscillations (e.g., [8], [9]). Several mathematical mechanisms have been suggested to explain and capture the sustained oscillatory dynamics. Models that have the potential to possess stable periodic solutions include predator-prey models with Holling type II functional response as discussed in [10], models that include seasonal forcing of the parameters (see [9], [11]), as well as models that incorporate delay (see [3], [4], [12] among many others).

One of the earliest systematic classification of functional responses is attributed

to Holling (see [1], [2]). Holling described three types of functional responses. Type I, given by mx, corresponds to the linear increase in uptake rate as a function of density of x. Type II, given by $\frac{mx}{a+x}$, describes the uptake rate that is decelerating due to the handling time necessary to process captured prey. Here, m is the maximal specific growth rate and a is the half-saturation constant. Finally, Type III, given by $\frac{mx^2}{(a+x)(b+x)}$, describes the uptake rate with a sigmoidal shape. It is an appropriate model for a predator with the ability to learn.

The Gause type predator-prey model with Holling type I functional response is given by

$$\frac{\mathrm{d}x(t)}{\mathrm{d}t} = rx(t)\left(1 - \frac{x(t)}{K}\right) - mx(t)y(t) \ , \tag{1.1a}$$

$$\frac{\mathrm{d}y(t)}{\mathrm{d}t} = -dy(t) + mYx(t)y(t) \ . \tag{1.1b}$$

Here, $x(t)$ and $y(t)$ represent the density of prey and predator populations at time t, respectively. Parameters r, K, m, d and Y are positive constants that denote the intrinsic reproduction rate, carrying capacity for the prey, capture rate of the prey, death rate of the predator in the absence of the prey and the growth yield of the predator, respectively.

Depending on parameter values, either the predator population goes extinct and the prey population reaches its environmental capacity, or the predator and prey coexist and their population sizes approach a coexistence equilibrium via damped oscillations. There are no sustained oscillatory solutions. For more details see [13], [14].

Fan and Wolkowicz in [4] studied the effects of incorporating discrete delay in system (1.1). The delay corresponds to the time lag between predator capturing the prey and its conversion to viable predator biomass. Their research focused on switches of stability of the coexistence equilibrium, the appearance of stable periodic solutions and subsequent bifurcation dynamics as the length of the delay increased. The following

is the system they considered:

$$\frac{\mathrm{d}x(t)}{\mathrm{d}t} = rx(t)(1 - \frac{x(t)}{K}) - mx(t)y(t) \ , \tag{1.2a}$$

$$\frac{\mathrm{d}y(t)}{\mathrm{d}t} = -dy(t) + mYx(t-\tau)y(t-\tau)e^{-d\tau} \ . \tag{1.2b}$$

Here, $\tau > 0$ is the delay and the $y(t-\tau)e^{-d\tau}$ term represents the proportion of predators that captured prey τ units of time ago and survived the time needed to process the prey. Fan and Wolkowicz [4] established that if the coexistence equilibrium does not exist, then the predator population dies out and the prey population reaches its environmental capacity. However, when the coexistence equilibrium exists, the dynamics are complicated and vary as τ varies. In their work, Wolkowicz and Fan showed that at $\tau = 0$ the coexistence equilibrium is globally asymptotically stable. As τ increases, for a suitable choice of the rest of the parameters, the coexistence equilibrium undergoes at least two Hopf bifurcations. They also showed that if there are more than two Hopf bifurcations, then there is an even number of them and they produce nested periodic branches. As a part of their numerical analysis, they indicated that the number of Hopf bifurcations grows as the death rate of the predator decreases. This indicates that the parameter can be treated as a secondary bifurcation parameter for the mentioned Hopf bifurcations.

Gourley and Kuang [15] investigated the dynamics of a two-stage predator-prey model with maturation delay. They divided the predator population into mature and immature compartments with different mortality rates. The delay was used to model the fact that it takes a certain amount of time for a predator to move from juvenile to adult category. If the juvenile death rate is equal to the adult death rate, then this model reduces to system (1.2). They showed that for an unspecified functional response, the coexistence equilibrium is globally asymptotically stable for very small delay and very large delay (as long as the equilibrium is biologically viable). They also showed that there exists a set of parameters such that sustained oscillatory solution

may appear.

Li et al. [16] investigated a Gause-type predator-prey model in which adult and juvenile death rates were taken to be different. In their work, the delay denoted the maturation period of the predator. They studied the dynamics of the system for Holling type I and Holling type II functional responses. They established the existence of stability switches due to Hopf bifurcations. These bifurcations occur in pairs that are connected and are nested. They also demonstrated that there is a range of parameters for which two or possibly more stable periodic solutions coexist.

Other studies considered models with delay incorporated into the prey dynamics. Song and Wei [17] considered the delay incorporated in the resource limitation term of the logistic equation. For the resulting system, they provided the conditions necessary for the coexistence equilibrium to undergo Hopf bifurcations. Using center manifold theorem and normal form theory, they calculated expressions that determine the direction of the Hopf bifurcations and the stability of the bifurcating periodic solutions. Their numerical simulations demonstrated that there exists a selection of parameters such that the coexistence equilibrium restabilizes for sufficiently large delay.

Yan and Zhang [18] considered a Gause-type predator-prey model with a delayed feedback resource regulating term in both the prey and predator equations. They showed that there exists a subset of parameter values such that as the delay increases the coexistence equilibrium undergoes a Hopf bifurcation resulting in the birth of a stable periodic solution. Their numerical explorations indicated that as the delay increases further, a chaotic attractor appears.

In the real world, the processing delay rarely has the same length at every instance, but rather follows a distribution with some mean value. In this thesis we study the effects of incorporating distributed delay in system (1.1) and compare the dynamics that result from using various distributions, including discrete delay. We classify these

distributions according to the effect they induce on the system. The system we consider is

$$\frac{\mathrm{d}x(t)}{\mathrm{d}t} = rx(t)\left(1 - \frac{x(t)}{K}\right) - mx(t)y(t) \ , \tag{1.3a}$$

$$\frac{\mathrm{d}y(t)}{\mathrm{d}t} = -dy(t) + mY\int_0^\infty x(t-s)y(t-s)e^{-ds}g(s)\,\mathrm{d}s. \tag{1.3b}$$

Here, $g(s)$ is called the kernel of the delay distribution and generally has the following properties:

$$\int_0^\infty g(s)\,\mathrm{d}s = 1,$$

$$\int_0^\infty sg(s)\,\mathrm{d}s = \tau,$$

where τ is called the mean delay.

In this thesis, among other things, we consider a special type of gamma distribution, the Erlang distribution. It is a distribution with an integer shape (or order) parameter $p \in \mathbb{Z},\ (p > 0)$ and scale parameter $a \in \mathbb{R},\ (a > 0)$. When we say "weak" kernel, we refer to the delay kernel with gamma distribution of order $p = 1$. The kernel of the general distribution is

$$g_a^p(s) = \frac{s^{p-1}a^p}{e^{as}(p-1)!} \ .$$

This distribution has support $[0, \infty)$ and is a "long-tail" distribution. The predator-prey model with such distribution can be reduced to an equivalent $p+2$ order ordinary differential equations system via the linear chain trick, which will be discussed in detail in Chapter 2.

Wolkowicz et al. (see [19], [20]) considered competition in chemostat with the gamma distributed delay in the nutrient conversion of species and monotonically increasing functional response. They showed that, for small delays, the limiting behavior of the model is identical to that of the system with discrete delay and to the behavior of the ordinary differential equations model.

In this thesis we also consider the uniform distribution:

$$g(s) = \begin{cases} \frac{\rho}{\tau}, & s \in [\tau(1-\frac{1}{2\rho}), \tau(1+\frac{1}{2\rho})],\ \rho > 0 \\ 0, & \text{otherwise .} \end{cases}$$

Observe that the greater the mean delay, the wider the support of the distribution and the smaller the weight assigned to a particular value of the delay.

Thiel et al. [21] analyzed three different models with uniformly distributed delay and observed that as the support of the distribution gets wider, the amplitude of oscillations gets smaller and overall the dynamics get simpler as compared to the dynamics of the systems with discrete delay. They hypothesized that smoothing over past behavior is the reason for this phenomenon.

Ma and Takeuchi [22] considered Lotka-Volterra model with distributed delays in both resource regulating terms and prey-to-predator biomass conversion. They showed that in the absence of a viable coexistence equilibrium, the equilibrium corresponding to survival of the prey is globally asymptotically stable for small delays. If the co-existence equilibrium of the system exists, then, for sufficiently small values of mean delay, it is also locally asymptotically stable.

Xu et al. [23] considered a ratio dependent predator-prey model with distributed time delay to account for gestation period of the predator. They used the Holling type II functional response. They considered the existence of the equilibria of the system and properties such as global stability and persistence of solutions. They showed that if a coexistence equilibrium exists, then solutions are uniformly persistent and the coexistence equilibrium is globally asymptotically stable, provided the mean delay is relatively small.

There are number of studies of systems with discrete and gamma distributed delay, using the delay as a bifurcation parameter (for example [24] [25] [26]), where the authors used the linear chain trick [27] to convert systems into systems with discrete

delay. The common theme is that for small enough mean delay, the coexistence equilibrium is locally asymptotically stable. The stability is lost through Hopf bifurcation. Normal form theory and central manifold theorem is used to asses stability and the direction of bifurcating periodic solutions.

Bernard et al. [28] developed a method for determining the stability of steady state solutions of linear general distributed delay differential equations. They provide a method of determining sufficient conditions for the stability of the equilibrium based only on the expected delay and the symmetry of the kernel distribution. They postulated that distributed delay increases the parametric region of stability of an equilibrium compared to the discrete delay.

Cooke and Grossman [29] have considered the ways in which two models with identical structure would differ if one has discrete delay and the other distributed delay. They showed that for a first order differential equation with discrete delay that was considered, if there exists a value of the delay such that a zero equilibrium loses its stability, then it never re-stabilizes again. Analysis of the same equation with gamma distributed delay showed that if there exists a value of delay, $\tau_1 > 0$ such that the equilibrium loses stability, then there also exists $\tau_2 > \tau_1$ at which the equilibrium re-stabilizes.

While many studies successfully have tackled the analytic description of the stability region for non-linear discrete delay systems and linear distributed delay systems, to our knowledge, there are no studies which give explicit analytical formulation of stability region for the nonlinear systems with general distributed delay.

Campbell and Jessop developed a method for approximating the stability region of an equilibrium for non-linear distributed delay equations, knowing only the first few moments of the delay distributions, using the analysis of the characteristic equation [30]. They also demonstrated a way of approximating the delay independent stability

region using Rouche's Theorem.

Yuan and Belair [31] developed a method of assessing the stability region for a number of differential equations with distributed delay using local stability analysis. They compared the results for the three most commonly used delay distributions: Dirac delta, uniform and general gamma distribution. They observed that for the equations considered, the region of stability with the distributed delay is larger than that corresponding to the discrete delay. They also discussed Hopf bifurcations that take place on the boundary of the stability region and compute the normal-form coefficients to determine the stability and direction of the bifurcated periodic solutions. The authors established that while for their system with discrete delay stability of the equilibrium once lost cannot be regained, in the system with the gamma distribution, as the mean delay grows the stability can be regained.

In this thesis, we apply the linear chain trick (as described in [32] and [27]) to the system with the uniform distribution. The system reduces to the discrete delay system with two delays, which we analyze using numerical bifurcation analysis tools. Any distribution with compact support (e.g. tent distribution) can be dealt with similarly.

One of the important aspects of local dynamics is the criticality of Hopf bifurcations if they exist. For systems with long-tail distributions such as gamma distribution, one can apply standard methods for reduction to the central manifold (since the number of eigenvalues with zero real parts is finite) and calculation of normal form (for example, the method described in [33]). However, for systems with compact support more complicated calculations are involved. Currently, there exist several methods (for example, see [34] and [35]) for symbolic calculations of center manifolds for the discrete delay differential equations. The method presented in [34] can handle central manifolds of the dimension two and higher but would not work for systems with multiplicity of pure imaginary eigenvalues higher than 1. Both of these methods find an explicit form

of the first Lyapunov coefficient. However, from a practical point of view, the analytic treatment is not generally possible and numerical treatment of the expression provides more meaningful results. Finally, software such as DDE-BIFTOOL and MATCONT also provide functions that calculate the first Lyapunov coefficient and normal form at Hopf bifurcation.

In Chapter 2, we show that model (1.3) can have up to three equilibria. The stability of the equilibrium corresponding to extinction of both species, an equilibrium corresponding to survival of the prey but extinction of the predator, as well as an equilibrium where both populations survive for systems with the general delay distributions is studied. We show that when the coexistence equilibrium exists, solutions are uniformly persistent.

Further, we consider analytic results for the "weak" kernel. We show that, as the mean delay increases from 0, the coexistence equilibrium loses its stability by undergoing Hopf bifurcation and then restabilizes by going through a subsequent Hopf bifurcation. We also show that the appearance of these Hopf bifurcations depends on the value of d (as seen in 1.3). As a result, we can numerically describe the stability region of the coexistence equilibrium as a subset of $Y - d - \tau$ space. Our numerical explorations with XPPAUT software and its AUTO interface further show that as d becomes sufficiently small the criticality of the second Hopf bifurcation changes from super- to sub-. This is in stark contrast with the discrete delay system, where the Bautin bifurcation [33] was not observed.

Numerical simulations for higher order gamma distributions show that the basic dynamic described previously holds for such distributions as well. Our numerical experiments also show that as the order of gamma distribution increases, a stable periodic solution undergoes an even number of period doubling bifurcations. The higher the order, the more period doubling bifurcations take place. Another bifurcation that manifests itself as the order of distribution increases is a saddle node of limit cycles

bifurcation that precedes the period doubling bifurcations. Those dynamics are similar to these detected by Fan and Wolkowicz in their work with discrete delay system [4]. While local stability of an equilibrium in uniform distribution systems is challenging to investigate analytically, we studied the bifurcation dynamics using DDE-BIFTOOL. The dynamics we observed were very similar to those of the discrete delay model including the change in number of Hopf bifurcations as d decreased.

1.2 The chemostat predator-prey model

In Chapter 3, we consider the dynamics of the predator-prey model in the chemostat. The chemostat can be thought of as a chain of three chambers: the feed bottle that contains fresh medium with limiting growth nutrients, the well-stirred vessel where the observed microbial dynamics take place and the collection vessel. Fresh medium is being constantly added to the growth chamber, contents of which are being removed at a rate that allows for the maintenance of constant volume.

This set up is very attractive to scientists from the fields of ecology, microbiology, and mathematical biology, as it allows simulation and observation of species dynamics in the controlled environment. More about various chemostat applications can be found in [36].

We consider the predator-prey model where the predator population consumes the prey population, while prey subsists on non-reproducing nutrient that is growth limiting at a low concentration. The following system describes this relationship:

$$\frac{\mathrm{d}s}{\mathrm{d}t} = \left(s^0 - s(t)\right) D_0 - \frac{x(t) f(s(t))}{\eta} \ , \tag{1.5a}$$

$$\frac{\mathrm{d}x}{\mathrm{d}t} = x(t)(-D + f(s(t))) - \frac{y(t) g(x(t))}{\xi} \ , \tag{1.5b}$$

$$\frac{\mathrm{d}y}{\mathrm{d}t} = -\Delta y(t) + g(x(t)) y(t) \ . \tag{1.5c}$$

Here, $s(t)$ denotes the concentration of nutrient, $x(t)$ is the density of the prey population and $y(t)$ is the density of the predator population at time t. Functions $f(s(t)) = \alpha s(t)$ ($\alpha > 0$) and $g(x(t)) = kx(t)$ ($k > 0$) denote the functional response of prey to nutrient concentration and predator to prey density. We select both functions to be Holling type I, since, in this case, there always exists a globally asymptotically stable equilibrium point in the absence of delay. The positive constants s^0, D, η, ξ denote the concentration of the growth limiting nutrient in the feed vessel, the dilution rate, and the growth yield constants, respectively. The sum of the dilution rate D_0 and the natural species-specific death rate of the prey is denoted D, and of the predator population is denoted Δ, respectively.

Dynamics of the predator mediated coexistence have been studied by Butler and Wolkowicz [37] under the assumption that $D_0 = D = \delta$. Model (1.5) was considered as a submodel. For the general monotone response function, they derived the conditions such that the solutions of the system are uniformly persistent. They also showed that, if both response functions are Holling type I, then the solutions converge to one of the three equilibria (determined by the rest of the parameters). However, if the predator response changes to Holling type II, then the coexistence equilibrium can lose stability through a Hopf bifurcation.

Fan and Wolkowicz [3] studied the dynamics of a model with both response functions being Holling type I and the discrete delay incorporated in the processing term of predator equation:

$$\frac{\mathrm{d}s}{\mathrm{d}t} = \left(s^0 - s(t)\right) D_0 - \frac{x(t) f(s(t))}{\eta} \,, \tag{1.6a}$$

$$\frac{\mathrm{d}x}{\mathrm{d}t} = x(t)(-D + f(s(t))) - \frac{y(t) g(x(t))}{\xi} \,, \tag{1.6b}$$

$$\frac{\mathrm{d}y}{\mathrm{d}t} = -\Delta y(t) + g(x(t-\tau)) y(t-\tau) e^{-\Delta\tau} \,. \tag{1.6c}$$

Here, τ is the time interval between capture of the prey and its conversion into viable predator biomass. The system can have up to three equilibria: one corresponding

to both prey and predator populations being extinct, second corresponding to the extinction of the predator population only and, finally, third equilibrium corresponding to the coexistence of populations (subject to some conditions on parameter space). The authors showed that, in the absence of the coexistence equilibrium, the dynamics of the discrete delay model are identical to those of the ordinary differential equations model. Once the delay was incorporated, given a suitable choice of parameters, the coexistence equilibrium lost its stability via supercritical Hopf bifurcation as τ increased from 0 and stable periodic solution appeared. Given a suitable choice of the rest of the parameters, as τ increases, the equilibrium can regain its stability via a subsequent supercritical Hopf bifurcation. Work by Humphreys, Wolkowicz and Teslya (currently in progress) has shown that there exists a secondary parameter that influences the number, as well as the location of Hopf bifurcations. It has also emerged, that as the secondary parameter changes, one of the stable periodic solutions born from a Hopf bifurcation can undergo a number of bifurcations, such as the saddle node of limit cycles, the period doubling and the torus bifurcations as τ changes. Moreover, the criticality of one of the Hopf bifurcations changes as the secondary parameter varies.

While in many respects the dynamics of Gause predator-prey model was comparable to that of the chemostat predator-prey model, once we consider the dynamics around the coexistence equilibrium, the qualitative difference becomes evident. Although both models may have more than two Hopf bifurcations, the location of these bifurcations is qualitatively different. In the predator-prey model the coexistence equilibrium changes its stability only twice (before ultimately disappearing), since the Hopf branches that arise are nested. Therefore, we do not expect a torus bifurcation in this model, since its "birthplace" is associated with double Hopf bifurcation. On the other hand, in chemostat there is no selection of parameters such that the periodic solution branches connecting Hopf bifurcations are nested.

We are interested to see how the dynamics of (1.6) changes if the processing delay

becomes distributed. Therefore, we consider the following model in Chapter 3:

$$\begin{aligned}
\frac{\mathrm{d}s}{\mathrm{d}t} &= \left(s^0 - s(t)\right) D_0 - \frac{x(t) f(s(t))}{\eta} \ , \\
\frac{\mathrm{d}x}{\mathrm{d}t} &= x(t)(-D + f(s(t))) - \frac{y(t) g(x(t))}{\xi} \ , \\
\frac{\mathrm{d}y}{\mathrm{d}t} &= -\Delta y(t) + \int_0^\infty g(x(t-u)) y(t-u) e^{-\Delta u} h(u)\, \mathrm{d}u,
\end{aligned}$$

where $h(u)$ is the kernel of the delay distribution with mean τ. We consider the equilibrium solutions and in particular the coexistence equilibrium when all of the species survive. We focus on different delay distributions, such as the gamma distribution of order 1 and 2 and the uniform distribution. We prove that in the former case, the coexistence equilibrium undergoes two Hopf bifurcations, losing stability and then re-stabilizing as the mean delay increases. We follow up with numerical bifurcation diagrams of the system for these distributions and compare them with bifurcation diagrams in the discrete delay case.

In Chapter 4, we summarize our findings about the dynamics of the Gause model and the chemostat predator-prey model with the distributed delay. We compare the dynamics induced by the gamma distribution and the uniform distribution to the dynamics of the discrete delay systems and to each other. We also discuss the differences and similarities between the dynamics of the Gause model and the chemostat model, focusing on Hopf bifurcations of the coexistence equilibrium and bifurcations of periodic solutions.

Chapter 2

A predator-prey model with distributed delay

2.1 The model

Consider the following predator-prey model:

$$\frac{\mathrm{d}x(t)}{\mathrm{d}t} = rx(t)\left(1 - \frac{x(t)}{K}\right) - f(x(t))y(t) \ ,$$
$$\frac{\mathrm{d}y(t)}{\mathrm{d}t} = -dy(t) + Y\int_0^\infty f(x(t-s))y(t-s)e^{-ds}g(s)\,\mathrm{d}s \ .$$

Here $x(t)$ and $y(t)$ represent the size of the prey and the predator populations at time t, respectively. The term $e^{-ds}y(t-s)$ represents the number of predators that have consumed prey at the time $t-s$ and survived until the time t. If the predator population is absent, then the growth dynamics of the prey population is described by the logistic model. If, on the other hand, the prey is absent, then the predator population decreases exponentially. Parameters r, K, d and Y are positive constants that denote the intrinsic reproduction rate, the carrying capacity for the prey, the death rate of the predator in the absence of the prey and the growth yield of the

predator, respectively. The function $f(x)$ denotes functional response of the predator to the prey population density. We set $f(x)$ to be Holling type I (as seen in [1] and [2]), i.e. $f(x) = mx$, where $m > 0$ is the attack rate of predator.

Therefore, the system we study is

$$\frac{\mathrm{d}x(t)}{\mathrm{d}t} = rx(t)\left(1 - \frac{x(t)}{K}\right) - mx(t)y(t) \ , \tag{2.2a}$$

$$\frac{\mathrm{d}y(t)}{\mathrm{d}t} = -dy(t) + Ym\int_0^\infty x(t-s)y(t-s)e^{-ds}g(s)\,\mathrm{d}s \ . \tag{2.2b}$$

Here, $g(s)$ is called the kernel of the delay distribution and generally has the following properties:

$$\int_0^\infty g(s)\,\mathrm{d}s = 1, \tag{2.3a}$$

$$\int_0^\infty sg(s)\,\mathrm{d}s = \tau, \tag{2.3b}$$

where τ is the mean delay between the capture of the prey by predator and the prey biomass turning into viable predator biomass.

Before proceeding further with the analysis, we non-dimensionalize the model (2.2) to reduce the number of parameters. We introduce the following change of variables and parameters:

$$x(\hat{t}) = a\hat{x}(\hat{t}),\ y(\hat{t}) = b\hat{y}(\hat{t}),\ d = c\hat{d}$$

$$Y = h\hat{Y},\ t = l\hat{t},\ s = l\hat{s}, \hat{g}(\hat{s}) = lg(l\hat{s})$$

where:

$$a = K,\ b = \frac{r}{m},\ c = r,\ h = \frac{r}{mYK},\ l = \frac{1}{r} \ .$$

We drop $\hat{}$ to obtain:

$$\frac{\mathrm{d}x(t)}{\mathrm{d}t} = x(t)(1 - x(t)) - x(t)y(t) \tag{2.5a}$$

$$\frac{\mathrm{d}y(t)}{\mathrm{d}t} = -dy(t) + Y\int_0^\infty x(t-s)y(t-s)e^{-ds}g(s)\,\mathrm{d}s \ . \tag{2.5b}$$

We will carry out a theoretical analysis of system (2.5), which, without loss to generality, can be applied to system (2.2).

2.2 Well-posedness and basic properties of the model

Denote by BC^2, the Banach space of bounded continuous functions mapping $(-\infty, 0]$ into $\mathbb{R}^2$ equipped with the uniform norm (i.e. if $\Gamma \in BC^2$, then $||\Gamma|| = \sup_{\theta\in(-\infty,0]} |\Gamma(\theta)|$, where $|\cdot|$ is any norm in $\mathbb{R}^2$). We consider initial data $\phi = (\phi_1, \phi_2) \in BC^2_+ = \{\phi \in BC^2 : \quad \phi_i(\theta) \geq 0, i = 1, 2, \quad \theta \leq 0\}$. Define $intBC^2_+ = \{\phi \in BC^2 : \quad \phi_i(\theta) > 0, i = 1, 2, \quad \theta \leq 0\}$. Denote the solutions of (2.2) with initial data $\phi \in BC^2_+$ at time t by $\pi(\phi, t)$ when they exist. From this point onward when saying positive solutions, we are referring to the solutions $\pi(\phi, t)$ with initial data $\phi \in intBC^2_+$. Later we show that in this case each component of $\pi(\phi, t)$ is positive for all $t > 0$.

Define $L > 0$ and assume that $g(s) = 0$ for all $s \in (L, \infty)$. We allow $L = \infty$.

Theorem 2.2.1. *Solutions of (2.5) with initial data in BC^2_+ exist and are unique and remain in BC^2_+.*

Proof. Since the right hand side of 2.5 is smooth and satisfies Lipschitz condition (see in Appendix B or [27], Theorem 3.7, Chapter 3, page 32), from the general theory of integro-differential equations it follows that for all non-negative bounded functions ϕ defined on $(-\infty, 0]$ and mapping into $\mathbb{R}^2_+$, there exists a unique solution of (2.5), $\pi(\phi, t)$ such that $\pi(\phi, \cdot)\big|_{(-\infty,0]} = \phi(t)$, on the interval $(-\infty, \infty)$. Therefore, solutions exist and are unique for all $t > 0$.

The boundary where $x(t) = 0$ is invariant, due to the uniqueness of solutions established earlier. If $x(0) = 0$, then $x(t) = 0$ for all $t \geq 0$. If $x(0) > 0$, then $x(t)$ will remain positive.

Since $y(t) \geq 0$ on $[-L, 0]$, then $\dot{y}(t) \geq -dy(t)$ for all $0 \leq t \leq L$. Therefore, by the Comparison Theorem in [38] (Theorem 1.4.1, page 15), $y(t) \geq 0$, for all $-L \leq t \leq L$. Arguing inductively, $y(t) \geq 0$, for an $t \in [L(n-1), Ln]$ and $n \in \mathbb{N}$, $n > 0$. Therefore,

$y(t) \geq 0$ for all $t > 0$. □

Proposition 2.2.2. *Solutions of (2.5) with positive initial data, remain positive for all* $t > 0$.

Proof. As established in the preceding theorem, since $x(0) > 0$, then $x(t) > 0$ for all $t > 0$.

We will prove that $y(t)$ is positive for all t by contradiction. Assume that $y(t)$ becomes zero for the first time at $\hat{t}$. This implies that $\dot{y}(\hat{t}) \leq 0$. However, once the value for $y(\hat{t})$ is substituted into (2.5b), we arrive on $\frac{\mathrm{d}y(\hat{t})}{\mathrm{d}t} = Y \int_0^\infty x(\hat{t}-s)y(\hat{t}-s)e^{-ds}g(s)\,\mathrm{d}s$, which is positive, a contradiction. □

Lemma 2.2.3. *Solutions of (2.5) with the initial data in* BC_+^2 *are bounded and* $\limsup_{t\to\infty} x(t) \leq 1$ *and* $\limsup_{t\to\infty} y(t) \leq \frac{Y(1+d)^2}{4d2} \int_0^\infty e^{-ds}g(s)\,\mathrm{d}s$.

Proof. Note that $\dot{x}(t) \leq x(t)(1-x(t))$. Consider $\dot{z}(t) = z(t)(1-z(t))$. If $z(0) \geq 0$, given any $\epsilon > 0$, there exists a $T > 0$ such that $z(t) < 1 + \epsilon$, for all $t \geq T$. Since by Theorem 2.2.1 $x(t)$ is non-negative for all t, using the Comparison theorem from [38], it follows that $\limsup_{t\to\infty} x(t) \leq 1$. To prove boundedness of $y(t)$, we consider the function $w(t)$:

$$w(t) = y(t) + Y \int_0^\infty x(t-s)e^{-ds}g(s)\,\mathrm{d}s\ . \tag{2.6}$$

The derivative of $w(t)$ with respect to t:

$$\dot{w}(t) = \dot{y}(t) + Y \int_0^\infty \dot{x}(t-s)e^{-ds}g(s)\,\mathrm{d}s\ .$$

Substitute the definitions for $\dot{x}(t-s)$ and $\dot{y}(t)$ to get:

$$\begin{aligned}
\dot{w}(t) &= -dy(t) + Y \int_0^\infty x(t-s)y(t-s)e^{-ds}g(s)\,\mathrm{d}s \\
&\quad + Y \int_0^\infty (x(t-s)(1-x(t-s)) - x(t-s)y(t-s))e^{-ds}g(s)\,\mathrm{d}s \\
&= -dy(t) + Y \int_0^\infty x(t-s)(1-x(t-s))e^{-ds}g(s)\,\mathrm{d}s\ .
\end{aligned}$$

From (2.6) follows:

$$y(t) = w(t) - Y \int_0^\infty x(t-s)e^{-ds}g(s)\,\mathrm{d}s \ .$$

Therefore,

$$\dot{w}(t) = -dw(t) + Y \int_0^\infty x(t-s)(1+d-x(t-s))e^{-ds}g(s)\,\mathrm{d}s \ .$$

Note that $\left(\frac{1+d}{2} - x(t-s)\right)^2 = (x(t-s))^2 + \frac{(1+d)^2}{4} - (1+d)x(t-s) \geq 0$. Therefore,

$$\dot{w}(t) \leq -dw(t) + \frac{Y(1+d)^2}{4} \int_0^\infty e^{-ds}g(s)\,\mathrm{d}s \ .$$

However, the differential equation

$$\dot{z}(t) = -dz(t) + \frac{Y(1+d)^2}{4} \int_0^\infty e^{-ds}g(s)\,\mathrm{d}s \tag{2.7}$$

has a solution

$$z(t) = z(0)e^{-dt} + \left(1 - e^{-dt}\right) \frac{Y(1+d)^2}{4d} \int_0^\infty e^{-ds}g(s)\,\mathrm{d}s \ . \tag{2.8}$$

For each $z(t)$ with $z(0) \geq 0$ and for every $\epsilon > 0$ there exists $T > 0$ such that $z(t) \leq \frac{Y(1+d)^2}{4d} \int_0^\infty e^{-ds}g(s)\,\mathrm{d}s + \epsilon$, for all $t > T$. Provided $w(0) = z(0)$, by the Comparison theorem [38], we conclude that $\limsup_{t\to\infty} w(t)$ is also bounded by $\frac{Y(1+d)^2}{4d} \int_0^\infty e^{-ds}g(s)\,\mathrm{d}s$, and therefore, so is $\limsup_{t\to\infty} y(t)$. □

Set

$$X^0 \equiv \{\phi(t) \in BC_+^2 : \quad \phi_1(0) > 0 \text{ and } \exists\theta \in [-L, 0] \text{ such that } \phi_1(\theta)\phi_2(\theta) > 0\} \ , \tag{2.9a}$$

$$X_1 \equiv \{\phi(t) \in BC_+^2 : \quad \phi_1(0) = 0\} \ , \tag{2.9b}$$

$$X_2 \equiv \{\phi(t) \in BC_+^2 : \quad \phi_1(0) > 0 \text{ and } \phi_1(\theta)\phi_2(\theta) = 0, \ \forall\theta \in [-L, 0]\} \ , \tag{2.9c}$$

$$X = X^0 \cup X_1 \cup X_2 \ . \tag{2.9d}$$

Observe several things implied by this definition:

(1) If $\phi \in X^0$, since it is continuous and $\phi_1(0) > 0$, then there exists $a > 0$, such that for all $\theta \in (-a, 0]$ $\phi_1(\theta) > 0$.

(2) If $\phi_1(\theta)\phi_2(\theta) = 0$ for all $\theta \in [-L, 0]$, then $\int_0^\infty \phi_1(-s)\phi_2(-s)e^{-ds}g(s)\,\mathrm{d}s = 0$.

(3) If $\phi \in X_2$, since ϕ is continuous, there exists $a > 0$ such that for all $\theta \in (-a, 0]$, $\phi_1(\theta) > 0$ and $\phi_2(\theta) = 0$.

Denote $(x(t), y(t)) = (x(t, \phi(t)), y(t, \phi(t)))$ to be the solution of (2.5) with the initial data $\phi(t)$ in X^0. Set

$$T(t)(\phi)(\theta) = (x(t+\theta), y(t+\theta)),\ \theta \in (-\infty, 0]\ .$$

Lemma 2.2.4. *If a solution of (2.5) has initial data in X^0, then for all $t > 0$ there exists $\theta \in [t - L, t]$ such that $x(\theta)y(\theta) > 0$. Moreover, there exists $M > 0$ such that $x(t) > 0$, $y(t) > 0$ and $\int_0^\infty x(t-s)y(t-s)e^{-ds}h(s)\,\mathrm{d}s > 0$, for all $t > M$.*

Proof. Observe that, since $\phi_1(0) > 0$, then $x(t) > 0$ for all $t > 0$. The proof of this statement is similar to that of Proposition 2.2.2.

Consider the case $\phi_2(0) > 0$. Then, since by Theorem 2.2.1 $y(t) \geq 0$ for all t and therefore $\dot{y}(t) \geq -dy(t)$, it follows that $y(t) > 0$ for all $t \geq 0$. The result follows.

Consider the case $\phi_2(0) = 0$. Observe that, since $\phi_1(t)$ and $\phi_2(t)$ are continuous functions, then there exist $t_1, t_2 \in \mathbb{R}$ such that $-L < t_1 < \theta_0 < t_2 \leq 0$ and $\phi_1(t)\phi_2(t) > 0$ for all $t \in [t_1, t_2]$. Therefore there exists time $T \leq L + t_1$ (if L is ∞ then inequality is strict) such that $\dot{y}(T) > 0$ and there exists $\epsilon > 0$ such that $y(t) > 0$ for all $t \in (T, T + \epsilon)$. Then, since $\dot{y}(t) \geq -dy(t)$, it follows that $y(t) > 0$ for all $t > T$. Since $\theta_0 \in [t_1, t_2] \subset [t_1, T]$, the result follows. □

Lemma 2.2.5. *Sets X^0, X_1 and X_2 are positively invariant under $T(t)$.*

Proof. From the Lemma 2.2.4 it follows that the set X^0 is positively invariant under $T(t)$.

If the solution has initial data in X_1, then, by (2.5a), $x(t) = 0$ for all $t > 0$. From Theorem 2.2.1 it follows that $y(t) \geq 0$ for all $t > 0$.

Consider the solutions with initial data in X_2. By (3) $y(0) = 0$ and since $y(t) = 0$ is a solution of (2.5b) with initial data $y(0) = 0$ and $\phi_1(\theta)\phi_2(\theta) = 0$ for all $\theta \in [-L, 0]$, then by the uniqueness of solutions in forward time, it follows that $y(t) = 0$ for all $t > 0$. Therefore, $\int_0^\infty x(t-s)y(t-s)e^{-ds}g(s)\,\mathrm{d}s = 0$ for all $t > 0$. The proof that $x(t) > 0$ for all $t > 0$ follows from Proposition 2.2.2. □

2.3 Equilibria and stability analysis for a general kernel

System (2.5) has three equilibria: $E_0 = (0, 0)$, $E_1 = (1, 0)$ and $E_+ = (x_+, y_+) = \left(\frac{d}{Y}\left(\int_0^\infty e^{-ds}g(s)\,\mathrm{d}s\right)^{-1}, 1 - \frac{d}{Y}\left(\int_0^\infty e^{-ds}g(s)\,\mathrm{d}s\right)^{-1}\right)$, where $x_+ > 0$, $y_+ > 0$ requires the following to hold:

$$Y\int_0^\infty e^{-ds}g(s)\,\mathrm{d}s > d. \tag{2.10}$$

We will refer to the above as the coexistence condition. If the inequality becomes equality, E_1 and E_+ coincide.

Since $\int_0^\infty e^{-ds}g(s)\mathrm{d}s < 1$, then $d < Y$ is a necessary but not sufficient condition for E_+ to exist. Intuitively, once the mean delay in the conversion of biomass becomes larger than the predator average life span, the predator population will die out. However, without knowing the expression of the distribution kernel it is impossible to give the critical value of τ.

To analyze the local dynamics we calculate the linearization of system (2.5) around

any equilibrium point (x^*, y^*):

$$\begin{bmatrix} \dot{x}(t) \\ \dot{y}(t) \end{bmatrix} = \begin{bmatrix} 1-2x^*-y^* & -x^* \\ 0 & -d \end{bmatrix} \begin{bmatrix} x(t)-x^* \\ y(t)-y^* \end{bmatrix} + \begin{bmatrix} 0 & 0 \\ Yy^* & Yx^* \end{bmatrix} \begin{bmatrix} \int_0^\infty (x(t-s)-x^*)e^{-ds}g(s)\,\mathrm{d}s \\ \int_0^\infty (y(t-s)-y^*)e^{-ds}g(s)\,\mathrm{d}s \end{bmatrix} . \tag{2.11}$$

2.3.1 Stability analysis of E_0

The linearization around E_0 takes the form:

$$\begin{bmatrix} \dot{x}(t) \\ \dot{y}(t) \end{bmatrix} = \begin{bmatrix} 1 & 0 \\ 0 & -d \end{bmatrix} \begin{bmatrix} x(t) \\ y(t) \end{bmatrix} .$$

The coefficient matrix has two eigenvalues, 1 and $-d$. Therefore, E_0 is always a saddle point, and hence, unstable.

Lemma 2.3.1. *E_0 is globally asymptotically stable with respect to solutions of (2.5) with initial data in X_1.*

Proof. By Lemma 2.2.5, it follows that $x(t) = 0$ for all $t > 0$.

Consider the case where $L = \infty$. If $\phi_1(\theta)\phi_2(\theta) = 0$ for all $\theta \in (-\infty, 0]$ and therefore $\int_0^\infty \phi_1(-s)\phi_2(-s)e^{-ds}g(s)\,\mathrm{d}s = 0$, then since $x(t) = 0$ for all $t > 0$, $\int_0^\infty x(t-s)y(t-s)e^{-ds}g(s)\,\mathrm{d}s = 0$ for all $t > 0$. Therefore, $\dot{y}(t) = -dy(t)$ for all $t > 0$. It follows that $\lim_{t\to\infty} y(t) = 0$.

If there exists $\theta \in (-\infty, 0]$ such that $\phi_1(\theta)\phi_2(\theta) > 0$, then there exists $T > 0$, such that $\int_0^\infty x(t-s)y(t-s)e^{-ds}g(s)\,\mathrm{d}s > 0$ for all $t > T$. On the other hand, since $x(t) = 0$ for all $t > 0$, then $\int_0^t x(t-s)y(t-s)e^{-ds}g(s)\,\mathrm{d}s = 0$ for all $t > 0$ and therefore,

$$\begin{aligned} \dot{y}(t) &= -dy(t) + Y\int_0^t x(t-s)y(t-s)e^{-ds}g(s)\,\mathrm{d}s + Y\int_t^\infty x(t-s)y(t-s)e^{-ds}g(s)\,\mathrm{d}s \\ &= -dy(t) + Y\int_t^\infty x(t-s)y(t-s)e^{-ds}g(s)\,\mathrm{d}s . \end{aligned}$$

The limit of $Y\int_t^\infty x(t-s)y(t-s)e^{-ds}g(s)\,\mathrm{d}s$ as $t\to\infty$ is 0. Therefore, $\lim_{t\to\infty} y(t)=0$.

Consider the case where $L<\infty$. Since $x(t)=0$ for $t>0$, then
$Y\int_t^\infty x(t-s)y(t-s)e^{-ds}g(s)\,\mathrm{d}s=0$ for all $t>L$. Then $\dot{y}(t)=-dy(t)$ for all $t>L$. The result follows. □

2.3.2 Stability analysis of E_1

Theorem 2.3.2. *E_1 is locally asymptotically stable if (2.10) is reversed and unstable if inequality (2.10) holds.*

Proof. The linearization around E_1 takes the following form:

$$\begin{bmatrix}\dot{x}(t)\\ \dot{y}(t)\end{bmatrix}=\begin{bmatrix}-1 & -1\\ 0 & -d\end{bmatrix}\begin{bmatrix}x(t)-1\\ y(t)\end{bmatrix}+\begin{bmatrix}0 & 0\\ 0 & Y\end{bmatrix}\begin{bmatrix}\int_0^\infty (x(t-s)-1)e^{-ds}g(s)\,\mathrm{d}s\\ \int_0^\infty y(t-s)e^{-ds}g(s)\,\mathrm{d}s\end{bmatrix}.$$

The corresponding characteristic equation is given by

$$p(\lambda)=(\lambda+1)\left(\lambda+d-Y\int_0^\infty e^{-(d+\lambda)s}g(s)\,\mathrm{d}s\right)=0\ . \tag{2.12}$$

From (2.12) it is clear that one of the roots of $p(\lambda)$ is -1. Therefore, to determine the stability of E_1 we consider the roots of the following equation:

$$\lambda=Y\int_0^\infty e^{-(d+\lambda)s}g(s)\,\mathrm{d}s-d\ . \tag{2.13}$$

Set the right-hand side of the (2.13) to be function $h(\lambda)$. Note that, $h(\lambda)$ is a monotonically decreasing continuous function of λ and as $\lambda\to\infty$, $h(\lambda)\to -d$. If the coexistence equilibrium exists and therefore (2.10) holds, then $h(0)>0$. Hence, by the Intermediate Value Theorem, equation (2.13) has at least one positive real root.

If, on the other hand, the coexistence equilibrium does not exist and the following condition holds:

$$Y\int_0^\infty e^{-ds}g(s)\,\mathrm{d}s<d. \tag{2.14}$$

then $h(0) < 0$ and therefore (2.13) has no positive real roots.

Next we consider complex roots $\lambda = \alpha + i\beta$ of (2.13). Equation (2.13) can now be written as a system of equations:

$$\begin{aligned}\alpha =& Y \int_0^\infty e^{-(d+\alpha)s} g(s) \cos(\beta s)\, \mathrm{d}s - d \ , \\ \beta =& Y \int_0^\infty e^{-(d+\alpha)s} g(s) \sin(\beta s)\, \mathrm{d}s \ .\end{aligned}$$

Note that

$$\alpha = Y \int_0^\infty e^{-(d+\alpha)s} g(s) \cos(\beta s)\, \mathrm{d}s - d \leq Y \int_0^\infty e^{-(d+\alpha)s} g(s)\, \mathrm{d}s - d = h(\alpha) \ .$$

Using similar type of reasoning as earlier in the proof, it follows, that if condition (2.14) holds, then (2.13) has no roots with positive real part.

To sum up, if the coexistence equilibrium does not exist, then E_1 is asymptotically stable, if, on the other hand, E_+ exists, E_1 is unstable. □

Global Asymptotic stability of E_1

Theorem 2.3.3. *If condition (2.14) is satisfied, then E_1 is globally asymptotically stable with respect to solutions with initial data in X^0.*

Proof. We use Lyapunov's Direct Method for delay differential equations (see [39], [40]). Consider the following function:

$$V(x(t), y(t)) = x(t) - 1 - \ln x(t) + \frac{1}{d} y(t) + \frac{Y}{d} \int_0^\infty \int_{-s}^0 x(t+\theta) y(t+\theta)\, \mathrm{d}\theta\, e^{-ds} g(s)\, \mathrm{d}s \ . \tag{2.16}$$

By Lemma 2.2.4, the double integral in the definition of V is always positive for solutions of (2.5) with initial data in X^0. Also, by Lemma 2.2.4, it follows that $x(t) > 0$ for all $t > 0$ and there exists $T > 0$ such that $y(t) > 0$ for all $t > T$. Note that the domain of $V(t)$ is $C((-\infty, \infty), int\mathbb{R}_+) \cap C((-\infty, \infty), \mathbb{R}_+)$ and that $V(x(t), y(t))$ is

0 if and only if $x(t) = 1$ and $y(t) = 0$ for all $t \in (-\infty, \infty)$. Otherwise, $V(t)$ is positive on X_0.

Note that:

$$\begin{aligned}\frac{\mathrm{d}}{\mathrm{d}t}\left(\int_{-s}^{0} x(t+\theta)y(t+\theta)\,\mathrm{d}\theta\right) &= \frac{\mathrm{d}}{\mathrm{d}t}\left(\int_{t-s}^{t} x(u)y(u)\,\mathrm{d}u\right) \\ &= \frac{\mathrm{d}}{\mathrm{d}t}\left(\int_{a}^{t} x(u)y(u)\,\mathrm{d}u - \int_{a}^{t-s} x(u)y(u)\,\mathrm{d}u\right) \\ &= x(t)y(t) - x(t-s)y(t-s)\ .\end{aligned}$$

Differentiate V with respect to t:

$$\begin{aligned}\dot{V}(t) &= \left(1 - \frac{1}{x(t)}\right)(x(t) - x^2(t) - x(t)y(t)) + \\ &\quad \left(-y(t) + \frac{Y}{d}\int_0^\infty x(t-s)y(t-s)e^{-ds}g(s)\,\mathrm{d}s\right) + \\ &\quad \frac{Y}{d}\int_0^\infty (x(t)y(t) - x(t-s)y(t-s))\,e^{-ds}g(s)\,\mathrm{d}s \\ &= x(t) - x^2(t) - x(t)y(t) - 1 + x(t) + \frac{Y}{d}x(t)y(t)\int_0^\infty e^{-ds}g(s)\,\mathrm{d}s \\ &= -(x(t)-1)^2 + x(t)y(t)\left(\frac{Y}{d}\int_0^\infty e^{-ds}g(s)\,\mathrm{d}s - 1\right)\ .\end{aligned}$$

Since (2.14) holds, then $\frac{Y}{d}\int_0^\infty e^{-ds}g(s)\,\mathrm{d}s - 1 < 0$ and therefore, if $(x(t), y(t)) \in X_0$, $\dot{V}(t) \leq 0$. Note that equality holds only when $x(t) = 1$ and $y(t) = 0$. Since E_1 is the largest invariant set where $\dot{V}(t) = 0$, then by the LaSalle Extension Theorem for delay equations [41], E_1 is globally asymptotically stable. □

Lemma 2.3.4. *E_1 is globally asymptotically stable with respect to solutions of (2.5) with initial data in X_2.*

Proof. By Lemma 2.2.5, $y(t) = 0$ for all $t > 0$. System (2.5) reduces to the standard logistic equation, solutions with non-negative conditions of which converge to 1 as $t \to \infty$. □

2.4 Properties of the model when E_+ exists

In what follows, we state some results about the dynamics of system (2.5), when E_+ exists. We restrict the kernel of the distribution $g(s)$ to be a function such that, if $g(s) = 0$ for all $s \in (a, b)$, except for one $x \in (a, b)$, then $g(x) = \infty$. It follows that if $\tau = 0$, then $g(s) = \delta_0(s)$.

2.4.1 Local dynamics at E_+

Now we investigate the local dynamics at E_+. In particular, we are interested in regions of local asymptotic stability of E_+ with respect to τ. Another aspect of interest is persistence of solutions, when E_+ exists.

The characteristic equation for the linearization around E_+ is:

$$\lambda^2 + (d + x^*)\lambda + x^* d + Y x^* \int_0^\infty e^{-(d+\lambda)s} g(s)\,\mathrm{d}s(1 - 2x^* - \lambda) = 0\ . \tag{2.17}$$

Lemma 2.4.1. *If (2.10) holds and $\tau = 0$, then E_+ is locally asymptotically stable.*

Proof. Since $\tau = 0$, then $g(s) = \delta_0(s)$. Equilibrium E_+ becomes $\left(\frac{d}{Y}, 1 - \frac{d}{Y}\right)$. Integral $\int_0^\infty e^{-\alpha s} g(s)\,\mathrm{d}s = 1$. The characteristic equation (2.17) becomes:

$$\lambda^2 + \left(d + \frac{d}{Y}\right)\lambda + \frac{d^2}{Y} + d\left(1 - 2\frac{d}{Y} - \lambda\right) = 0\ . \tag{2.18}$$

The equation simplifies to the following quadratic equation:

$$\lambda^2 + \frac{d}{Y}\lambda + d\left(1 - \frac{d}{Y}\right) = 0\ . \tag{2.19}$$

From the fact that both $1 - \frac{d}{Y} > 0$ and $\frac{d}{Y} > 0$, it follows that the equation has roots with negative real parts. □

Theorem 2.4.2. *As τ increases from zero, the number of roots of (2.17) with positive real part can change only if a root appears on or crosses the imaginary axis as τ increases from 0.*

Proof. For $g(\lambda) = (d + x^*)\lambda + x^*d + Yx^* \int_0^\infty e^{-(d+\lambda)s} g(s)\,\mathrm{d}s(1 - 2x^* - \lambda)$ it is easy to see that

$$\limsup_{\lambda\to\infty} |\lambda^{-2} g(\lambda)| = 0 < 1 \ .$$

Therefore, by Theorem 1.4 (in [42] Chapter 3, page 66), no root of (2.17) with positive real part can enter from infinity as τ bifurcates from 0. Since Lemma 2.4.1 holds, the result follows. □

Note that if condition (2.10) holds $\lambda = 0$ is not a root of (2.17).

Lemma 2.4.3. *If condition (2.10) holds, then (2.17) has no positive real roots.*

Proof. Consider $\lambda \in \mathbb{R}$. Set $f(\lambda) = \lambda^2 + (d + x^*)\lambda + x^*d$ and $h(\lambda) = Yx^* \int_0^\infty e^{-(d+\lambda)s} g(s)\,\mathrm{d}s(\lambda - (1 - 2x^*))$. Then (2.17) can be written as $f(\lambda) - h(\lambda) = 0$. Note that $f(\lambda) > 0$ for all $\lambda \geq 0$ and $f(0) = x^*d$.

Consider the case $1 - 2x^* \geq 0$. Then $h(\lambda) \leq 0$ for all $\lambda \leq 1 - 2x^*$. For $\lambda > 1 - 2x^*$, $h(\lambda) \leq k(\lambda) = d(\lambda - (1 - 2x^*))$. However, $f(\lambda) > k(\lambda)$ for $\lambda > 1 - 2x^*$ and therefore $f(\lambda)$ and $h(\lambda)$ do not intersect in the right half plane.

Consider the case $1 - 2x^* < 0$. Then $h(0) = -d(1 - 2x^*)$ and $f(0) > h(0)$. Note that for $\lambda > 1 - 2x^*$, $h(\lambda) \leq k(\lambda) = d(\lambda - (1 - 2x^*))$. However, $f(\lambda) > k(\lambda)$ for $\lambda > 1 - 2x^*$ and therefore $f(\lambda)$ and $h(\lambda)$ do not intersect in the right half plane.

□

Next, we find an estimate of the parametric region of local stability of E_+, i.e. the set of parameters where equation (2.17) has no roots with positive real part. In the previous lemma we have shown that when condition (2.10) holds, the characteristic equation (2.17) has no real non-negative roots. In what follows, Rouché's Theorem [43] (Chapter 6.2, Theorem 6.2.5, page 387) is used to approximate the region of stability of E_+.

Theorem 2.4.4. *If $1/3 < x^* < 1$, then E_+ is locally asymptotically stable.*

Proof. Define (2.17) into $f(\lambda) = \lambda^2+(d+x^*)\lambda+x^*d$ and $h(\lambda) = Yx^* \int_0^\infty e^{-(d+\lambda)s} g(s)\,\mathrm{d}s(1-2x^*-\lambda)$. Then (2.17) can be written as $f(\lambda)+h(\lambda) = 0$.

Note that $f(\lambda)$ has two real negative roots if (2.10) holds. Define $\Gamma_1 = \{\lambda \in \mathbb{C} : \lambda = Re^{\theta i},\ R > 0,\ -\pi/2 \le \theta \le \pi/2\}$, $\Gamma_2 = \{\lambda \in \mathbb{C} : \lambda = \beta i,\ -R \le \beta \le R,\ R, \beta \in \mathbb{R},\ R > 0\}$ and $\Gamma = \Gamma_1 \cup \Gamma_2$. We show that for all $\lambda \in \Gamma$, as $R \to \infty$ $|f(\lambda)| > |h(\lambda)|$, since then, by Rouché's theorem it follows that $f(\lambda)+h(\lambda)$ has no root with positive real part.

Consider contour Γ_1. Note that

$$|e^{-\lambda s}| = |e^{-Re^{i\theta}s}| = |e^{-R(\cos\theta - i\sin\theta)s}| \le e^{-R(\cos\theta)s}\ .$$

Therefore $|e^{-\lambda s}|$ is maximized at $\theta = \pi/2,\ -\pi/2$ and therefore $|e^{-\lambda s}| \le 1$. Note that

$$\begin{aligned} |f(\lambda)| &\ge R^2 - (d+x^*)R - x^*d\ , \\ |h(\lambda)| &\le Yx^* \int_0^\infty e^{-ds} g(s)\mathrm{d}s||1-2x^*| + R| = d||1-2x^*| + R|\ . \end{aligned}$$

For R large enough $|f(\lambda)| > |h(\lambda|)$ for $\lambda \in \Gamma_1$.

Consider contour Γ_2. Similarly, note that $|e^{-\lambda s}| \le 1$. Then

$$\begin{aligned} f(\lambda) &= -\beta^2 + x^*d + y(d+x^*)i, \\ h(\lambda) &= Yx^* \int_0^\infty e^{-(d+\beta i)s} g(s)\mathrm{d}s(1-2x^*-\beta i)\ . \end{aligned}$$

Therefore,

$$\begin{aligned} |f(\lambda)|^2 &= (-\beta^2 + x^*d)^2 + \beta^2(d+x^*)^2, \\ |h(\lambda)|^2 &\le k^2(\lambda) = Y^2(x^*)^2 \left(\int_0^\infty e^{-ds} g(s)\mathrm{d}s\right)^2 ((1-2x^*)^2 + \beta^2) \\ &= d^2((1-2x^*)^2 + \beta^2)\ . \end{aligned}$$

Then,

$$|f(\lambda)|^2 - k^2(\lambda) \;=\; \beta^4 + \beta^2(x^*)^2 - d^2\left(1 - 4x^* + 3(x^*)^2\right) \ .$$

Note that if $1 - 4x^* + (3x^*)^2 < 0$, then $|f(\lambda)|^2 - k^2 > 0$ for all y and therefore E_+ is stable. In other words, if $\frac{1}{3} < x^* < 1$, then E_+ is stable. If, on the other hand, $1 - 4x^* + (3x^*)^2 > 0$, then $|f(\lambda)|^2 - k^2(\lambda)$ becomes negative for some $y > 0$. Therefore, $1/3 < x^* < 1$ is our first approximation of the stability region. □

2.4.2 Global dynamics

We begin by considering the case of mean delay $\tau = 0$.

Lemma 2.4.5. *If (2.10) holds and $\tau = 0$, then E_+ is globally asymptotically stable with respect to solutions of (2.5) with $x(0) > 0$ and $y(0) > 0$.*

Proof. Since $\tau = 0$, then $g(s) = \delta_0(s)$ and therefore, system (2.5) reduces to its ODE prototype:

$$\dot{x}(t) = x(t)(1 - x(t) - y(t)) \ , \tag{2.20a}$$

$$\dot{y}(t) = -dy(t) + Yx(t)y(t) \ . \tag{2.20b}$$

Solutions with positive initial conditions will remain positive for all $t > 0$. Using the Dulac criterion with $h(x, y) = \frac{1}{xy}$, we observe that there are no periodic solutions lying in $int\mathbb{R}^2_+$. Observe that only the solutions with initial conditions on the y-axis converge to E_0, while solutions on the x-axis, not including the origin, converge to E_1. On the other hand, E_1 repels the solutions with initial data not on the x-axis. Using straightforward phase plane argument, one can see that neither E_0, nor E_1 is in the ω-limit set of solutions with initial data in $int\mathbb{R}^2_+$. Then, by Poincaré-Bendixson Theorem, E_+ is globally asymptotically stable. □

Lemma 2.4.6. *Let $(x(t), y(t))$ be a solution of (2.5) with initial data in $X^0 \cup X_2$. There is no positive monotonically increasing sequence $\{t_n\}$, with $t_n \longrightarrow \infty$ as $n \longrightarrow \infty$ such that $(x(t_n), y(t_n))$ converges to E_0.*

Proof. Note that for every solution with initial data in $X^0 \cup X_2$, $x(t) > 0$ for all $t \geq 0$. We proceed using proof by contradiction. Assume that there exists a positive, monotonically increasing sequence $\{t_n\}$, with $t_n \longrightarrow \infty$ as $n \longrightarrow \infty$ such that $\dot{x}(t_n) \leq 0$ and $(x(t_n), y(t_n)) \to E_0$ as $n \to \infty$. For every $\epsilon > 0$, there exists $T > 0$ such that $x(t_n) < \epsilon$ and $y(t_n) < \epsilon$, for all $t_n > T$. Set $\epsilon < 1/2$. Then $\dot{x}(t_n) > x(t_n)(1 - 2\epsilon) > 0$, for sufficiently large n, a contradiction. □

Lemma 2.4.7. *If $g(s)$ is a non-negative, continuous almost everywhere function satisfying (2.3), then for every $\epsilon > 0$ there exists $b_\epsilon \geq 0$ such that $\int_{b_\epsilon}^{\infty} g(s)\,\mathrm{d}s < \epsilon$.*

Proof. We proceed using proof by contradiction. Assume that there exists an $\bar{\epsilon} > 0$, such that $\int_b^{\infty} g(s)\,\mathrm{d}s \geq \bar{\epsilon}$, for all $b \geq 0$. Define $\{c_k\} = \int_k^{\infty} g(s)\,\mathrm{d}s,\ k = 1, 2, \ldots$. Then, $\{c_k\}$ is a decreasing sequence bounded below by $\bar{\epsilon}$. Define $a_k = 1 - c_k,\ k = 1, 2, \ldots$. Then, $\{a_k\}$ is an increasing sequence, bounded above by $1 - \bar{\epsilon}$. Therefore, there exists $a \in \mathbb{R}$ such that $a_k \to a \leq 1 - \bar{\epsilon}$, as $k \longrightarrow \infty$. However, since $\int_0^{\infty} g(s)\,\mathrm{d}s = 1$, $a_k = 1 - \int_k^{\infty} g(s)\,\mathrm{d}s = \int_0^k g(s)\,\mathrm{d}s \longrightarrow \int_0^{\infty} g(s)\,\mathrm{d}s = 1$ as $k \to \infty$, a contradiction. □

Lemma 2.4.8. *If (2.10) holds, then no solution of (2.5) with initial data in X^0 converges to E_1.*

Proof. By Lemma 2.2.4, it follows that for any solution of system (2.5) with initial data in X^0, there exists $T \geq 0$ such that $y(t) > 0$ for all $t > T$. We proceed using proof by contradiction. Assume that there exists a positive, monotonically increasing sequence $\{t_n\}$, with $t_n \longrightarrow \infty$ as $n \longrightarrow \infty$ such that $y(t_n) \geq y(t_{n+1})$, $y(t) \geq y(t_n)$, $0 \leq t < t_n$, and $\dot{y}(t_n) \leq 0$. By (2.10), there exists $\gamma > 0$, such that $Y \int_0^{\infty} e^{-ds} g(s)\,\mathrm{d}s = d + 2\gamma$. By Lemma 2.4.7, we can select b sufficiently large so that $Y \int_b^{\infty} e^{-ds} g(s)\,\mathrm{d}s \leq$

$Y\int_b^\infty g(s)\,\mathrm{d}s < \gamma$. For any $s \in [0,b]$, we can also select t_n large enough so that $t_n - s > 0$ and so $y(t_n - s) > y(t_n)$ for all $s \in (0,b]$, for n sufficiently large. Since we assume that $x(t) \longrightarrow 1$ as $t \longrightarrow \infty$, then $x(t_n - s) > \frac{d}{d+\gamma}$, for all $s \in (0,b]$ for n sufficiently large. Then,

$$\begin{aligned}
\dot{y}(t_n) &= -dy(t_n) + Y\int_0^\infty x(t_n - s)y(t_n - s)e^{-ds}g(s)\,\mathrm{d}s \\
&\geq -dy(t_n) + Y\int_0^b \left(\frac{d}{d+\gamma}\right) y(t_n)e^{-ds}g(s)\,\mathrm{d}s \\
&> y(t_n)\left(-d + \left(\frac{d}{d+\gamma}\right)(d+\gamma)\right) = 0\ ,
\end{aligned}$$

i.e., $\dot{y}(t_n) > 0$, for all sufficiently large n, a contradiction. □

Define $x^\infty = \limsup_{t\to\infty} x(t)$, $x_\infty = \liminf_{t\to\infty} x(t)$, $y^\infty = \limsup_{t\to\infty} y(t)$ and $y_\infty = \liminf_{t\to\infty} y(t)$.

Lemma 2.4.9. *Let $(x(t), y(t))$ be a solution of (2.5) with initial data in $X^0 \cup X_2$. Then $x^\infty \geq \min\left\{1, \frac{d}{Y\int_0^\infty e^{-ds}g(s)\,\mathrm{d}s}\right\}$.*

Proof. We proceed using proof by contradiction. Assume

$$x^\infty < \min\left\{1, \frac{d}{Y\int_0^\infty e^{-ds}g(s)\,\mathrm{d}s}\right\}\ . \tag{2.21}$$

By the Fluctuation Lemma, there exists a positive sequence $\{t_n\}$, such that $\lim_{n\to\infty} t_n = \infty$, $\lim_{n\to\infty} y(t_n) = y^\infty$, and $\lim_{n\to\infty} \dot{y}(t_n) = 0$.

There exists $T > 0$ such that $x(t) < x^\infty + \epsilon$ and $y(t) < y^\infty + \epsilon$, for all $t \geq T$. Take $t_n > T$. Then $x(t_n - s) < x^\infty + \epsilon$ and $y(t_n - s) < y^\infty + \epsilon$, for all $s \in [0, t_n - T]$.

Consider

$$\begin{aligned}
\int_0^\infty x(t_n - s)y(t_n - s)e^{-ds}g(s)\,\mathrm{d}s = \quad & \int_0^{t_n - T} x(t_n - s)y(t_n - s)e^{-ds}g(s)\,\mathrm{d}s \\
& + \int_{t_n - T}^\infty x(t_n - s)y(t_n - s)e^{-ds}g(s)\,\mathrm{d}s\ .
\end{aligned}$$

Since $x(t)$ and $y(t)$ are bounded for $t \in (-\infty, \infty)$, there exists $K > 0$, such that $x(t)y(t) < K$. Therefore, $\int_{t_n-T}^{\infty} x(t_n - s)y(t_n - s)e^{-ds}g(s)\,\mathrm{d}s \leq \int_{t_n-T}^{\infty} Ke^{-ds}g(s)\,\mathrm{d}s$ converges to 0, as $n \to \infty$. It follows that

$$\int_0^{\infty} x(t_n - s)y(t_n - s)e^{-ds}g(s)\,\mathrm{d}s \leq (x^{\infty} + \epsilon)(y^{\infty} + \epsilon)\int_0^{\infty} e^{-ds}g(s)\,\mathrm{d}s\ ,$$

for sufficiently large n. Then, letting $n \to \infty$ and $\epsilon \to 0+$

$$0 = \dot{y}(t_n) \leq -dy(t_n) + Yx^{\infty}y^{\infty}\int_0^{\infty} e^{-ds}g(s)\,\mathrm{d}s$$

Since $\lim_{n\to\infty} y(t_n) = y^{\infty}$, then

$$0 \leq -dy^{\infty} + Yx^{\infty}y^{\infty}\int_0^{\infty} e^{-ds}g(s)\,\mathrm{d}s\ .$$

Since by (2.21), $x^{\infty} < \frac{d}{Y\int_0^{\infty} e^{-ds}g(s)\,\mathrm{d}s}$, then $y^{\infty} = 0$. Therefore, $\lim_{t\to\infty} y(t) = 0$. From (2.5a), it follows that $x^{\infty} = \lim_{t\to\infty} x(t) = 1$, a contradiction. □

Lemma 2.4.10. *Let $(x(t), y(t))$ to be a solution of (2.5) with initial data in $X^0 \cup X_2$. Then there exists $\epsilon_x > 0$ such that $x_{\infty} > \epsilon_x$.*

Proof. Recall that $T : \mathbb{R}_+ \times X \to X$ denotes the semiflow generated by model (2.5). Consider the function $\rho : X \to \mathbb{R}_+$, defined for $(\phi(t), \psi(t)) \in X^0$ by $\rho((\phi, \psi)) = \phi(0)$ so that $\rho(T(t, (\phi, \psi))) = x(t)$. By Lemma 2.2.4, $\rho((\phi, \psi)) > 0$ implies that $\rho(T(t, (\phi, \psi))) > 0$ for all $t \geq 0$. Therefore, the semi-flow is uniformly weakly ρ-persistent. By an argument similar to that given in Theorem 5.29 of [36] together with Lemma 2.2.3, T is a continuous semiflow that has a compact attractor of bounded sets. Therefore, T is uniformly ρ-persistent by Theorem 5.2 of [36], and hence there exists $\epsilon_x > 0$, such that $x_{\infty} \geq \epsilon_x$, for all solutions with $x(0) > 0$. □

Lemma 2.4.11. *Consider solutions of (2.5) with initial data in X^0. If (2.10) holds, then there exists $\epsilon > 0$ such that $y^{\infty} > \epsilon$.*

Proof. We denote the Laplace transform of a function $f(t)$ as $\widehat{f}(\lambda) = \int_0^\infty e^{-\lambda t} f(t)\, dt$, and note that the Laplace transform of $y(t)$ exists for all $\lambda > 0$, since $y(t)$ is bounded by Lemma 2.2.3. Taking the Laplace transform on both sides of of (2.5b) and simplifying we obtain:

$$\begin{aligned}(\lambda + d)\widehat{y}(\lambda) &= y(0) + Y\widehat{xy}(\lambda)\int_0^\infty e^{-\lambda s}e^{-ds}g(s)\mathrm{d}s \\ &\quad + Y\int_0^\infty e^{-\lambda u}\int_u^\infty x(u-s)y(u-s)e^{-ds}g(s)\mathrm{d}s\; du.\end{aligned}$$

There exists $\delta > 0$ such that $x(t) \geq (x_\infty - \delta)$ for all $t \geq 0$, and so $\widehat{xy}(\lambda) \geq (x_\infty - \delta)\widehat{y}(\lambda)$.

$$(\lambda + d)\widehat{y}(\lambda) \geq Y(x_\infty - \delta)\widehat{y}(\lambda)\int_0^\infty e^{-\lambda s}e^{-ds}g(s)\mathrm{d}s.$$

By Lemma 2.2.4, $y(t) > 0$ for all sufficiently large t, and hence $\widehat{y}(\lambda) > 0$, we can divide by $\widehat{y}(\lambda)$ to obtain

$$(\lambda + d) \geq Y(x_\infty - \delta)\int_0^\infty e^{-\lambda s}e^{-ds}g(s)\mathrm{d}s.$$

After a shift of time, if necessary, we can take the limit as $\delta, \lambda \to 0^+$ to obtain $x_\infty \leq \frac{d}{Y\int_0^\infty e^{-ds}g(s)\mathrm{d}s}$.

Since (2.10) holds, it is possible to select $\epsilon > 0$ such that $\frac{d}{\int_0^\infty e^{-ds}g(s)\mathrm{d}s} < 1 - \epsilon$. We proceed using proof by contradiction. Assume that there is initial data $\phi \in X^0$ such that $y^\infty < \epsilon/4$. Therefore, there exists $T_0 > 0$ such that $y(t) < \epsilon/2$ for all $t > T_0$. Then, by (2.5a),

$$\dot{x}(t) \geq x(t)(1 - x(t) - \epsilon/2)\ ,$$

for all $t > T_0$. Therefore, by the Comparison Theorem (see [38]), $x_\infty \geq 1 - \epsilon/2$, a contradiction. □

Theorem 2.4.12. *If (2.10) holds, then solutions of (2.5) with initial data in X^0 are uniformly persistent, i.e., there exists $\epsilon > 0$ such that $x_\infty > \epsilon$ and $y_\infty > \epsilon$.*

Proof. By Lemma 2.4.10, there exists $\epsilon_x > 0$ such that $x_\infty > \epsilon_x$.

Define $\rho : X \to \mathbb{R}_+$ by $\rho((\phi, \psi)) = \min\{\phi(0), \psi(0)\}$. Then $\rho(T(t, (\phi, \psi))) = \min\{x(t), y(t)\}$. By Lemma 2.2.4, shifting time if necessary, there is no loss of generality if we assume that $\psi(0) = y(0) > 0$. Therefore, $\rho(T(t, (\phi, \psi))) > 0$ for all $t \geq 0$. Since by Lemma 2.4.11, $y(t)$ is uniformly weakly persistent, then, by a similar argument to that given in Theorem 5.29 of [36] together with Lemma 2.2.3, T is uniformly weakly ρ-persistent. Since, by Lemma 2.2.3, T has a compact attractor of bounded sets, by Theorem 5.2 in [36], T is uniformly persistent. □

To sum up, if E_+ exists, solutions of (2.5) are uniformly persistent. The specific dynamic is the subject of the discussion to follow.

This concludes the results that are common to all distributions. To get more insight into the local dynamics at E_+ we will consider analytically the gamma distribution of order $p = 1$ and $p = 2$ analytically, and the gamma distribution of higher orders and the uniform distribution numerically.

2.5 Dynamics of the model with the gamma distribution as the delay kernel

The general gamma distribution is given by

$$g_a^p(s) = \frac{s^{p-1}a^p}{e^{as}(p-1)!} \ . \tag{2.22}$$

The distribution has support $[0, \infty)$ and is an example of "long-tail" distribution.

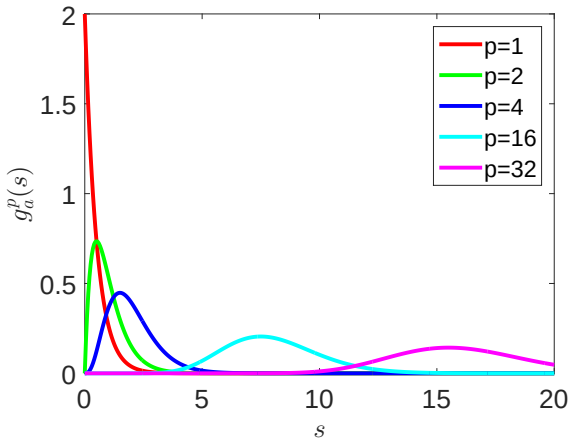

Figure 2.1: Graphs of the gamma distribution with $a = 2$ and various values for p.

The mean delay $\tau = \int_0^\infty s e^{-ds} g(s)\,\mathrm{d}s$ is given by

$$\tau = \frac{p}{a}\ .$$

Observe that

$$\int_0^\infty e^{-\alpha s} g_a^p(s)\,\mathrm{d}s = \frac{a^p}{(a+\alpha)^p}\ , \forall \alpha \in \mathbb{R}, \alpha \geq 0.$$

The coexistence equilibrium is $E_+ = (x_+, y_+) = \left(\frac{d(a+d)^p}{Ya^p}, 1 - \frac{d(a+d)^p}{Ya^p}\right)$, where $x_+ > 0$ and $y_+ > 0$ hold when:

$$Ya^p > d(a+d)^p\ . \tag{2.23}$$

In this section we refer to this inequality as "coexistence" condition. The critical value of mean delay τ, τ_c when E_+ ceases to exist is given by:

$$\tau_c = \frac{p}{d}\left(\left(\frac{Y}{d}\right)^{1/p} - 1\right)\ .$$

Observe that if $Y > d$, then there is a range of τ for which E_+ exists and as d decreases, this range becomes wider.

Linearization around E_+ has the following characteristic equation:

$$\left(\lambda + \frac{d(a+d)^p}{Ya^p}\right)((\lambda+d)(a+d+\lambda)^p - d(a+d)^p) + d(a+d)^p\left(1 - \frac{d(a+d)^p}{Ya^p}\right) = 0\ .$$

For the general value of p the characteristic equation is a polynomial of order $p+2$ and has at most $p+2$ roots, in contrast to the characteristic equation of the discrete delay model, which is transcendental and has infinitely many roots. When E_+ exists, all of the coefficients of the characteristic equation are positive.

2.5.1 Hopf bifurcations in the system with $p = 1$

We consider gamma distribution of order $p = 1$, i.e., an exponential distribution $g(s) = ae^{-as}$. The corresponding characteristic equation after simplification is:

$$\lambda^3 + \lambda^2\left(\frac{d(a+d)}{Ya} + a + 2d\right) + \lambda(a+2d)\frac{d(a+d)}{Ya} + d(a+d)\left(1 - \frac{d(a+d)}{Ya}\right) = 0\ . \tag{2.24}$$

The coexistence condition:

$$\frac{d(a+d)}{Ya} < 1\ . \tag{2.25}$$

Theorem 2.5.1. *If (2.25) holds and*

$$a^3 + \left(\frac{d}{Y} + 5d - Y\right)a^2 + \left(\frac{3d^2}{Y} + 5d^2\right)a + \frac{2d^3}{Y} = 0 \tag{2.26}$$

has two positive real roots a_c^1 and a_c^2, with $a_c^1 < a_c^2$, then E_+ undergoes two Hopf bifurcations as τ increases from 0, losing stability at $\tau_c^1 = 1/a_c^2$ and re-stabilizing at $\tau_c^2 = 1/a_c^1$.

Proof. Observe that $k(a)$ always has at least one negative root.

To find pure imaginary roots of (2.24) substitute $\lambda = \omega i$ ($\omega > 0$) in (2.24) to obtain:

$$-i(a\omega^3) - \left(\frac{d(a+d)}{Y} + a^2 + 2da\right)\omega^2 + i(a+2d)\frac{d(a+d)}{Y}\omega + d(a+d)\left(a - \frac{d(a+d)}{Y}\right) = 0\ .$$

Separate pure and imaginary parts:

$$-a\omega^3 + (a+2d)\frac{d(a+d)}{Y}\omega = 0 \ , \tag{2.27a}$$

$$-\left(\frac{d(a+d)}{Y} + a^2 + 2da\right)\omega^2 + d(a+d)\left(a - \frac{d(a+d)}{Y}\right) = 0 \ . \tag{2.27b}$$

Solve (2.27a) and (2.27b) for ω^2:

$$\omega^2 = \frac{(a+2d)}{a}\frac{d(a+d)}{Y} \ , \tag{2.28a}$$

$$\omega^2 = d(a+d)\left(a - \frac{d(a+d)}{Y}\right) \Big/ \left(\frac{d(a+d)}{Y} + a^2 + 2da\right) \ . \tag{2.28b}$$

Therefore, we have shown that

$$\left(\frac{d(a+d)}{Y} + a^2 + 2da\right)(a+2d)\frac{d(a+d)}{Y} = da(a+d)\left(a - \frac{d(a+d)}{Y}\right) \tag{2.29}$$

is a necessary condition for (2.24) to have pure imaginary roots and it is equivalent to

$$k(a) = a^3 + \left(\frac{d}{Y} + 5d - Y\right)a^2 + \left(\frac{3d^2}{Y} + 5d^2\right)a + \frac{2d^3}{Y} = 0 \ . \tag{2.30}$$

If (2.26) has two positive real roots a_c^1 and a_c^2 such that $a_c^1 < a_c^2$, then $k'(a_c^1) < 0$ and $k'(a_c^2) > 0$. On the other hand, if (2.26) has only one positive real root a_c it means $k'(a_c) = 0$.

Next we show that the transversality condition (see [29]) holds only if (2.26) has two positive real roots. If we multiply equation (2.24) by a ($a \neq 0$), we obtain an equivalent cubic polynomial of the form

$$f(\lambda, a) = b_3(a)\lambda^3 + b_2(a)\lambda^2 + b_1(a)\lambda + b_0(a) \tag{2.31}$$

where

$$b_3(a) = a, \tag{2.32a}$$

$$b_2(a) = \frac{d(a+d)}{Y} + a^2 + 2da, \tag{2.32b}$$

$$b_1(a) = (a+2d)\frac{d(a+d)}{Y}, \tag{2.32c}$$

$$b_0(a) = d(a+d)\left(a - \frac{d(a+d)}{Y}\right) \ . \tag{2.32d}$$

Condition (2.25) ensures that all the coefficients of (2.31) are positive. If $k(a) = b_3b_0 - b_2b_1 = 0$ holds, then (2.31) has a pair of pure imaginary values $\lambda = \pm i\omega$, such that $\omega^2 = \frac{b_1}{b_3} = \frac{b_0}{b_2}$.

Differentiate (2.31) with respect to a:

$$\lambda' \left(3b_3\lambda^2 + 2b_2\lambda + b_1\right) + b_3'\lambda^3 + b_2'\lambda^2 + b_1'\lambda + b_0' = 0 \ .$$

Here, we denote by $'$ the derivative with respect to a.

Solve for λ':

$$\lambda' = -\frac{b_3'\lambda^3 + b_2'\lambda^2 + b_1'\lambda + b_0'}{3b_3\lambda^2 + 2b_2\lambda + b_1} \ .$$

Evaluate the derivative at $a = a_c^i$ and recall that at such a, $\lambda = \omega i$:

$$(\alpha + \beta i)'\big|_{a=a_c^i} = -\frac{-b_3'\omega^3 i - b_2'\omega^2 + b_1'\omega i + b_0'}{-3b_3\omega^2 + b_1 + 2b_2\omega i}\Big|_{a=a_c^i} \ .$$

Multiply and divide the equation by $-3b_3\omega^2 + b_1 - 2b_2\omega i$:

$$(\alpha + \beta i)'\big|_{a=a_c^i} = -\frac{(-b_2'\omega^3 i - b_2'\omega^2 + b_1'\omega i + b_0')(-3b_3\omega^2 + b_1 - 2b_2\omega i)}{(-3b_3\omega^2 + b_1)^2 + (2b_2\omega)^2}\Big|_{a=a_c^i} \ .$$

Cross-multiply the brackets and separate the real part:

$$\alpha'\big|_{a=a_c^i} = -\frac{2b_2\omega(-b_3'\omega^3 + b_1'\omega) + (b_0' - b_2'\omega^2)(b_1 - 3b_3\omega^2)}{(-3b_3\omega^2 + b_1)^2 + (2b_2\omega)^2}\Big|_{a=a_c^i} \ .$$

Therefore, if we want to assess the sign of the real part of expression it will be sufficient to consider the real part of the numerator only:

$$\text{sign}(\alpha)'\big|_{a=a_c^i} = \text{sign}(-(2b_2\omega(-b_3'\omega^3 + b_1'\omega) + (b_0' - b_2'\omega^2)(b_1 - 3b_3\omega^2))) \ .$$

Consider the expression:

$$-(2b_2\omega(-b_3'\omega^3 + b_1'\omega) + (b_0' - b_2'\omega^2)(b_1 - 3b_3\omega^2)) =$$
$$-(-2b_2b_3'\omega^4 + 2b_2b_1'\omega^2 + b_0'b_1 - 3b_3b_0'\omega^2 - b_1b_2'\omega^2 + 3b_3b_2'\omega^4) \ .$$

Group the terms:

$$\text{sign}(\alpha') = -\text{sign}(\omega^4(3b_3b_2' - 2b_2b_3') + \omega^2(-3b_3b_0' - b_1b_2' + 2b_2b_1') + b_0'b_1) \ .$$

Recall that $\omega^2 = \frac{b_0}{b_2} = \frac{b_1}{b_3}$. Therefore, the expression becomes

$$\begin{aligned} \text{sign}(\alpha') &= -\text{sign}\left(\frac{b_0^2}{b_2^2}(3b_3b_2' - 2b_2b_3') + \frac{b_1}{b_3}(-3b_3b_0' - b_1b_2' + 2b_2b_1') + b_0'b_1\right) \\ &= -\text{sign}\left(\frac{2b_1}{b_3}(b_2'b_1 + b_1'b_2 - b_0b_3' - b_3b_0')\right) \ . \end{aligned}$$

We recognize the expression in the brackets as $-k'(a)$. If $k(a)$ has only one positive real root a_c, then $k'(a_c) = 0$ and therefore the transversality condition does not hold.

On the other hand, if $k(a)$ has two positive real roots a_c^1 and a_c^2, then at a_c^1, $k'(a) < 0$ and since $b_3, b_2, b_1, b_0 > 0$, then $\frac{\partial}{\partial a} Re(\lambda)\big|_{a=a_c^1} < 0$. Similarly, $k'(a_c^2) > 0$ and since $b_3, b_2, b_1, b_0 > 0$, then $\frac{\partial}{\partial a} Re(\lambda)\big|_{a=a_c^2} > 0$. □

Theorem 2.5.2. *Set*

$$\Delta = 4\left(\frac{1}{Y^2} + \frac{1}{Y} + 10\right)d^2 - 2(1 + 5Y)\,d + Y^2 \ .$$

If $d < \frac{5Y^3 + Y^2 - Y^2\sqrt{15Y^2+9Y}}{10Y^2+Y+1}$ *and*

$$\begin{aligned} \left(\frac{-\left(\frac{d}{Y} + 5d - Y\right) + \Delta}{3}\right)^3 + \left(\frac{d}{Y} + 5d - Y\right)\left(\frac{-\left(\frac{d}{Y} + 5d - Y\right) + \Delta}{3}\right)^2 \\ + \left(\frac{3d^2}{Y} + 5d^2\right)\left(\frac{-\left(\frac{d}{Y} + 5d - Y\right) + \Delta}{3}\right) + \frac{2d^3}{Y} < 0 \ , \end{aligned} \tag{2.33}$$

then there exist two values of $a > 0$ *at which (2.24) has a pair of pure imaginary roots.*

Proof. Recall that in order for equation (2.24) to have pure imaginary roots $k(a) = 0$ should hold. Note that $k(a)$ is a cubic polynomial in a. Since $a = 1/\tau$, we are interested in positive real roots of $k(a)$. Since $k(0) > 0$ and $\lim_{a\to-\infty} k(a) = -\infty$, it follows that $k(a)$ has at least one negative real root. If the remaining two roots are real, they are

of the same sign. Positive real roots of (2.26) correspond to the values of a at which (2.24) has pure imaginary roots. In order for (2.26) to have positive real roots, it must have two local extrema in the positive half plane and if a_{min} is a local minimum of $k(a)$, then $k(a_{min}) < 0$.

To find the location of the local extrema of $k(a)$, consider:

$$k'(a) = 3a^2 + 2a\left(\frac{d}{Y} + 5d - Y\right) + \frac{3d^2}{Y} + 5d^2 = 0 \ . \tag{2.34}$$

$k'(a)$ is a quadratic equation. In order for it to have two real roots, the discriminant of $k'(a)$ must be positive, i.e.:

$$\Delta(d) = 4\left(\frac{1}{Y^2} + \frac{1}{Y} + 10\right)d^2 - 2\left(1 + 5Y\right)d + Y^2 > 0 \ . \tag{2.35}$$

$\Delta(d)$ is a quadratic in d and $\lim_{d\to\pm\infty} = \infty$. The roots are given by:

$$d_1 = \frac{5Y^3 + Y^2 - Y^2\sqrt{3Y(5Y+3)}}{10Y^2 + Y + 1} \ , \tag{2.36a}$$

$$d_2 = \frac{5Y^3 + Y^2 + Y^2\sqrt{3Y(5Y+3)}}{10Y^2 + Y + 1} \ . \tag{2.36b}$$

Note that d_1 and d_2 are real and are both positive, since $d_2 > 0$ and both the constant term and leading coefficient of $\Delta(d)$ are positive. This implies that the two roots have the same sign.

In order for (2.34) to have two distinct real roots, either $0 < d < d_1$ or $d > d_2$ must hold. If in addition, the coefficient of a in (2.34) is negative and the coefficient of a^2 is positive, then $k'(a)$ has two positive real distinct roots. This is satisfied, if and only if

$$(0 < d < d_1 \text{ or } d > d_2) \text{ and } \left(\frac{d}{Y} + 5d - Y\right) < 0 \ .$$

Solving the second inequality for d we obtain :

$$(0 < d < d_1 \text{ or } d > d_2) \text{ and } d < \frac{Y^2}{5Y+1} \ . \tag{2.38}$$

However, if $d > d_2$, (2.38) is violated, since $d_2 > \frac{Y^2}{5Y+1}$, by (2.36b). On the other hand, if

$$0 < d < d_1 \tag{2.39}$$

holds, then by (2.36a) system (2.38) is always satisfied. Therefore, if $d < d_1$, then (2.34) has two extrema in the positive half plane.

Now consider the sign of $k(a_{min})$.

$$a_{min} = \frac{-\left(\frac{d}{Y} + 5d - Y\right) + \sqrt{\Delta(d)}}{3} \tag{2.40}$$

Then the condition $k(a_{min}) < 0$ is equivalent to (2.33). Note that

$$\lim_{d \to 0+} k(a_{min}) < 0$$

Therefore, it is possible to select d sufficiently small so that both (2.33) and $d < d_1$ hold. □

These results illuminate the shape of the border of the stability region of E_+. Our results did not suggest limitations on Y, save for it being positive. For a fixed value of Y there is a range of values of $d(Y)$ such that E_+ is locally asymptotically stable when it exists. On the other hand, if the pair $(Y, d(Y))$ is such that (2.24) has pure imaginary roots for two different values of $a = a_c^i$, then at both a_c^1 and a_c^2, E_+ undergoes a Hopf bifurcation, losing stability at a_c^1 and re-stabilizing at a_c^2.

Finally, if the set of values of d and Y is such that (2.24) has pure imaginary roots for only one value of $a = a_c$, then E_+ is locally asymptotically stable for all values of a (except possibly, for $a = a_c$).

For each value of $Y \in [0.2, 1]$, we proceeded numerically to solve the system of inequalities (2.39) and (2.33) for d, and found pairs (Y, d) for which two Hopf bifurcations at E_+ are possible (blue region on the Figure 2.2). We then considered (2.33) as an equality and for each value of Y found a critical value of $d = d_c(Y)$, so that

for all such (Y, d) there is only one value of τ when the characteristic equation has pure imaginary roots and the transversality condition does not hold (red curve on the Figure 2.2). In the white region on Figure (2.2), E_+ is locally asymptotically stable when it exists.

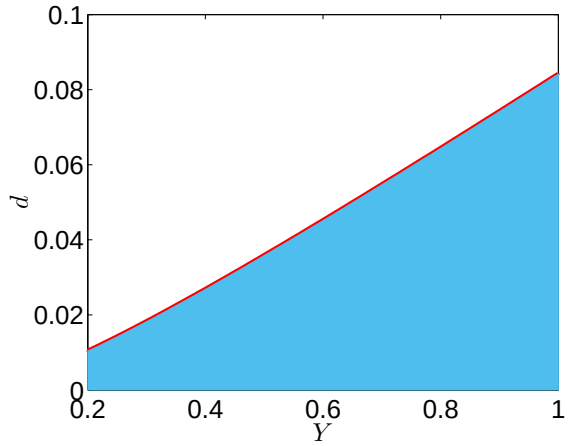

Figure 2.2: The region where Hopf bifurcations occurs in $Y - d$ space as τ $(= \frac{1}{a})$ varies in system (2.5) with the gamma distribution of order $p = 1$ used as the delay kernel. For each point in the blue shaded region there exist two values of a at which E_+ undergoes Hopf bifurcation. In the white region there are no Hopf bifurcations. The regions are separated by the red curve, for each point on which there is only one value of a such that the characteristic equation has pure imaginary roots, however, the transversality condition does not hold.

We created a mesh in $Y - d$ space based on the shaded region of (2.2) and using (2.26) numerically calculated the values of a_c^i, $i = 1, 2$ at which E_+ loses and subsequently regains stability. As the result we produced the 3-dimensional manifold (Figure 2.3) inside of which E_+ is unstable. The code underlying the calculations can be found in Appendix A.

There are several things of note with respect to this figure. We fixed Y and varied d to change the potential number of Hopf bifurcations, but our diagram indicates that

Y could have been used in the identical fashion. While we produced the mesh using $Y = 0.2 - 1$, it can be extended at both ends.

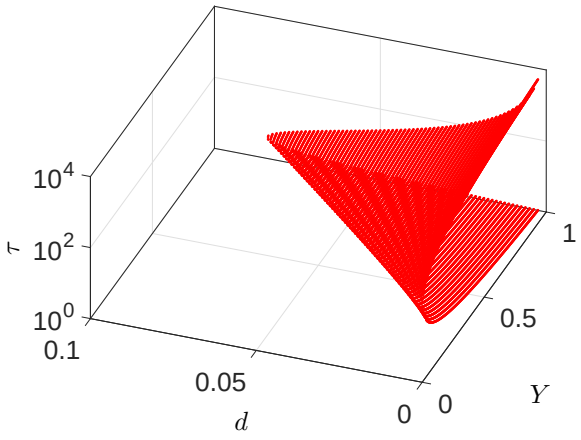

Figure 2.3: The envelope of the Hopf bifurcations in $Y - d - \tau$ space for system (2.5) with the gamma distribution of order $p = 1$ used as the delay kernel. Inside the fold E_+ is unstable and outside it is stable, if it exists.

2.5.2 Hopf bifurcations in the system with $p = 2$

Next we consider system (2.5) with the gamma distribution of order $p = 2$ used as the delay kernel. We will give conditions for the existence of critical values of τ, such that the characteristic equation corresponding to linearization of system (2.5) around E_+ has pure imaginary roots. Moreover, we will give the conditions when such roots are indicative of Hopf bifurcation.

The characteristic equation corresponding to the gamma distribution of order $p = 2$ is

$$\left(\lambda + \frac{d(a+d)^2}{Ya^2}\right)\left((\lambda+d)(a+d+\lambda)^2 - d(a+d)^2\right) + d(a+d)^2\left(1 - \frac{d(a+d)^2}{Ya^2}\right) = 0\,. \tag{2.41}$$

Once the brackets are open, expression multiplied by Ya^2 and terms collected, the

equation takes the form:

$$b_4(a)\lambda^4 + b_3(a)\lambda^3 + b_2(a)\lambda^2 + b_1(a)\lambda + b_0(a) = 0 \ ,$$

where

$$\begin{aligned} b_4(a) &= Ya^2 \ , \\ b_3(a) &= 2Ya^3 + 3Ya^2d + a^2d + 2ad^2 + d^3 \ , \\ b_2(a) &= (a+d)(Ya^3 + 3Ya^2d + 2a^2d + 5ad^2 + 3d^3) \ , \\ b_1(a) &= d(a+d)^3(a+3d) \ , \\ b_0(a) &= d(a+d)^2(Ya^2 - a^2d - 2ad^2 - d^3) \ . \end{aligned}$$

Observe that all the coefficients are polynomial in a and are positive if E_+ exists.

Theorem 2.5.3. *Consider an equation of the form* $p(\lambda) = b_4(a)\lambda^4 + b_3(a)\lambda^3 + b_2(a)\lambda^2 + b_1(a)\lambda + b_0(a) = 0$. *If* $k(a) = b_4(a)b_1^2(a) - b_1(a)b_2(a)b_3(a) + b_0(a)b_3^2(a) = 0$ *has positive real root* a_c *such that* $k'(a_c) \neq 0$, *then when* $a = a_c$, $p(\lambda)$ *has pure imaginary roots and* $\frac{\partial Re(\lambda)}{\partial a}\big|_{a=a_c} \neq 0$.

Proof. Set $\lambda = i\omega$ ($\omega \in \mathbb{R}$, $\omega > 0$) and substitute into $p(\lambda)$ to obtain:

$$p(i\omega) = b_4(a)\omega^4 - ib_3(a)\omega^3 - b_2(a)\omega^2 + ib_1(a)\omega + b_0(a) = 0 \ .$$

Isolate real and imaginary parts:

$$b_4(a)\omega^4 - b_2(a)\omega^2 + b_0(a) = 0 \ , \tag{2.42a}$$

$$-b_3(a)\omega^2 + b_1(a) = 0 \ . \tag{2.42b}$$

Solve (2.42b) for ω^2 and substitute into (2.42a) to obtain:

$$k(a) = b_4(a)b_1^2(a) - b_1(a)b_2(a)b_3(a) + b_0(a)b_3^2(a) = 0 \ .$$

If $k(a)$ has positive real roots a_c, then (2.41) has pure imaginary roots when $a = a_c$. Moreover, these are roots are $\lambda = \pm i\omega = \pm i\sqrt{\frac{b_1(a)}{b_3(a)}}$.

Next we check the sign of $\frac{\partial Re(\lambda)}{\partial a}\big|_{a=a_c}$. Note that

$$k'(a) = -b_3^2 b_0' + (b_2 b_3 - 2b_1 b_4)b_1' + b_1 b_3 b_2' + (b_1 b_2 - 2b_0 b_3)b_3' - b_1^2 b_4' \ .$$

Differentiate $p(\lambda)$ with respect to a:

$$\lambda'(4\lambda^3 b_4 + 3b_3\lambda^2 + 2b_2\lambda + b_1) + b_4'\lambda^4 + b_3'\lambda^3 + b_2'\lambda^2 + b_1'\lambda + b_0' = 0 \ .$$

Solve for λ':

$$\lambda' = -\frac{b_4'\lambda^4 + b_3'\lambda^3 + b_2'\lambda^2 + b_1'\lambda + b_0'}{4\lambda^3 b_4 + 3b_3\lambda^2 + 2b_2\lambda + b_1} \ .$$

Recall that at critical values of $a = a_c$, $\lambda = i\omega$. It follows

$$(\beta + \gamma i)'\big|_{a=a_c} = -\frac{b_4'\omega^4 - b_3'\omega^3 i - b_2'\omega^2 + b_1'\omega i + b_0'}{-4\omega^3 b_4 i - 3b_3\omega^2 + 2b_2\omega i + b_1} \ .$$

After multiplication and division of the expression by $b_1 - 3b_3\omega^2 - i(2b_2\omega - 4b_4\omega^3)$, the denominator of the ratio on the right becomes positive. Therefore, if we want to assess the sign of the real part of expression it will be sufficient to consider the real part of the numerator only:

$$\text{sign}(\beta') = \text{sign}\left(-\left((b_4'\omega^4 - b_2'\omega^2 + b_0')(b_1 - 3b_3\omega^2) + (b_1'\omega - b_3'\omega^3)(2b_2\omega - 4b_4\omega^3)\right)\right) \ .$$

Open brackets, substitute $\omega^2 = \frac{b_1}{b_3}$ and multiply by b_3^3:

$$\begin{aligned}\text{sign}(\beta') = \text{sign}(-(&b_1^3 b_3 b_4' - 3b_1^3 b_3 b_4' - b_1^2 b_3^2 b_2' + 3b_1^2 b_3^2 b_2' + b_1 b_3^3 b_0' - 3b_1 b_3^3 b_0' \\ &+2b_1 b_2 b_3^2 b_1' - 4b_1^2 b_3 b_4 b_1' - 2b_1^2 b_2 b_3 b_3' + 4b_1^3 b_4 b_3'))\ .\end{aligned}$$

Collect terms and factor out $2b_1$:

$$\text{sign}(\beta') = \text{sign}(-2b_1(-b_3^3 b_0' + (b_2 b_3^2 - 2b_1 b_3 b_4)b_1' + b_1 b_3^2 b_2' + (2b_1^2 b_4 - b_1 b_2 b_3)b_3' - b_1^2 b_3 b_4'))\ .$$

Replace $b_1^2 b_4$ by $b_1 b_2 b_3 - b_0 b_3^2$ and factor out b_3:

$$\text{sign}(\beta') = \text{sign}(-2b_1 b_3(-b_3^2 b_0' + (b_2 b_3 - 2b_1 b_4)b_1' + b_1 b_3 b_2' + (b_1 b_2 - 2b_0 b_3)b_3' - b_1^2 b_4'))\ .$$

Therefore, $\text{sign}(\beta') = \text{sign}(2b_1 b_3 k'(a_c))$. □

By Theorem 2.5.3 system (2.5) with gamma distributed delay of order $p = 2$ undergoes a Hopf bifurcation provided that $k(a)$ has a root a_c such that $k'(a)_c \neq 0$. Note that $k(a)$ for the system is a polynomial of degree 9:

$$\begin{aligned} k(a) &= 2Y^2a^9 - (4Y^3 - 23Y^2d - 4Yd)a^8 \\ &\quad -(12Y^3d - 88Y^2d^2 + 4Y^2d - 40Yd^2 - 2d^2)a^7 \\ &\quad -(9Y^3d^2 - 151Y^2d^3 + 14Y^2d^2 - 151Yd^3 + Yd^2 - 20d^3)a^6 \\ &\quad -(-120Y^2d^4 + 16Y^2d^3 - 286Yd^4 + 4Yd^3 - 80d^4)a^5 \\ &\quad -(-36Y^2d^5 + 6Y^2d^4 - 292Yd^5 + 6Yd^4 - 170d^5)a^4 \\ &\quad -(-154Yd^6 + 4Yd^5 - 210d^6)a^3 - (-33Yd^7 + Yd^6 - 152d^7)a^2 \\ &\quad +60d^8a + 10d^9 \ . \end{aligned} \tag{2.43}$$

Therefore, whenever there exists a_c^1 satisfying the above conditions, there exists a second value a_c^2 with similar properties. Thus, similar to the previously considered case of "weak" kernel, for the systems with gamma kernel with $p = 2$ Hopf bifurcations occur in pairs.

The coefficient next to a^9 is positive and $k(0) = 10d^9 > 0$. Therefore, $k(a)$ has at least one negative real root and possibly 8 positive real roots, each of which could mark a Hopf bifurcation. Since $\text{sign}\left(\frac{\partial Re(\lambda)}{\partial a}\big|_{a=a_c}\right) = \text{sign}(k'(a))$, we expect for the periodic solution bubbles (if they occur) to follow sequentially. However, in our numerical simulations we have never observed appearance of more than two Hopf bifurcations. Finally, while in the case of $p = 1$ we were able to explicitly establish that for d sufficiently small, E_+ undergoes Hopf bifurcation, we were not able to analyze $k(a)$ in the same fashion for the case $p = 2$. However, the numerical simulations in the following section indicate that such a relationship exist.

2.6 Numerical results

In this section we confirm previously obtained results concerning the dynamics at E_+ for the system with "weak" kernel and will extend them farther with the help of numerical bifurcation analysis. We investigate the dynamics of the system with the general gamma distribution and the uniform distribution. These were chosen since they have different types of support. Gamma distribution kernel is continuous and positive on $(0, \infty)$, while uniform distribution has compact support $[\tau(1+\frac{1}{2\rho}), \tau(1-\frac{1}{2\rho})]$ and is identically zero outside of it. As the result, the system with gamma distributed delay has characteristic equation that is a polynomial, while the system with uniformly distributed delay has characteristic equation that is a transcendental equation. Linear chain trick applied to the former changes the system into ODE system, while the later becomes discrete delay system. We study bifurcation dynamics at equilibrium E_+ using τ as primary bifurcation parameter and d as the secondary. We have fixed $Y = 0.6$ for most of the diagrams, except when noted otherwise.

We observed that the dynamics across various distributions had many features in common and were similar in many respects to the dynamics of the system with discrete delay.

Our goal is to find the conditions under which the system dynamics with the two distributions are similar to each other and to these of the system with discrete delay. In the system with "weak" kernel the insight from the analytic results showed us that if the value of d is below a certain threshold value, then E_+ goes through two Hopf bifurcations as τ increases from 0. Similar dynamics have been numerically detected in the system with uniformly distributed delay and discrete delay system.

For the two types of distribution, we have also detected other global bifurcation dynamics when d becomes sufficiently small and τ changes its value. Finally, we compare the stability region of E_+ in $d - Y - \tau$ space for systems with discrete delay

to that of the system with gamma distributed delay of order $p = 1$.

This section contains two types of diagrams: orbit and bifurcation. Orbit diagrams were obtained by creating a mesh of values for the bifurcation parameter and then, for each point of the mesh, time series were generated. We integrated for the time intervals long enough so that trajectories of the solutions converge to an attractor (e.g. equilibrium or periodic orbit). Then, the local minima and maxima of $x(t)$ were plotted. The integration for a particular value of parameter was done through XPPAUT and then the obtained data was analyzed using a MATLAB script. Bifurcation diagrams were created using XPPAUT interface to the continuation package AUTO and DDE-BIFTOOL MATLAB package that enables numerical bifurcation and stability analysis of delay differential equations with one or more discrete or state-dependent delays. In bifurcations diagram the maximum and minimum amplitude of the x-component of the solution is plotted on the ordinate axis. Stable equilibria are depicted with solid blue line, unstable - dashed red line. Stable periodic solutions are depicted with solid green line, unstable - dashed red line.

The code used for the generation of diagrams is located in Appendix A.

Gamma distribution

We used the linear chain trick (as described in [27]) to convert the system with the gamma distributed delay into a system of ODEs and analyzed the bifurcation dynamics of the new system using the mean delay τ as the bifurcation parameter.

Set $g(s)$ to have general gamma distribution $g_a^p(s)$. Set

$$y_i(t) = \int_0^\infty x(t)y(t)e^{-ds}g_a^i(s)\,\mathrm{d}s\ , i = 1 \dots p.$$

Differentiate $y_i(t)$, with respect to t:

$$\begin{aligned}
\dot{y}_1(t) &= ax(t)y(t) - (a+d)y_1 \ , \\
\dot{y}_i(t) &= ay_{i-1}(t) - (a+d)y_i(t) \ , i = 2 \dots p \ .
\end{aligned}$$

System (2.5) becomes:

$$\begin{aligned}
\dot{x}(t) &= x(t) - x^2(t) - x(t)y(t) \ , \\
\dot{y}(t) &= -dy(t) + Yy_p(t) \ , \\
\dot{y}_1(t) &= ax(t)y(t) - (a+d)y_1 \ , \\
\dot{y}_i(t) &= ay_{i-1}(t) - (a+d)y_i(t) \ , i = 2 \dots p \ .
\end{aligned}$$

with initial conditions

$$\begin{aligned}
x(0) &= \phi(0) \ , \\
y(0) &= \psi(0) \ , \\
y_i(0) &= \int_0^\infty \phi(-s)\psi(-s)e^{-ds} g_a^i(s) \, \mathrm{d}s \ ,
\end{aligned}$$

where (ϕ, ψ) are initial data functions for $(x(t), y(t))$ that map from the interval $(-\infty, 0]$ onto $\mathbb{R}^2_+$. The system is now finite dimensional. Recall, that using the results of our analytic findings we can describe the region of instability of E_+ by creating a mesh out of the area under the curve on the Figure 2.2 and finding corresponding values of τ where Hopf bifurcation takes place. Fan and Wolkowicz [4] in their work with discrete delay system gave conditions on parameter space such that equilibrium E_+ undergoes two Hopf bifurcations. Using approach similar to what we did before, we have created a mesh in $Y - d$ space and for each point in the mesh found values of τ at which E_+ undergoes Hopf bifurcation. We plotted the results in $Y - d - \tau$ space (Figure 2.4). The code underlying the calculations can be found in Appendix (A).

We observe that shapes of stability regions boundaries for the "weak" kernel system and discrete delay system are identical. Note that, there is no restriction on Y, except for it being positive.

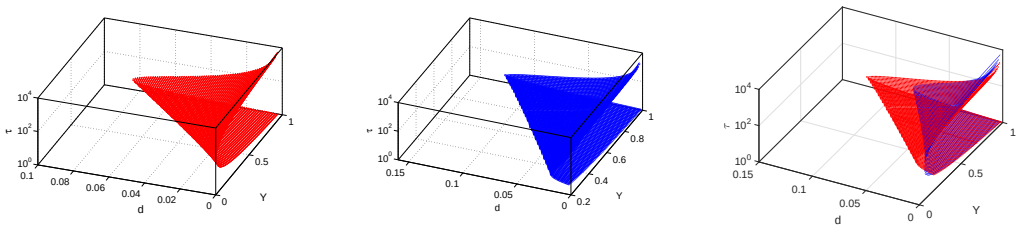

Figure 2.4: Hopf bifurcations envelope in $Y-d-\tau$ space for system (2.5) with $Y = 0.6$. Figure (a): gamma distribution of order p=1. Figure (b): discrete delay. Figure (c): juxtaposition of the regions for the two distributions

We fixed $Y = 0.6$ and compared two-parameter description of stability region of E_+ for the two systems (Figure 2.5). The shapes of the region are identical, but the region of instability of E_+ for gamma distribution is smaller. We stated previously that in system (3.6) with the general gamma distribution as d decreases the region of existence of E_+ is increasing. The similar effect is observed in the system with discrete delay, where the critical value of τ, $\tau_c = d^{-1} \ln \frac{Y}{d}$ (as seen in [4]) increases as d decreases.

Consider the dynamics depicted in the Figure 2.6. In the system with discrete delay for $0.07 < d < Y$, E_+ is locally asymptotically stable while it exists (Figure 2.6a). At $d \approx 0.07$ two supercritical Hopf bifurcations appear. An example of such dynamics is depicted at Figure 2.6b. Equilibrium E_+ is stable at $\tau = 0$ and remains so until $\tau \approx 2.299$ when E_+ goes through the first Hopf bifurcation and real parts of a pair of complex eigenvalues change from negative to positive, a stable periodic orbit appears. As τ increases to 34.96, E_+ goes through the second Hopf bifurcation, where the real parts of the pair of complex eigenvalues become negative, a stable periodic orbit disappears and E_+ restabilizes.

As $d \approx 0.016$ a second set of Hopf bifurcations occurs between the previous two.

An example of such dynamics is depicted on the Figure 2.6c. Equilibrium E_+ is stable at $\tau = 0$ and remains so until $\tau \approx 1.859$ when E_+ goes through the first Hopf bifurcation, and real parts of a pair of complex eigenvalues change from negative to positive. As τ approaches $\tau \approx 66.98$ real parts of a second pair of complex roots do the same, supercritical Hopf bifurcation takes place and an semi-stable periodic solution appears. The as τ increases to 102.8, real part of the second pair of complex eigenvalues becomes negative and the unstable periodic orbit disappears. As τ increases through 150.4, E_+ goes through the fourth Hopf bifurcation, a stable periodic orbit disappears and E_+ restabilizes.

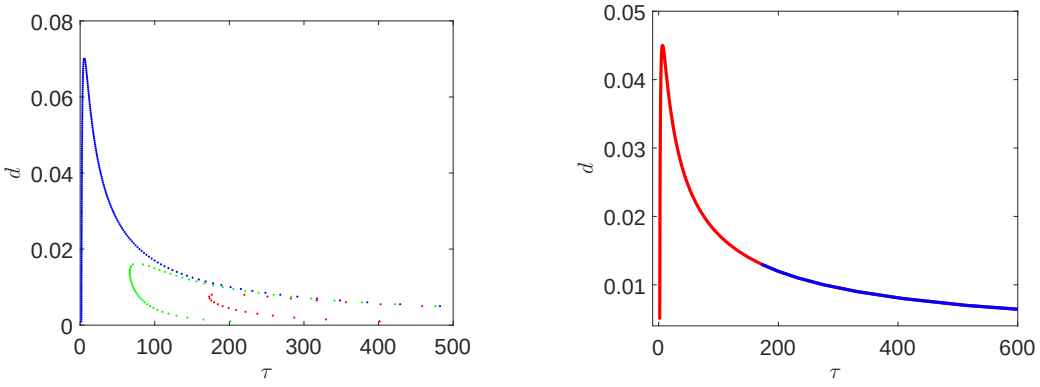

(a) (b)

Figure 2.5: Two parameter bifurcation diagram for system (2.5) with $Y = 0.6$. Figure (a): discrete delay. Blue - two Hopf bifurcations through which switches in stability of E_+ occurs. Outside of the blue region E_+ is locally asymptotically stable. Green denotes Hopf bifurcations that are located in between the previous pair of bifurcations, red denotes the innermost set of Hopf bifurcations. All bifurcations are supercritical. Figure (b): gamma distribution of order $p = 1$. Red denotes supercritical Hopf bifurcation, blue denotes subcritical Hopf bifurcation. Outside of the red-blue curve E_+ is locally asymptotically stable.

As d decreases, new pairs of Hopf bifurcations appear such that the corresponding

pairs of complex eigenvalues cross the axis to the left in the reverse order of their crossing it to the right. We refer to periodic solution curves connecting any pair of two Hopf bifurcations as "bubbles".

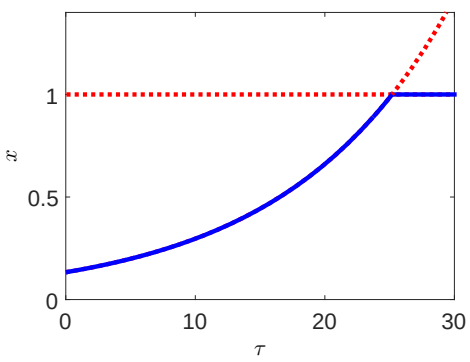

(a) $d = 0.08$

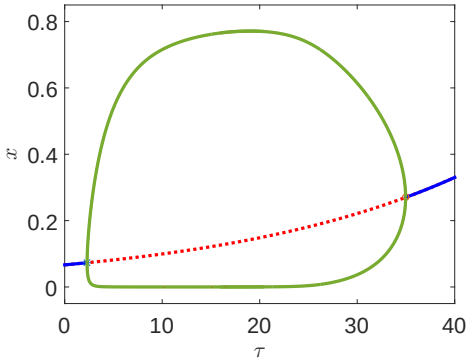

(b) $d = 0.04$

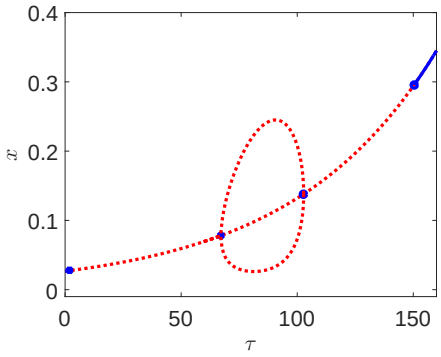

(c) d=0.016

Figure 2.6: Bifurcation diagrams showing the difference in the number of Hopf bifurcations at E_+ for various values of d in system (2.5) with discrete delay, $Y = 0.6$. Figure (a): E_+ is locally asymptotically stable when it exists. Figure (b): E_+ loses its stability at the first Hopf bifurcation at $\tau_1 = 2.299$ and restabilizes at the second Hopf bifurcation at $\tau_2 = 34.96$. Figure (c): nested periodic "bubbles" occur, that are consistent with Figure 2.5a. When $d = 0.016$, E_+ undergoes four Hopf bifurcations as τ increases from 0. First the real parts of a pair of complex eigenvalues change from negative to positive and therefore, E_+ loses stability. Next, at the second bifurcation, the real parts of another pair of complex roots change from negative to positive and then cross back at the third bifurcation. Finally, E_+ regains stability.

Now consider the dynamics in the system with the gamma distribution of order $p = 1$. If $0.045 < d < Y$, E_+ is locally asymptotically stable while it exists (Figure 2.7a). At $d \approx 0.045$ two supercritical Hopf bifurcations appear. An example of such dynamics is depicted at Figure 2.7b. Equilibrium E_+ is stable at $\tau = 0$ and remains so until $\tau \approx 2.12$ when E_+ goes through the first Hopf bifurcation and a pair of complex eigenvalues crosses the imaginary axis, a stable periodic orbit appears. As τ increases to 75.43, E_+ goes through the second Hopf bifurcation, where the pair of complex eigenvalues crosses the imaginary axis back, a stable periodic orbit disappears and E_+ restabilizes again.

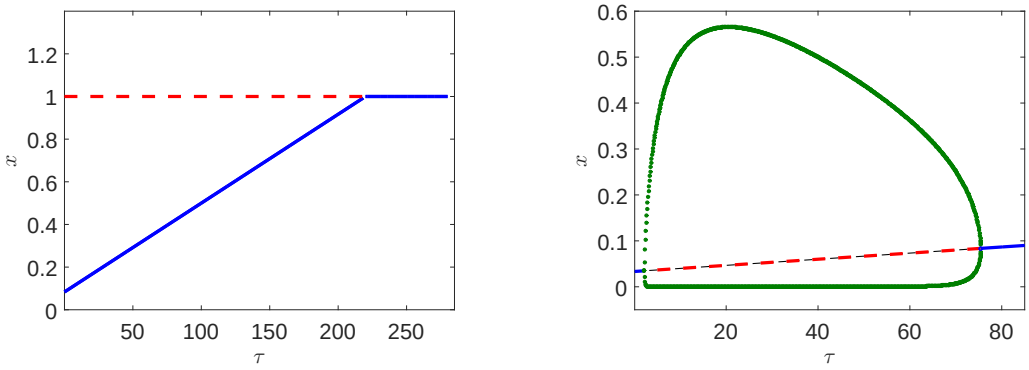

(a) $d = 0.05$ (b) $d = 0.02$

Figure 2.7: Bifurcation diagrams showing the change in bifurcation dynamics as d decreases for system (2.5) with gamma distribution of order $p = 1$ used as the delay kernel and $Y = 0.6$. Figure (a): E_+ is stable while it exists. Figure (b): equilibrium E_+ loses stability through the first Hopf bifurcation at $\tau_1 = 2.12$ and restabilizes as τ passes the second Hopf bifurcation point at $\tau_2 = 75.43$.

The numerical simulations in both "weak" kernel distributed delay system and the discrete delay system suggest that as d decreases the region of instability of E_+ as well as the maximal amplitude of stable periodic solution increase (Figure 2.8).

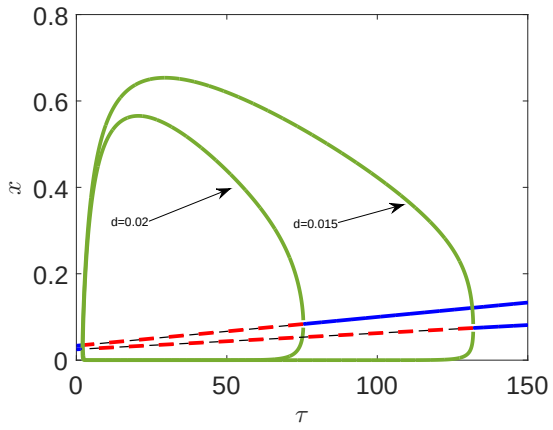

Figure 2.8: Bifurcation diagram for system (2.5) with the gamma distribution of order $p = 1$ used as the delay kernel and $Y = 0.6$. A decrease in d causes an increase in the region of instability of E_+.

Figure 2.5 captures another difference in the local bifurcation dynamics for the two distributions: change of criticality of Hopf bifurcations as d decreases. In the system with the discrete delay we used built-in first Lyapunov coefficient calculator in DDE-BIFTOOL package to asses the criticality of the two outer Hopf bifurcations. For the values of d that we considered, both Hopf bifurcations remain supercritical. For the system with gamma distribution we used a method described by Kuznetsov [33] to calculate the Lyapunov first coefficient for each point on Figure 2.5b (a description of the method and the MATLAB script can be found in Appendix A).

As d decreases to 0.013, the second Hopf bifurcation changes from supercritical to subcritical and the saddle node of limit cycles bifurcation appears. Therefore, the second Hopf bifurcation undergoes a Bautin bifurcation, a two-parameter bifurcation in which criticality of a Hopf bifurcation is changed (indicated by the sign of the first Lyapunov coefficient). An example of such dynamics for $d = 0.01$ can be observed on Figure 2.9. As τ decreases to 275.9, two complex eigenvalues cross the axis and a subcritical Hopf bifurcation takes place. As a result, an unstable periodic orbit is

born. As τ increases, the orbit undergoes a saddle node of limit cycles bifurcation at $\tau = 279.2$ where it collides with stable periodic solution and both cease to exist. For the range of $\tau = 275.9 - 279.2$, the system experiences bi-stability: solutions can be attracted to either E_+ or stable periodic orbit around it, depending on the initial data (Figure 2.9). There is an unstable periodic orbit separating the two attractors.

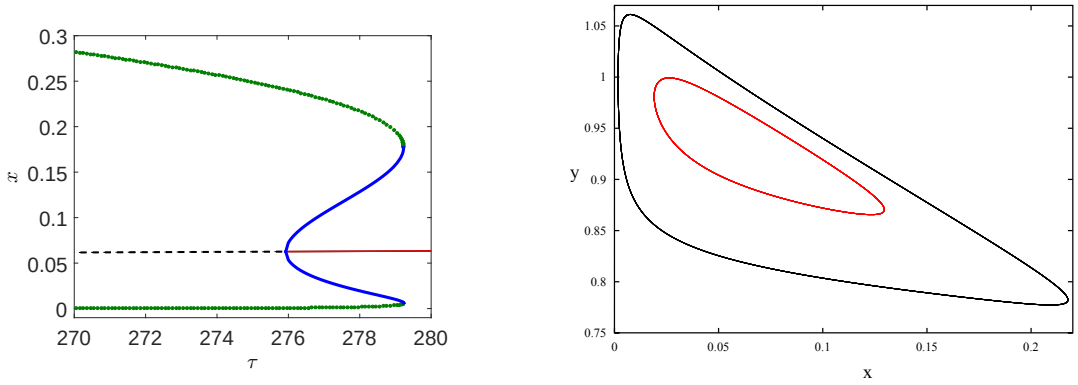

(a) (b)

Figure 2.9: System (2.5) using the gamma distribution of order $p = 1$ as the delay kernel with $Y = 0.6$ and $d = 0.01$. Figure (a): bifurcation diagram illustrating a subcritical Hopf bifurcation and a saddle node of limit cycles bifurcation. Figure (b): projection of two periodic orbits into phase space for $\tau = 278$. The outer one is asymptotically stable, while the inner one is unstable.

Next we address additional Hopf bifurcations that might involve E_+. Observe that Figure 2.5a indicates that as d decreases, additional pairs of Hopf bifurcations appear in the bifurcation diagram for system (2.5) with the discrete delay. The figure shows three such pairs, but results of Fan and Wolkowicz [4] suggest that there could be infinitely many of them. Notice that as d changes the bifurcations do not change their placement relative to other pairs of Hopf bifurcations.

On the other hand, there are no secondary Hopf bifurcations in the system with gamma distribution of order $p = 1$. This is the consequence of $k(a)$ being polynomial

of order 3 with at least one negative root.

Results of Fan and Wolkowicz [4] indicate that the bifurcation dynamics at E_+ for system (2.5) with discrete delay are very rich. There is a number of bifurcations that stable periodic solution undergoes as τ changes, provided d is sufficiently small (Figure 2.10). However, in the case of gamma distribution with $p = 1$, the previously described bifurcations are the only ones observed. This is in contrast to the dynamics exhibited by the discrete delay system (the periodic solution that arises through the first Hopf bifurcation undergoes a pair of saddle node of limit cycles bifurcations, followed by the cascade of period doubling bifurcations). Moreover, from [4] it follows that the dynamics becomes richer as d decreases.

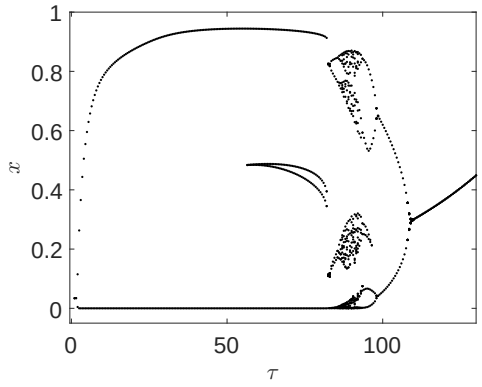

Figure 2.10: Orbit diagram of system (2.5) with discrete delay, $Y = 0.6$, and $d = 0.02$ illustrating bifurcation dynamics at E_+.

This concludes the exploration of dynamics of system (2.5) with the gamma distribution of order $p = 1$ used as the delay kernel. Next, we consider the change in local dynamics at E_+ for the general gamma distribution with various values of p, all other parameters being the same.

While we have not conducted the theoretical analysis of the stability of E_+ for order of gamma distributions higher than $p = 2$ analytically, there are several things that are

anticipated. Note that for a given gamma distribution of order p, the corresponding characteristic equation is $p+2$-order polynomial and therefore no more then $floor((p+2)/2)$ pairs of eigenvalues can move across imaginary axis and therefore, we expect no more than $floor((p+2)/2)$ nested periodic solutions to occur. Moreover, for the distributions with $p = 2$ and $p = 3$, the critical values of a_c where the characteristic equation has pure imaginary roots are roots of polynomial $k_p(a)$. The product of signs of $\frac{\partial Re(\lambda)}{\partial a}\big|_{a=a_c}$ at adjacent values of a_c will be less than 0, which implies if there are several "bubbles", they appear in sequence.

We investigate how the instability region of E_+ changes as the order of the distribution increases and whether any bifurcations of periodic solutions manifest themselves.

We start from the local bifurcations at E_+. We used numerical bifurcation analysis to study the local dynamics at E_+ for $p = 2, 4, 8$. We start by fixing the values of parameters $Y = 0.6$ and $d = 0.02$ and producing bifurcation diagrams. Following that, we compare the bifurcation diagrams for the values $d = 0.02$ and $d = 0.015$ to observe the effect of diminishing d on the dynamics across various kernels. In each case, for the parameter values chosen we observed that, similar to "weak" kernel dynamics, E_+ undergoes two supercritical Hopf bifurcations as τ increases from zero, before ultimately losing the stability in transcritical bifurcation (Figure 2.11a). From Figures 2.11a and Figure 2.11b it is evident that our observation for the case of $p = 1$ extends to the larger p - as d decreases region of instability of E_+ increases with respect to τ. Finally, it appears that the region of instability of E_+ has a limiting set as $p \to \infty$ (Figure 2.12a) and that limiting set is the region of instability in the system with the discrete delay (Figure 2.12b).

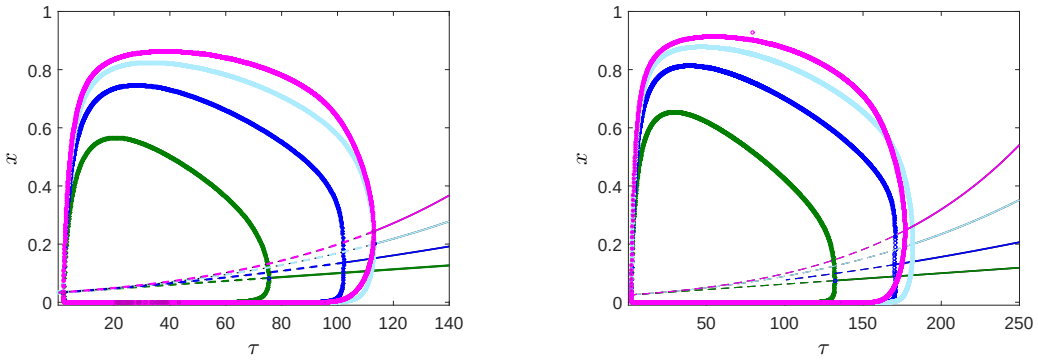

(a) $d = 0.02$ (b) $d = 0.015$

Figure 2.11: Bifurcation diagrams for system (2.5) with gamma distribution of the delay kernel and $Y = 0.6$ showing the change in local dynamics at E_+ as p increases and d decreases. Green - $p = 1$, blue - $p = 2$, cyan - $p = 4$, magenta - $p = 8$. As p increases the region of instability of E_+ appears to approach a limiting set. As the value of d decreases the region of instability of E_+ increases.

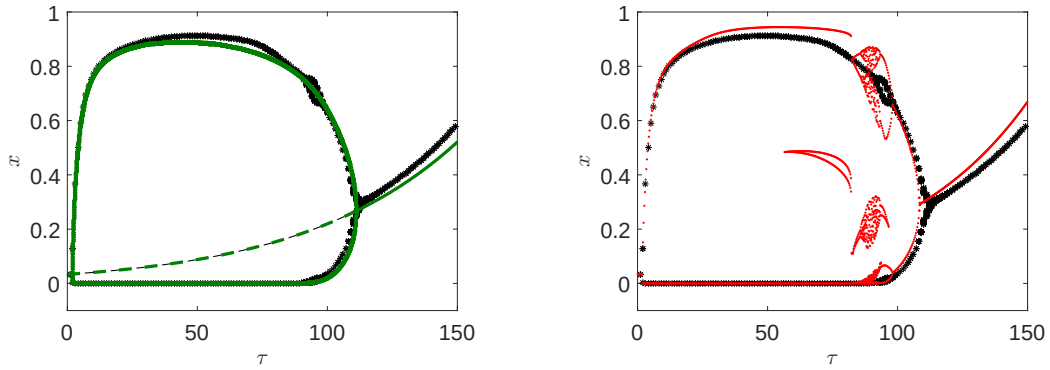

(a) (b)

Figure 2.12: Orbit diagrams for system (2.5) with $Y = 0.6$, $d = 0.02$ showing that as p increases the region of instability in the system with gamma distribution approaches that of the system with the discrete delay. Figure(a): gamma distribution. Green - $p = 16$, black - $p = 32$. Figure (b): black - gamma distribution with $p = 32$, red - discrete delay.

Using a process similar to that described for the system with the gamma distribution of order $p = 2$, we used the expression (2.43) that gives the condition on parameter space in order for E_+ to undergo Hopf bifurcations and constructed two-parameter bifurcation diagram in $d - \tau$ space (provided fixed $Y = 0.6$). Its shape is similar to that of calculated for system (2.5) with $p = 1$ and the discrete delay. We hypothesize that the region of stability of E_+ in terms of $d - \tau$ space (provided fixed Y) looks similar for all p (Figure 2.13).

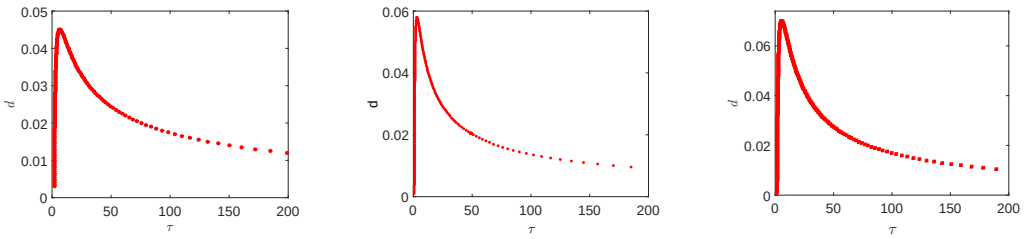

(a) $p = 1$ (b) $p = 2$ (c) Discrete delay

Figure 2.13: Two-parameter bifurcation diagrams for system (2.5) with $Y = 0.6$ depicting Hopf bifurcations that facilitate stability switches of E_+. Figure (a) and Figure (b): gamma distribution used as the delay kernel. Figure (c): discrete delay. The shape of the boundary of instability region of E_+ is similar between the three distributions.

Next we investigate the saddle node of limit cycles bifurcation associated with subcritical Hopf bifurcation. From our numerical simulations it is evident that for sufficiently small d, it also appears for the system with $p = 2$ as demonstrated in the Figure 2.15.

The question at hand is whether the Bautin bifurcation is preserved for the higher order gamma distribution. To address this, we calculated two parameter following of the two outer Hopf bifurcations in $d - \tau$ space for the gamma kernel distributions of order $p = 2, 3$. To do that we used the method described earlier. Subsequently, for each point on these curves we calculated the first Lyapunov coefficient, using the method mentioned earlier. The code underlying the calculations is similar to the code for the case $p = 1$ in Appendix A. The results are shown on the Figure 2.14.

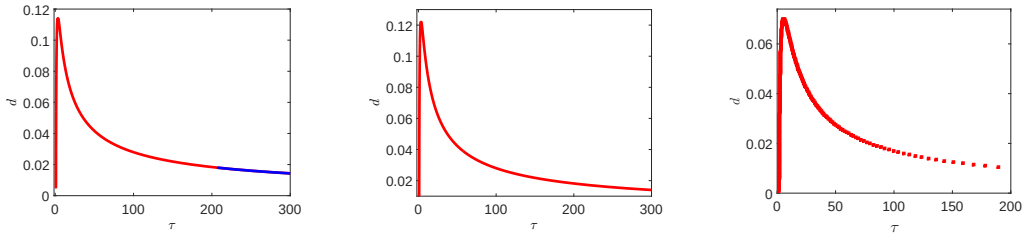

(a) $p = 2$ (b) $p = 3$ (c) Discrete delay

Figure 2.14: Two-parameter bifurcation diagram for system (2.5) with $Y = 0.6$ depicting Hopf bifurcations that facilitate stability switches of E_+. Red - supercritical Hopf bifurcation, blue - subcritical Hopf bifurcation. Figure (a) and Figure (b): gamma distribution, Figure (c): discrete delay. For the higher order gamma distributions a Bautin bifurcation does not appear, which is similar to the discrete delay case.

Our results indicated that in the case of $p = 2$, a Bautin bifurcation takes place, i.e. the rightmost Hopf bifurcation changes from supercritical to subcritical. Also, note that in the case of $p = 2$, the Bautin bifurcation occurs at a higher value of d than in the $p = 1$ case. However, in the case of $p = 3$, for all values of d that we considered, the rightmost Hopf bifurcation remains supercritical. We hypothesize that the Bautin bifurcation disappears relatively quickly as p increases and is not preserved for the higher order gamma distribution systems.

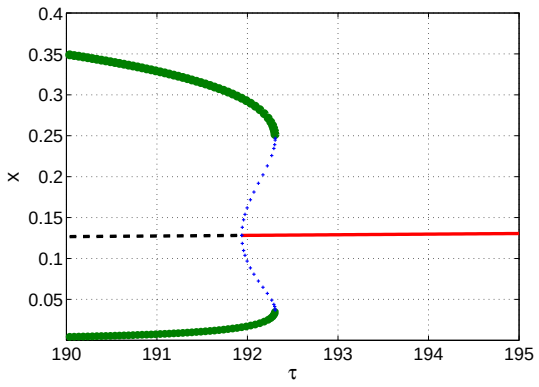

Figure 2.15: Bifurcation diagram for system (2.5) with gamma distribution of order $p = 2$ used as the delay kernel with $Y = 0.6$ and $d = 0.014$. As τ increases E_+ restabilizes via a subcritical Hopf bifurcation with an accompanying saddle node of limit cycles bifurcation.

Figure 2.12b shows that system (2.5) with the discrete delay has rich bifurcation dynamics as τ changes. Stable periodic solution around E_+ undergoes two saddle node of limit cycles bifurcations followed by the series of period doubling bifurcations.

In the numerical experiments we observed that for systems with the gamma distributed delay and p sufficiently large, stable periodic solution undergoes a pair of period doubling bifurcations as τ changes. We further stipulate that the bifurcation dynamics becomes even richer as the value of d is decreasing. In particular, a saddle node of limit cycles bifurcation appears prior to a period doubling bifurcations as τ increases (Figure 2.16).

To sum up, in the predator-prey model with the gamma distributed delay it is always possible to select a pair $(Y, d(Y))$ such that the coexistence equilibrium undergoes two Hopf bifurcations. This is a feature shared with the discrete delay system. For the lower order distributions, a rich dynamics present in the discrete delay model does not manifest itself. However, for the higher order of the gamma distribution richer

dynamics emerge, such as a cascade of period doubling bifurcations and two saddle node of limit cycles bifurcations. Decreasing magnitude of d has similar effect for the higher values of p. Finally, for the lower order of gamma distribution there appears Bautin bifurcation in which rightmost Hopf bifurcation changes from supercritical to subcritical and the periodic solution born at that Hopf bifurcation changes from stable to unstable. This bifurcation disappears for the higher order of distributions and is not observed in the discrete delay system.

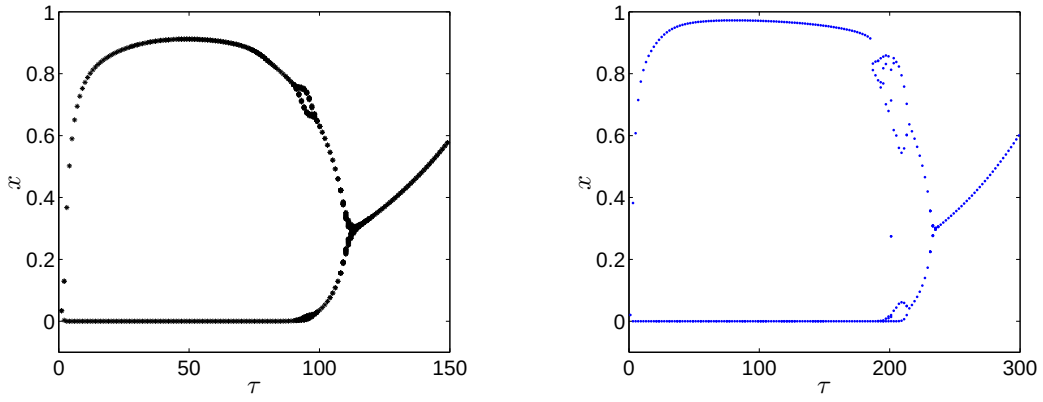

(a) $d = 0.02$ (b) $d = 0.012$

Figure 2.16: Bifurcation diagrams for system (2.5) with the gamma distribution of order $p = 32$ used as the delay kernel and $Y = 0.6$. Figure (a): stable periodic solution undergoes a pair of period doubling bifurcations. Figure (b): as d decreases, richer global bifurcation dynamics emerges: as τ increases stable periodic solution undergoes a pair of saddle node of limit cycles bifurcations, followed by a cascade of period doubling bifurcations.

Uniform distribution

In this section we consider system (2.5) with the uniform distribution used as the delay kernel. We define the kernel as follows:

$$g(s) = \begin{cases} \frac{\rho}{\tau}, & s \in [\tau(1-\frac{1}{2\rho}), \tau(1-\frac{1}{2\rho})],\ \rho > 0 \\ 0, & \text{otherwise .} \end{cases}$$

Examples of such distributions are depicted in Figure 2.17.

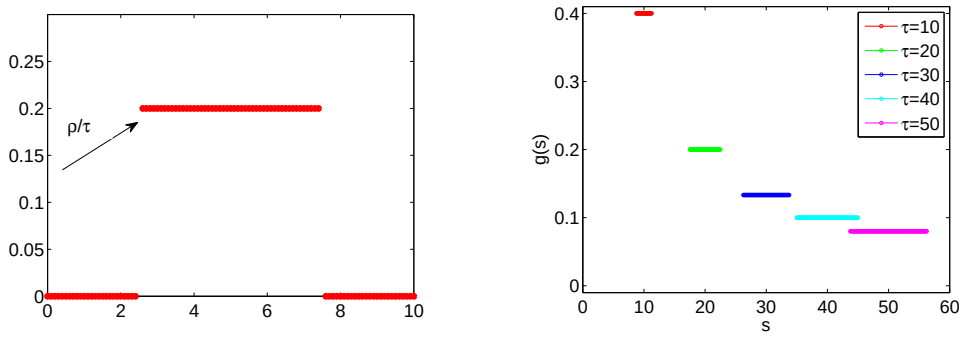

(a) $\rho = 1$, $\tau = 5$ (b) $\rho = 4$

Figure 2.17: Examples of uniform distribution kernels

The expression for the coexistence equilibrium is $E_+ = (x^*, y^*) = \left(\frac{d^2 \tau e^{d\tau}}{Y\rho\left(e^{\frac{d\tau}{2\rho}} - e^{-\frac{d\tau}{2\rho}}\right)}, 1 - \frac{d^2 \tau e^{d\tau}}{Y\rho\left(e^{\frac{d\tau}{2\rho}} - e^{-\frac{d\tau}{2\rho}}\right)} \right)$. While it is difficult to solve for the exact value of τ at which E_+ ceases to be biologically relevant, it is possible to see that such a value exists using the following argument. As $\tau \to 0+$, $E_+ \to (\frac{d}{Y}, 1 - \frac{d}{Y})$. On the other hand, as $\tau \to \infty$, the x-component of E_+ approaches ∞ and the y-component of E_+ becomes negative. Therefore, E_+ ceases to be in $int\mathbb{R}^2_+$.

In order to obtain the characteristic equation corresponding to the linearization of system (2.5) at the coexistence equilibrium, we applied the linear chain trick to the system. Define:

$$I(t) = \int_0^\infty x(t-s)y(t-s)e^{-ds}g(s)\,\mathrm{d}s\ .$$

Differentiate $I(t)$ with respect to t and apply integration by parts to obtain

$$\begin{aligned}\frac{\mathrm{d}I(t)}{\mathrm{d}t} &= -\int_0^\infty \frac{\partial}{\partial s}\left[x(t-s)y(t-s)\right]e^{-ds}g(s)\,\mathrm{d}s \\ &= \frac{\rho}{\tau}\left(e^{-d\tau_1}x(t-\tau_1)y(t-\tau_1) - e^{-d\tau_2}x(t-\tau_2)y(t-\tau_2)\right) - dI(t)\ ,\end{aligned}$$

where

$$\tau_1 = \tau\left(1-\frac{1}{2\rho}\right)\ ,$$
$$\tau_2 = \tau\left(1+\frac{1}{2\rho}\right)\ .$$

System (2.5) with the uniform distribution used as the delay kernel becomes

$$\dot{x}(t) = x(t)(1-x(t)) - x(t)y(t)\ , \tag{2.45a}$$
$$\dot{y}(t) = -dy(t) + YI(t)\ , \tag{2.45b}$$
$$\dot{I}(t) = \frac{\rho}{\tau}\left(e^{-d\tau_1}x(t-\tau_1)y(t-\tau_1) - e^{-d\tau_2}x(t-\tau_2)y(t-\tau_2)\right) - dI(t)\ . \tag{2.45c}$$

where the initial data for (x,y), $\phi = (\phi_1, \phi_2)$ is in the Banach space of bounded continuous functions mapping $[-\tau_2, 0]$ into $\mathbb{R}^2_+$, equipped with the uniform norm and $I(0) \in \mathbb{R}$, $I(0) \geq 0$. Note that for the complete correspondence to system (2.5), $I(0) = \int_0^\infty \phi_1(s)\phi_2(s)e^{-ds}g(s)\,\mathrm{d}s$ should hold.

The characteristic equation for the linearization of system (2.45) at E_+ is the following transcendental equation:

$$\lambda^2 + (d+x^*)\lambda + dx^* + (1-2x^*-\lambda)\frac{d^2e^{-\lambda\tau}\left(e^{\frac{(d+\lambda)\tau}{2\rho}} - e^{-\frac{(d+\lambda)\tau}{2\rho}}\right)}{(\lambda+d)\left(e^{\frac{d\tau}{2\rho}} - e^{-\frac{d\tau}{2\rho}}\right)} = 0\ .$$

The equation has three transcendental terms that are positive simultaneously. This makes theoretical analysis difficult. Instead, we use DDEBIF-TOOL and XPPAUT to produce bifurcation diagrams and orbit diagrams.

We start from the local dynamics at E_+. Consider the bifurcation diagram in Figure 2.18. It captures two outer Hopf bifurcations at τ_1 and τ_2, such that outside of (τ_1, τ_2), E_+ is stable when it exists. The basic dynamics for the system with the uniformly distributed delay is similar to the dynamics previously observed in the system with the discrete delay and gamma distribution with $p = 1$ and $p = 2$. If $0.07456 < d < Y$, E_+ is stable when exists (Figure 2.19); when $d < 0.07456$, E_+ undergoes two Hopf bifurcations as τ increases, losing stability at the first bifurcation and re-stabilizing at the second (Figure 2.19b).

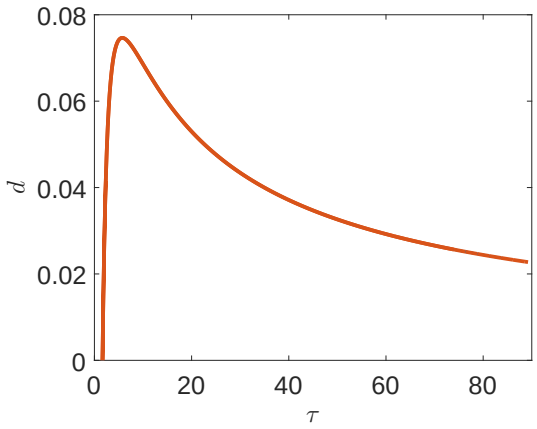

Figure 2.18: Part of a two-parameter bifurcation diagram for system (2.5) with the uniform distribution used as the delay kernel and $Y = 0.6$ and $\rho = 10$ following the supercritical Hopf bifurcations.

For each point on the curve depicted on the Figure 2.18 we calculated the Lyapunov first coefficient using built in DDE-BIFTOOL functionality. We learned that for the range of parameters that we considered both Hopf bifurcations remain supercritical.

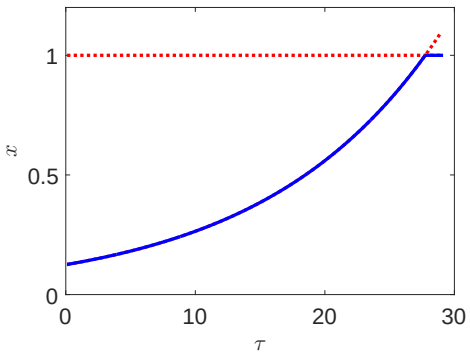

(a) $d = 0.075$

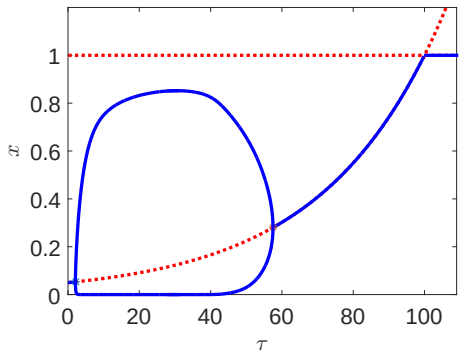

(b) $d = 0.03$

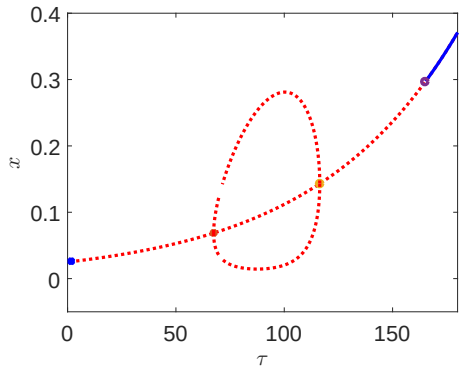

(c) $d = 0.015$

Figure 2.19: Bifurcation diagrams for system (2.5) with the uniform distribution used as the delay kernel, $\rho = 10$ and $Y = 0.6$. Figure (a): E_+ is locally asymptotically stable while it exists. Figure (b): equilibrium E_+ loses its stability at the first Hopf bifurcation $\tau_1 = 2.089$ and restabilizes at the second Hopf bifurcation at $\tau_2 = 57.46$. Figure (c): nested periodic "bubbles". As τ increases through the first bifurcation point, first pair of complex roots crosses the imaginary axis and therefore E_+ loses stability. As τ increases further through the second bifurcation point, a second pair of complex roots crosses the imaginary axis. At the third bifurcation the second pair of roots crosses back across the axis and at the fourth bifurcation the first pair of roots also crosses back and E_+ regains stability.

We observe that as d decreases the number of Hopf bifurcations at E_+ increases, the bifurcations appear in pairs and are nested (Figure 2.19c). We hypothesize that as d decreases new pairs of Hopf bifurcations emerge in the similar pattern.

We proceed now to investigate bifurcation dynamics of the stable periodic solution that connects the two outermost bifurcations. We fixed parameter values $d = 0.02$, $Y = 0.6$ and $\rho = 10$ and studied bifurcation dynamics using DDE-BIFTOOL. We learned that as τ decreases stable periodic solution undergoes a number of bifurcations (Figure 2.20). At $\tau_1 = 97.95$, a Floquet multiplier leaves unit circle at -1, the stable periodic solution loses its stability and new stable periodic solution emerges with twice the period of the first solution. As τ decreases to $\tau_2 = 93.17$, Floquet multiplier associated with new stable periodic solution map leaves the unit circle through -1, and the currently stable solution loses its stability and third stable periodic solution emerges with twice the period.

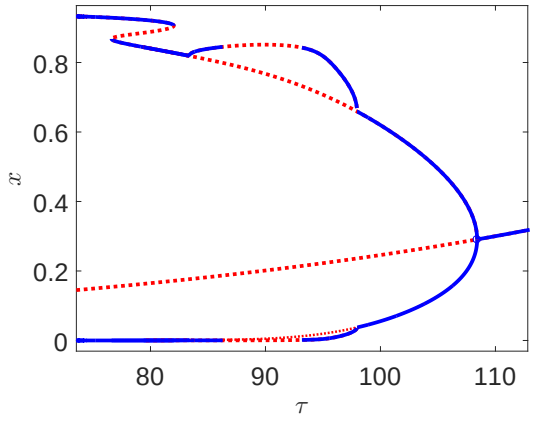

Figure 2.20: Bifurcation diagram for system (2.5) with the uniform distribution used as the delay kernel and $Y = 0.6$, $d = 0.02$, $\rho = 10$ that shows the change in the dynamics at the coexistence equilibrium as τ changes. As τ decreases past the rightmost Hopf bifurcation the stable periodic solution undergoes at least four period doubling bifurcations. Following that, as τ decreases, the stable periodic solution undergoes two saddle node of limit cycles bifurcations, and hence, the system exhibits bi-stability on the interval $\tau \approx 76.65 - 82.03$.

As τ decreases to $\tau_3 = 86.78$, a Floquet multiplier associated with the appearance of the third stable periodic solution enters the unit circle through -1, third stable periodic ceases to exists and second periodic solution is stable again. At $\tau = 83.28$ Floquet multiplier associated with the appearance of the second stable periodic solution re-enters the unit circle through -1 and the solution disappears and the first stable solution restabilizes again. As τ decreases to 76.63 a Floquet multiplier leaves unit circle through 1, saddle node of limit cycles bifurcation takes place and as the result the periodic solution loses the stability and switches the direction with respect to τ, and a stable periodic solution appears. Finally, as τ increases to 82.02 unstable and stable periodic solutions collide and disappear.

We observed that the periodic solution goes through four period doubling bifur-

cations and could not investigate further with DDE-BIFFTOOL due to numerical instability, but our further numerical experiments showed that there are more period doubling bifurcations. However, Figure 2.20 suggests, that if there are more than four period doubling bifurcations, Floquet multiplier associated with them re-enter unit circle in the reverse order of which they left it.

There are several aspects of note here. Recall that the occurrence of both the pair of saddle node of limit cycle bifurcations and period doubling bifurcations are subject to d being sufficiently small. This is a feature shared with the discrete delay system and higher order gamma distribution system.

To get a fuller picture in the region of period doubling we fixed $Y = 0.6$, $d = 0.02$ and $\rho = 10$ and produced orbit diagram for the uniform distributed delay model (Figure 2.21a and Figure 2.21b). We then compare it to the similar diagram for the system with discrete delay (Figure 2.21c and Figure 2.21d).

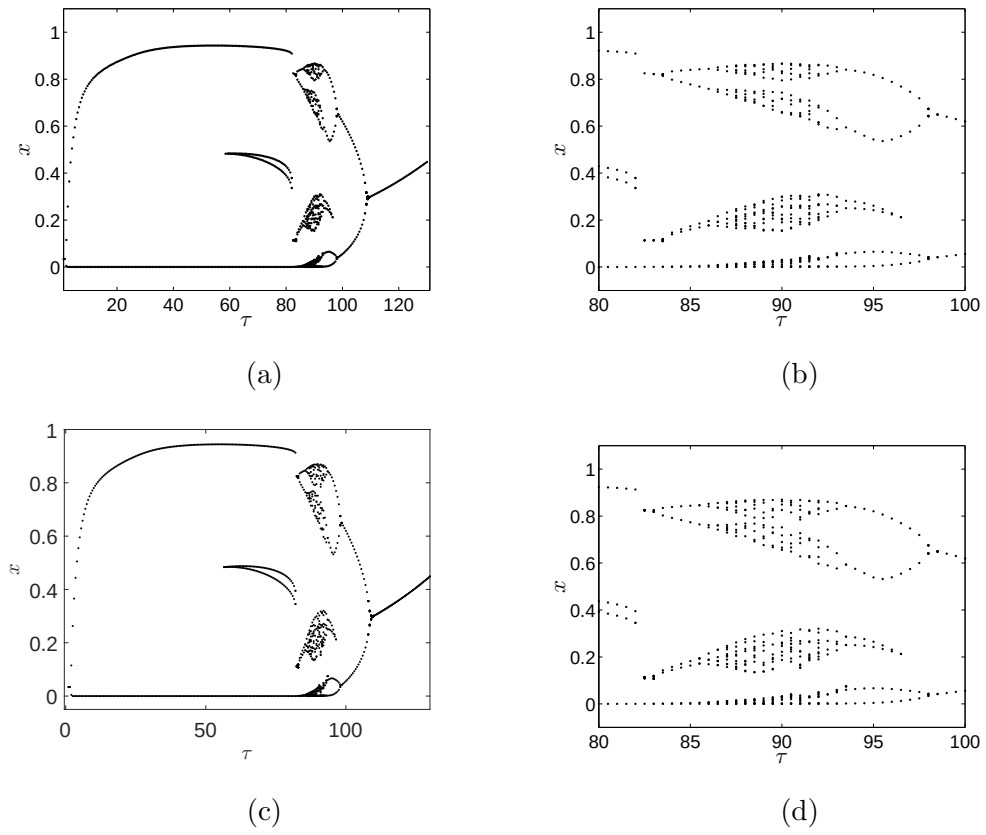

Figure 2.21: Orbit diagrams for system (2.5) with $Y = 0.6$, $d = 0.02$ showing the similarities between the systems' dynamics. Figure (a) and (b): uniform distribution of the delay kernel with $\rho = 10$. Figure (c) and (d): discrete delay.

We notice that the bifurcation dynamic is similar for the two systems: there are two saddle node of limit cycle bifurcations, followed by the cascade of period doubling bifurcations as τ increases.

To investigate whether any new bifurcations emerge as d decreases further in the system with the uniform distribution, we fixed $Y = 0.6$ and $d = 0.012$ and created an orbit diagram (Figure 2.22). We detected another set of period doubling bifurcation preceding the first set (as τ increases).

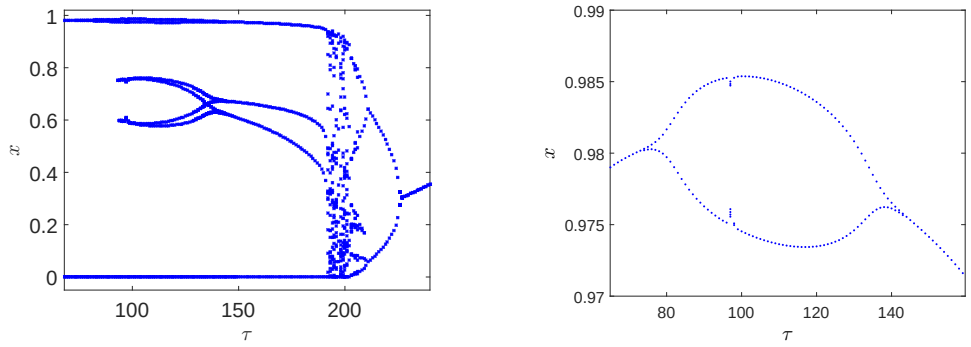

(a) (b)

Figure 2.22: Orbit diagrams for system (2.5) with the uniform distribution used as the delay kernel and $Y = 0.6$, $d = 0.012$ and $\rho = 10$. Figure (a): complete diagram. Figure (b): magnified fragment of the diagram showing a new set of period doubling bifurcations.

As τ increases past $\tau = 74$, a Floquet multiplier leaves the unit circle through -1, stable periodic solution loses its stability and a new stable solution with twice the period appears. As τ increases to 142, the Floquet multiplier moves inside the circle through -1, stable periodic solution disappears and initial periodic solution restabilizes. An example of the dynamic can be observe on the Figure 2.23.

We also noticed that the pair of saddle node of limit cycle bifurcations moved inside the period doubling cascade, as well as there appears now to be a chaotic attractor. We hypothesize that as d decreases it passes a threshold value where a chaotic attractor is born. We reduced the value of d to 0.009 and produced orbit diagram of the chaotic attractor region (Figure 2.24).

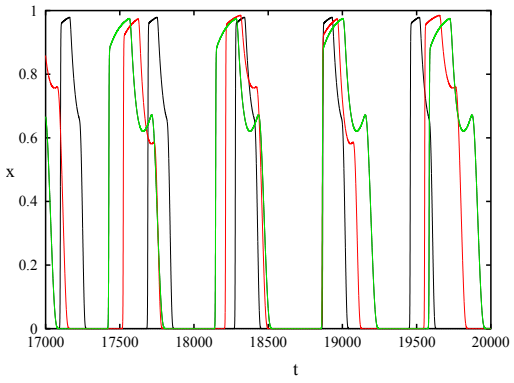

(a) Time trajectory

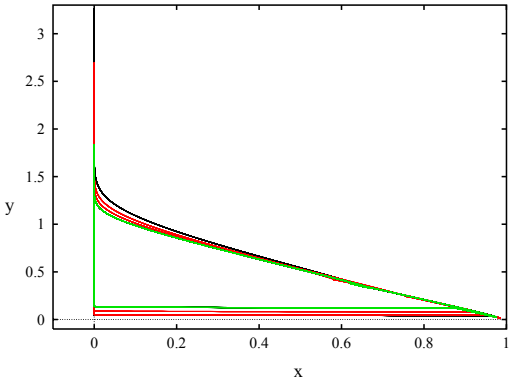

(b) Phase portrait

Figure 2.23: System (2.5) with the uniform distribution used as the delay kernel and $Y = 0.6$, $d = 0.012$, $\rho = 10$. Black corresponds to $\tau = 65$, red corresponds to $\tau = 105$, green corresponds to $\tau = 145$. As τ increases, the stable periodic solution loses stability and a new stable periodic solution with twice the period appears. As τ increases further, the stable periodic solution disappears and the initial periodic solution restabilizes.

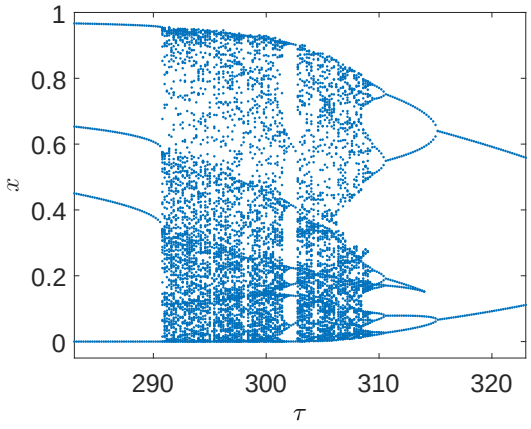

Figure 2.24: A fragment of the orbit diagram for system (2.5) with the uniform distribution used as the delay kernel and $Y = 0.6$, $d = 0.009$ and $\rho = 10$ showing a chaotic attractor.

Note that the chaotic attractor region in the orbit diagram stops suddenly as τ decreases. We hypothesize that there is an interval of values of τ such that there is a bi-stability in the system between the limit cycle and a chaotic attractor. While we have not done this, one way to show our hypothesis is true is to take value of τ slightly smaller than where the chaotic attractor disappears and find initial data such that solutions will be attracted to the chaotic attractor.

The appearance of the second set of period doubling bifurcations was not previously observed in the system with the discrete delay. However, to obtain numerical bifurcation diagrams for the discrete delay model with low values of d is numerically challenging, since the linearization matrix becomes ill-conditioned. To overcome the numerical instability that appears when d becomes too small we have rescaled the predator-prey model with discrete delay. The original model is

$$\begin{aligned}\frac{\mathrm{d}x}{\mathrm{d}t} &= rx(t)\left(1-\frac{x(t)}{K}\right) - mx(t)y(t)\ ,\\ \frac{\mathrm{d}y}{\mathrm{d}t} &= -dy(t) + mYe^{-\tau}x(t-\tau)y(t-\tau)\ ,\end{aligned}$$

where the meaning of the parameters is the same as the one given at the beginning of the chapter. Set

$$\begin{aligned}\hat{t} = dt, \hat{x}(\hat{t}) = \frac{x(\hat{t})}{K},\ \hat{y}(\hat{t}) = my(t),\\ \hat{\tau} = d\tau\ , \hat{r} = \frac{r}{d}, \hat{Y} = \frac{mKY}{d}\ .\end{aligned}$$

After the substitution and dropping of $\hat{}$ we obtain the following system:

$$\frac{\mathrm{d}x}{\mathrm{d}t} = rx(t)(1-x(t)) - x(t)y(t)\ , \tag{2.48a}$$

$$\frac{\mathrm{d}y}{\mathrm{d}t} = -y(t) + Ye^{-\tau}x(t-\tau)y(t-\tau)\ . \tag{2.48b}$$

Consider the orbit diagram for the obtained system with parameter values $r = 20$ and $Y = 64$ on the Figure 2.25a.

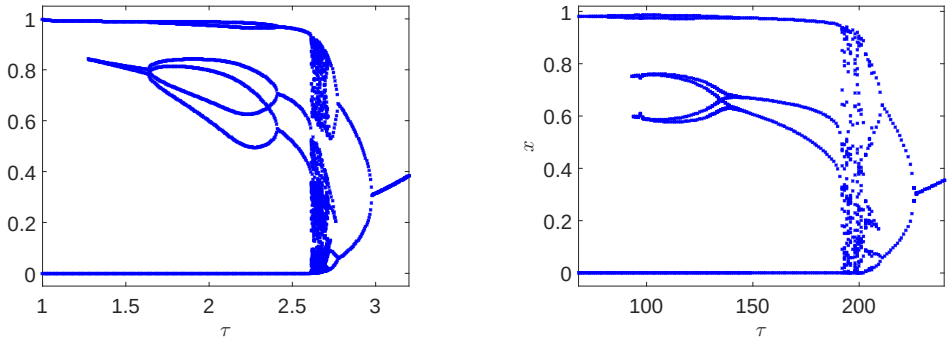

(a) (b)

Figure 2.25: Orbit diagram showing the second set of period doubling bifurcations. Figure (a): system (2.48) with $Y = 64$ and $r = 20$. Figure (b): system (2.5) with the uniform distribution of the delay kernel and $Y = 0.6$, $d = 0.012$.

Our results confirm that the discrete delay system can have a second set of period doubling bifurcations that precedes the saddle node of limit cycles bifurcations. Also, in the orbit diagram of the rescaled discrete delay system, a chaotic attractor is indicated, which is similar to what we observed in the uniform distribution system.

We compare chaotic attractors in the discrete delay model and the uniform distribution model (Figure 2.26 and Figure 2.27). The appearance of the attractor in both of the models, not only depends on τ but also on the value of secondary parameter.

Finally, we compare the fragments of the orbit diagrams for system (2.5) with discrete delay and uniform distribution (Figure 2.27). We notice that the path to chaos is different for the two models as τ decreases. In the discrete delay system, the path to the attractor is a cascade of period doubling bifurcations. On the other hand, for the uniform distribution system, the system goes through three period doubling bifurcations and two saddle node of limit cycle bifurcations before period doubling bifurcations cascade commences, culminating in chaotic attractor. Observe that for the uniform distribution system we see that at least one pair of Floquet multipliers

that left unit circle via a period doubling bifurcation returned back inside via the following period doubling bifurcation, while in the discrete delay system, each period doubling bifurcation is accompanied by the multipliers leaving the unit circle.

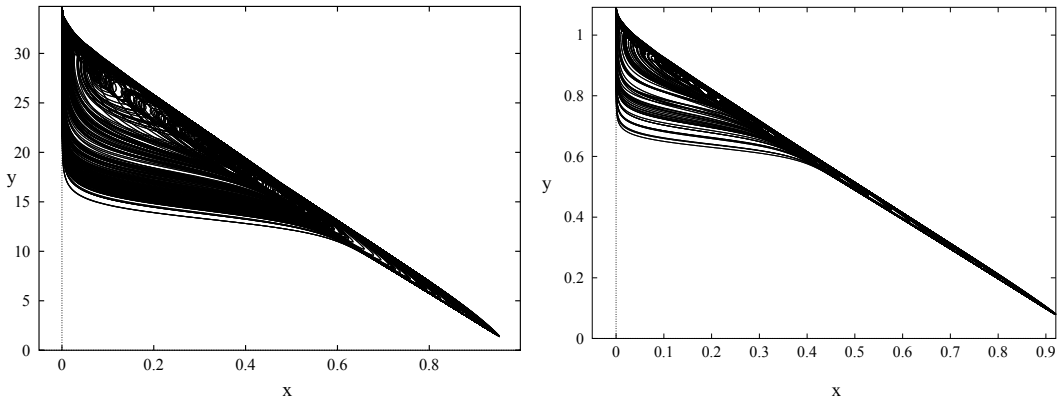

(a) (b)

Figure 2.26: Projection of solutions on the phase space showing a chaotic attractor. Figure (a): system (2.48) with $r = 30$, $Y = 64$ and $\tau = 2.6$. Figure (b): system (2.5) with the uniform distribution of the delay kernel and $d = 0.012$, $Y = 0.6$, $\rho = 10$ and $\tau = 198$.

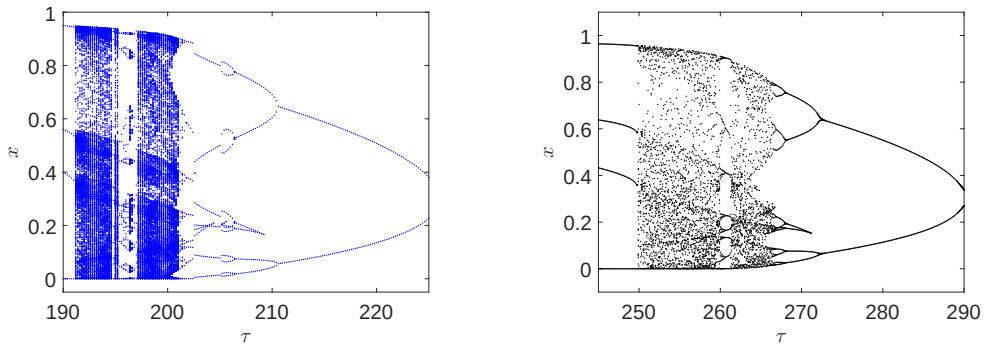

(a) (b)

Figure 2.27: A fragment of orbit diagram showing a chaotic attractor for system (2.5). Figure (a): uniform distribution of the kernel with $Y = 0.6$, $d = 0.012$ and $\rho = 10$. Figure (b): discrete delay with $Y = 0.6$ and $d = 0.012$. The path to chaotic attractor as τ decreases are different depending on the delay distribution.

2.7 Conclusion

Fan and Wolkowicz in their work [4] considered the predator-prey model with the discrete delay. They conclusively proved that there exists a parameter set so that two stability switches for E_+ equilibrium happen in the biologically realistic state space as τ increases from zero. In this section we considered Gause-type predator-prey model with distributed delay. We discovered, that in the absence of E_+, the dynamics of the system are similar to these of the discrete delay model and ordinary differential equations model.

For a general delay distribution, we described the set of initial data such that all components of the solutions with such data eventually become positive and remain positive. Using Rouché's Theorem we calculated the conservative approximation to the region of stability of the coexistence equilibrium. We also showed that the mechanism

through which E_+ loses the stability, as mean delay changes, is a Hopf bifurcation.

While it is difficult to study stability switches for the general delay, we showed analytically that in the case of "weak" kernel distribution there exists a set of parameters so that the coexistence equilibrium undergoes two Hopf bifurcations as τ increases from zero. Our numerical simulations suggest that this is also the case for the higher order gamma distributions.

Gamma distribution systems of lower order did not replicate the rich bifurcation dynamics observed in the discrete delay systems for the range of parameters that we considered. However, once the distribution order becomes high enough ($p = 32$), we observed that the stable periodic solution goes through a pair of period doubling bifurcations, which is something that was observed in the discrete delay model. Moreover, when d is low enough, we also witnessed a pair of saddle node of limit cycle bifurcations as τ changes. Our hypothesis is that if the order of the distribution is high enough, it is possible to select d low enough so that a pair of saddle node of limit cycle bifurcations occur.

On the other hand, gamma distribution delay systems dynamics offers a number of differences from the dynamics of the discrete delay. Due to the fact that the characteristic equations for the gamma distribution are polynomial, there is a finite number of periodic solution "bubbles" around E_+ that might appear as the result of decrease of d. Also, for the lower order gamma distributions we observed that the rightmost Hopf bifurcation changes from supercritical to subcritical if d is sufficiently low. The Bautin bifurcation disappears for the higher order distributions and is not observed in the discrete delay system.

We analyzed the dynamics of the predator-prey model with the uniform distribution numerically. Our bifurcation analysis showed that the dynamics is closer to the discrete delay model dynamics than to the dynamics of the gamma distribution sys-

tem. Having fixed Y it is possible to select values of d such that either E_+ is locally asymptotically stable for all τ, or undergoes only two Hopf bifurcations, or has several nested "bubbles", as τ changes. Also, it is possible to select d sufficiently low so that a stable periodic solution undergoes a series of period doubling bifurcations and a pair of saddle node bifurcations. All the bifurcation dynamics observed in the system with the discrete delay were present in the system with the uniform delay distribution including the order of their appearance with respect to τ.

We also discovered that as d becomes sufficiently low a second set of period doubling bifurcations appears as τ increases from the leftmost Hopf bifurcation, something that was not previously noted in the discrete delay system. Since in the predator-prey model with the discrete delay the linearization matrix becomes ill-conditioned when the value of d becomes too low, we rescaled the original model as to scale death rate to 1. The orbit diagrams with parameter values $Y = 64$ and $r = 20$ for the resulting system showed that the second set of the period doubling bifurcations, prior to the cascade of period doubling bifurcations is also present in the discrete delay system (we used r as a secondary parameter). We noticed that while in the discrete delay model, the pair of saddle node of limit cycle bifurcations always precedes the period doubling cascade, in the uniform distribution, as d decreases the saddle node of limit cycle bifurcations moves to the right into the cascade.

Chapter 3

A predator-prey model with distributed delay in the chemostat

3.1 The model

Consider the predator-prey model in the chemostat:

$$\begin{aligned}
\frac{\mathrm{d}s}{\mathrm{d}t} &= \left(s^0 - s(t)\right) D_0 - \frac{f(s(t))x(t)}{\eta}\ , \\
\frac{\mathrm{d}x}{\mathrm{d}t} &= x(t)(-D + f(s(t))) - \frac{g(x(t))y(t)}{\xi}\ , \\
\frac{\mathrm{d}y}{\mathrm{d}t} &= -\Delta y(t) + \int_0^\infty g(x(t-u))y(t-u)e^{-\Delta u}h(u)\,\mathrm{d}u.
\end{aligned}$$

Here $s(t)$ denotes the concentration of nutrient in the growth chamber, $x(t)$ the density of the prey population and $y(t)$ the density of the predator population at time t. Function $h(s)$ is called the kernel of the delay distribution and has the following properties:

$$\int_0^\infty h(u)\,\mathrm{d}u = 1, \tag{3.2a}$$

$$\int_0^\infty uh(u)\,\mathrm{d}u = \tau, \tag{3.2b}$$

where τ is the mean delay between the capture of the prey to its conversion into viable predator biomass.

The functions $f(s(t)) = \alpha s(t)$ $(\alpha > 0)$ and $g(x(t)) = Kx(t)$ $(K > 0)$ denote the functional response of prey to the nutrient concentration and predator to prey density, respectively. We have selected both to be the Holling type I functional response, since in this case the corresponding ODE system always has a globally asymptotically stable equilibrium point (i.e. no stable periodic solution is possible). If after the introduction of the delay stable periodic solutions appear, it is the result of incorporating the delay.

The system reduces to

$$\frac{\mathrm{d}s}{\mathrm{d}t} = \left(s^0 - s(t)\right) D_0 - \frac{\alpha s(t) x(t)}{\eta} \,, \tag{3.3a}$$

$$\frac{\mathrm{d}x}{\mathrm{d}t} = x(t)(-D + \alpha s(t)) - \frac{K x(t) y(t)}{\xi} \,, \tag{3.3b}$$

$$\frac{\mathrm{d}y}{\mathrm{d}t} = -\Delta y(t) + K \int_0^\infty x(t-u) y(t-u) e^{-\Delta u} h(u) \,\mathrm{d}u. \tag{3.3c}$$

Here the positive constants s^0, D_0, η, ξ denote the concentration of the growth limiting nutrient in the feed vessel, the dilution rate, and the growth yield constants, respectively. The sum of the dilution rate D_0 and the natural species specific death rate of the prey is denoted D and of the predator population is denoted Δ, respectively.

Denote by BC^3, the Banach space of bounded continuous functions mapping $(-\infty, 0]$ into $\mathbb{R}^3$ equipped with the uniform norm. We consider initial data $\phi = (\phi_1, \phi_2, \phi_3) \in BC^3_+ = \{\phi \in BC^3 : \quad \phi_i(\theta) \geq 0,\, i = 1, 2, 3, \quad \theta \leq 0\}$. Define $intBC^3_+ = \{\phi \in BC^3 : \quad \phi_i(\theta) > 0,\, i = 1, 2, 3, \quad \theta \leq 0\}$. Denote the solutions of (3.3) with initial data $\phi \in BC^3_+$ at time t by $\pi(\phi, t)$. Later we will show that solutions with such initial data exist and are unique in forward time. From this point onward when saying positive solutions, we are referring to the solutions $\pi(\phi, t)$ with initial data $\phi \in BC^3_+$. Later we will show that each component of $\pi(\phi, t)$ is non-negative for

all $t > 0$.

Before proceeding with the analysis of the model we non-dimensionalize it. We set

$$\hat{t} = D_0 t,\ \hat{s}(\hat{t}) = \frac{s(\hat{t})}{s^0},\ \hat{x}(\hat{t}) = \frac{x(\hat{t})\alpha}{D_0\eta},\ \hat{y}(\hat{t}) = \frac{Ky(\hat{t})}{\xi D_0},$$
$$\hat{u} = D_0 u\ , \hat{\alpha} = \frac{\alpha s^0}{D_0}, \hat{D} = \frac{D}{D_0},\ \hat{K} = \frac{K\eta}{\alpha},\ \hat{\Delta} = \frac{\Delta}{D_0}\ , \hat{h}(\hat{u}) = \frac{1}{D_0}h(\hat{u}/D_0).$$

After the substitution and dropping of $\hat{}$ the following system was obtained:

$$\begin{aligned}
\frac{\mathrm{d}s}{\mathrm{d}t} &= 1 - s(t) - s(t)x(t)\ , \\
\frac{\mathrm{d}x}{\mathrm{d}t} &= x(t)(-D + \alpha s(t)) - x(t)y(t)\ , \\
\frac{\mathrm{d}y}{\mathrm{d}t} &= -\Delta y(t) + K\int_0^\infty x(t-u)y(t-u)e^{-\Delta u}h(u)\,\mathrm{d}u.
\end{aligned}$$

In the interest of convenience we will further simplify this system by setting $\Delta = D = 1$ to obtain

$$\frac{\mathrm{d}s}{\mathrm{d}t} = 1 - s(t) - s(t)x(t)\ , \tag{3.6a}$$
$$\frac{\mathrm{d}x}{\mathrm{d}t} = x(t)(-1 + \alpha s(t)) - x(t)y(t)\ , \tag{3.6b}$$
$$\frac{\mathrm{d}y}{\mathrm{d}t} = -y(t) + K\int_0^\infty x(t-u)y(t-u)e^{-u}h(u)\,\mathrm{d}u. \tag{3.6c}$$

The remaining three parameters are α, K, and the distribution $h(u)$. We will carry out theoretical analysis for system (3.6), which, without loss to generality, can be applied to system (3.3).

3.2 Well-posedness and basic properties of the model

Define $L > 0$ and assume that $h(u) = 0$ for all $s \in (L, \infty)$. We allow $L = \infty$.

Theorem 3.2.1. *Solutions of (3.6) with initial data in BC^3_+ exist on $[0, \infty)$ and are unique, and remain in BC^3_+ for all $t > 0$. Moreover, $s(t) > 0$ for all $t > 0$.*

Proof. From the general theory of integro-differential equations [27], it follows that for each function $\phi \in BC^3_+$, there exists a unique solution of (3.6), $\pi(\phi, t)$, such that $\pi(\phi, \cdot)\big|_{(-\infty,0]} = \phi(t)$.

Note that there exists $b > 0$ such that $s(t) > 0$, for all $t \in (0, b)$. Assume that there exists $\hat{t} > 0$ such that $s(\hat{t}) = 0$ and $s(t) > 0$, $t \in (0, \hat{t})$. This implies that $\dot{s}(\hat{t}) \leq 0$. However, by (3.6a), $\frac{\mathrm{d}s(\hat{t})}{\mathrm{d}t} = 1 > 0$, a contradiction. Therefore, $s(t) > 0$, $t \geq 0$. By equation (3.6b) $x(t) = x(0)e^{\int_0^t -1+\alpha s(u)-y(u)\,\mathrm{d}u} \geq 0$.

Finally, since $y(t) \geq 0$ on $[-L, 0]$, then $\dot{y}(t) \geq -dy(t)$ for all $0 \leq t \leq L$. And therefore by the Comparison Theorem in [38] $y \geq 0$ for all $-L \leq t \leq L$. Arguing inductively, $y(t) \geq 0$ on $[L(n-1), Ln]$ for all $n \in \mathbb{N}$, $n > 0$. Therefore, $y(t) \geq 0$ for all $t > 0$. □

Proposition 3.2.2. *Solutions of (3.6) with positive initial data will remain positive for all $t > 0$.*

Proof. By Theorem 3.2.1, it follows that $s(t) > 0$ for all $t \geq 0$. We prove that $x(t)$ and $y(t)$ are positive for all $t \geq 0$ by contradiction.

Assume that there exists $\hat{t} > 0$ such that $x(\hat{t}) = 0$ and $x(t) > 0$ for all $t \in [0, \hat{t})$. Therefore $x'(\hat{t}) \leq 0$. Divide (3.6b) by $x(t)$ to obtain

$$\frac{\dot{x}(t)}{x(t)} = -1 + \alpha s - y \ , \ t \in [0, \hat{t}).$$

Integrating from 0 to $\hat{t}$, we obtain $x(\hat{t}) = x(0)e^{\int_0^{\hat{t}} -1+\alpha s-y\,\mathrm{d}t} > 0$. We arrive at a contradiction. Therefore, $x(t) > 0$, for all $t \geq 0$.

Assume that $y(t)$ becomes 0 for the first time at some time $\hat{t} > 0$. Therefore, $y'(\hat{t}) \leq 0$. By (3.6c) $y'(\hat{t}) = K\int_0^\infty x(t-u)y(t-u)e^{-u}h(u)\,\mathrm{d}u > 0$. We arrive at a contradiction. □

Lemma 3.2.3. *Solutions of (3.6) with initial data in BC^3_+ are bounded and* $\limsup_{t\to\infty} s(t) \leq 1$, $\limsup_{t\to\infty} x(t) \leq \alpha$ *and* $\limsup_{t\to\infty} y(t) \leq \alpha K \int_0^\infty e^{-u} h(u)\,\mathrm{d}u$.

Proof. Note that $\dot{s}(t) \leq 1 - s(t)$. For each solution $z(t)$ of $\dot{z}(t) = 1 - z(t)$, given any $\epsilon > 0$, there exists $T > 0$ such that $z(t) < 1 + \epsilon$, for all $t > T$. Using the Comparison theorem from [38] and the fact that $s(t)$ is non-negative for all t, it follows that $\limsup_{t\to\infty} s(t) \leq 1$.

Set $w(t) = \alpha s(t) + x(t)$. Differentiating $w(t)$ with respect to t we obtain

$$\dot{w} = \alpha - \alpha s - \alpha s x - x + \alpha s x - xy = \alpha - \alpha s - x - xy \ \leq \alpha - w.$$

For each solution $z(t)$ of $\dot{z}(t) = \alpha - z(t)$, given any $\epsilon > 0$, there exists $T > 0$ such that $z(t) < \alpha + \epsilon$, for all $t > T$. Using the Comparison theorem from [38] and the fact that $w(t) = \alpha s(t) + x(t) \geq 0$ for all $t \geq 0$, it follows that $\limsup_{t\to\infty} w(t) \leq \alpha$. Since $\limsup_{t\to\infty} s(t) \geq 0$, therefore $\limsup_{t\to\infty} x(t) \leq \alpha$.

Finally, set $z(t) = y(t) + K\int_0^\infty e^{-u} h(u)\,(x(t-u) + \alpha s(t-u) - \alpha)\,\mathrm{d}u$. Differentiate $z(t)$ with respect to t to obtain

$$\begin{aligned}
\dot{z}(t) &= -y(t) + K\int_0^\infty e^{-u} h(u)\,[x(t-u)(y(t-u) + \alpha s(t-u) - 1 - y(t-u))]\,\mathrm{d}u \\
&\quad + K\int_0^\infty e^{-u} h(u)\,[\alpha - \alpha s(t-u) - \alpha x(t-u) s(t-u)]\,\mathrm{d}u \\
&= -y(t) + K\int_0^\infty e^{-u} h(u)\,[-x(t-u) - \alpha s(t-u) + \alpha]\,\mathrm{d}u\ .
\end{aligned}$$

Therefore, $\dot{z}(t) = -z(t)$. It follows that $\lim_{t\to\infty} z(t) = 0$. Hence,

$$\begin{aligned}
0 &= \lim_{t\to\infty} \left[y(t) + K\int_0^\infty e^{-u} h(u)\,(x(t-u) + \alpha s(t-u) - \alpha)\,\mathrm{d}u \right] \\
&\geq \limsup_{t\to\infty} \left[y(t) - \alpha K \int_0^\infty e^{-u} h(u)\,\mathrm{d}u \right]\ .
\end{aligned}$$

Therefore, $\limsup_{t\to\infty} y(t) \leq \alpha K \int_0^\infty e^{-u} h(u)\,\mathrm{d}u$. □

Lemma 3.2.4. *If $(s(t), x(t), y(t))$ is a solution of (3.6) with initial data in BC^3_+, then*

(1) *If* $\alpha < 1$, *then* $\lim_{t\to\infty} x(t) = 0$.

(2) *If* $\alpha \geq 1$, *then* $\limsup_{t\to\infty} x(t) \leq \alpha - 1 + \frac{1}{\sum_{i=0}^{k} \alpha^i}$ *for all* $k \geq 0$.

Proof. If $\alpha < 1$, there exists $\delta > 0$ such that $\alpha(1+\delta) < 1$. By Theorem 3.2.1, there exists $T > 0$ such that $s(t) \leq 1 + \delta$ for all $t > T$. It follows

$$\dot{x} \leq -x + \alpha x s \leq -x + \alpha(1+\delta)x \ .$$

The solution of equation $\dot{z}(t) = (-1 + \alpha(1+\delta))z(t)$ goes to 0, as $t \to \infty$. By the Comparison Theorem in [38], $\limsup_{t\to\infty} x(t) \leq 0$. Since, $x(t) \geq 0$, then, if $\alpha < 1$, $\lim_{t\to\infty} x(t) = 0$.

To show part (2), we used proof by induction. The case $k = 0$ is true, by Theorem 3.2.1, since $\alpha - 1 + \frac{1}{\sum_{i=0}^{0} \alpha^i} = \alpha$.

Assume that the inequality holds for an integer $k = n > 0$, i.e.

$$\limsup_{t\to\infty} x(t) \leq \alpha - 1 + \frac{1}{\sum_{i=0}^{n} \alpha^i} \ . \tag{3.7}$$

Then given any $\epsilon > 0$, there exists $T > 0$ such that $x(t) < \alpha - 1 + \frac{1}{\sum_{i=0}^{n} \alpha^i} + \epsilon$ for $t > T$. Therefore, $\dot{s}(t) > 1 - s(t) - s(t)(\alpha - 1 + \frac{1}{\sum_{i=0}^{n} \alpha^i} + \epsilon)$. For all sufficiently large t by the Comparison Theorem in [38],

$$\liminf_{t\to\infty} s(t) > \frac{1}{\alpha + \frac{1}{\sum_{i=0}^{n} \alpha^i} + \epsilon} \ .$$

Letting $\epsilon \to 0$, it follows that

$$\liminf_{t\to\infty} s(t) \geq \frac{1}{\alpha + \frac{1}{\sum_{i=0}^{n} \alpha^i}} \ .$$

Since $\alpha s(t) > 0$, $\liminf_{t\to\infty} \alpha s(t) + \limsup_{t\to\infty} x(t) \leq \limsup_{t\to\infty} \big[\alpha s(t) + x(t)\big] \leq \alpha$.

Therefore

$$\limsup_{t\to\infty} x(t) \leq \alpha - \frac{\alpha}{\alpha + \frac{1}{\sum_{i=0}^{n} \alpha^i}} = \alpha - \frac{\sum_{i=0}^{n} \alpha^{i+1}}{\sum_{i=0}^{n} \alpha^{i+1} + 1} = \alpha - \frac{\sum_{i=0}^{n} \alpha^{i+1}}{\sum_{i=0}^{n+1} \alpha^i} = \alpha - 1 + \frac{1}{\sum_{i=0}^{n+1} \alpha^i} \ .$$

This completes the induction. □

Theorem 3.2.5. *If $(s(t), x(t), y(t))$ is a solution of (3.6) with initial data in BC^3_+, then*

(1) *If $\alpha > 1$, then $\limsup_{t\to\infty} x(t) \leq \alpha - 1$.*

(2) *If $\alpha = 1$, then $\lim_{t\to\infty} x(t) = 0$.*

Proof. Since the previous lemma is true for all positive integers k, therefore $\limsup_{t\to\infty} x(t) \leq \lim_{k\to\infty} \alpha - 1 + \frac{1}{\sum_{i=0}^{k} \alpha^k} = \alpha - 1$. If $\alpha = 1$, then $\limsup_{t\to\infty} x(t) \leq 0$. Since we have shown that $x(t)$ remains non-negative for all t, then $\lim_{t\to\infty} x(t) = 0$. □

Set

$$X^0 \equiv \{\phi(t) \in BC^3_+ : \quad \phi_2(0) > 0 \text{ and } \exists\theta \in [-L, 0] \text{ such that } \phi_2(\theta)\phi_3(\theta) > 0\} , \tag{3.8a}$$

$$X_1 \equiv \{\phi(t) \in BC^3_+ : \quad \phi_2(0) = 0\} , \tag{3.8b}$$

$$X_2 \equiv \{\phi(t) \in BC^3_+ : \quad \phi_2(0) > 0 \text{ and } \phi_2(\theta)\phi_3(\theta) = 0, \ \forall\theta \in [-L, 0]\} , \tag{3.8c}$$

$$X = X^0 \cup X_1 \cup X_2 . \tag{3.8d}$$

Observe several things implied by this definition:

(1) If $\phi \in X^0$, since it is continuous and $\phi_2(0) > 0$, then there exists $a > 0$, such that for all $\theta \in (-a, 0]$ $\phi_2(\theta) > 0$.

(2) If $\phi_2(\theta)\phi_3(\theta) = 0$ for all $\theta \in [-L, 0]$, then $\int_0^\infty \phi_2(-u)\phi_3(-u)e^{-u}h(u)\,\mathrm{d}u = 0$.

(3) If $\phi \in X_2$, since ϕ is continuous, there exists $a > 0$ such that for all $\theta \in (-a, 0]$, $\phi_2(\theta) > 0$ and $\phi_3(\theta) = 0$.

Denote $(s(t), x(t), y(t)) = (s(t, \phi(t)), x(t, \phi(t)), y(t, \phi(t)))$ to be the solution of (3.6) with the initial data $(\phi(t))$ in X^0. Set

$$T(t)(\phi)(\theta) = (s(t + \theta), x(t + \theta), y(t + \theta)), \ \theta \in (-\infty, 0] .$$

Lemma 3.2.6. *If a solution of (3.6) has initial data in X^0, then for all $t > 0$ there exists $\theta \in [t - L, t]$ such that $x(\theta)y(\theta) > 0$. Moreover, there exists $T > 0$, such that $s(t) > 0$, $x(t) > 0$ and $y(t) > 0$ and $\int_0^\infty x(t-u)y(t-u)e^{-u}h(u)\,\mathrm{d}u > 0$, for all $t > T$.*

Proof. Observe that, since $\phi_1(0) \geq 0$ and $\phi_2(0) > 0$, then $s(t) > 0$ and $x(t) > 0$ for all $t > 0$. The proof of this statement is similar to that of Proposition 3.2.2.

Consider the case $\phi_3(0) > 0$. Then, since by Theorem 3.2.1 $y(t) \geq 0$ for all t and therefore $\dot{y}(t) \geq -y(t)$, it follows that $y(t) > 0$ for all $t \geq 0$. The result follows.

Consider the case $\phi_3(0) = 0$. Observe that, since $\phi_2(t)$ and $\phi_3(t)$ are continuous functions then there exist $t_1, t_2 \in \mathbb{R}$ such that $-L < t_1 < \theta_0 < t_2 \leq 0$ and $\phi_2(t)\phi_3(t) > 0$ for all $t \in [t_1, t_2]$. Therefore there exists time $T \leq L + t_1$ (if L is ∞ then inequality is strict) such that $\dot{y}(T) > 0$ and there exists $\epsilon > 0$ such that $y(t) > 0$ for all $t \in (T, T + \epsilon)$. Then, since $\dot{y}(t) \geq -y(t)$, it follows that $y(t) > 0$ for all $t > T$. Since $\theta_0 \in [t_1, t_2] \subset [t_1, T]$, the result follows. □

Lemma 3.2.7. *Sets X^0, X_1 and X_2 are positively invariant under $T(t)$.*

Proof. From the Lemma 3.2.6 and the fact that $s(t) > 0$ for $t > 0$ whenever $\phi_1(0) \geq 0$ it follows that the set X^0 is positively invariant under $T(t)$.

If the solution has initial data in X_1, then, by (3.6b), $x(t) = 0$ for all $t > 0$. From Theorem 3.2.1 it follows that $s(t) \geq 0$, $y(t) \geq 0$ for all $t > 0$.

Consider the solutions with initial data in X_2. By (3) $y(0) = 0$ and since $y(t) = 0$ is a solution of (3.6c) with initial data $y(0) = 0$ and $\phi_2(\theta)\phi_3(\theta) = 0$ for all $\theta \in [-L, 0]$, by the uniqueness of solutions in forward time, it follows that $y(t) = 0$ for all $t > 0$. Therefore, $\int_0^\infty x(t-u)y(t-u)e^{-u}h(u)\,\mathrm{d}u = 0$ for all $t > 0$. The proof that $s(t) \geq 0$ and $x(t) > 0$ for all $t > 0$ follows from Theorem 3.2.1. □

3.3 Stability results with general delay

System (3.6) has three equilibria: $E_0 = (1, 0, 0)$, $E_1 = \left(\frac{1}{\alpha}, \alpha - 1, 0\right)$, and $E_+ = \left(\frac{K\int_0^\infty e^{-u}h(u)\,\mathrm{d}u}{K\int_0^\infty e^{-u}h(u)\,\mathrm{d}u+1}, \frac{1}{K\int_0^\infty e^{-u}h(u)\,\mathrm{d}u}, \frac{\alpha K\int_0^\infty e^{-u}h(u)\,\mathrm{d}u}{K\int_0^\infty e^{-u}h(u)\,\mathrm{d}u+1} - 1\right)$. E_0 always exists. Existence of E_1 requires

$$\alpha > 1 \ . \tag{3.9}$$

Existence of E_+ requires

$$(\alpha - 1)K \int_0^\infty e^{-u}h(u)\,\mathrm{d}u > 1 \ . \tag{3.10}$$

Set $X(t) = [s(t), x(t), y(t)]^T$.

The linearization of system (3.6) around an equilibrium $E_* = (s_*, x_*, y_*)$ is given by

$$\dot{X}(t) = AX(t) + B\int_0^\infty e^{-u}h(u)X(t-u)\,\mathrm{d}u \ , \tag{3.11}$$

where

$$A = \begin{bmatrix} -1 - x_* & -s_* & 0 \\ \alpha x_* & \alpha s_* - 1 - y_* & -x_* \\ 0 & 0 & -1 \end{bmatrix}, \ B = \begin{bmatrix} 0 & 0 & 0 \\ 0 & 0 & 0 \\ 0 & Ky_* & Kx_* \end{bmatrix}.$$

3.3.1 Stability at E_0

At E_0, (3.11) becomes

$$\begin{bmatrix} \dot{s}(t) \\ \dot{x}(t) \\ \dot{y}(t) \end{bmatrix} = \begin{bmatrix} -1 & -1 & 0 \\ 0 & \alpha - 1 & 0 \\ 0 & 0 & -1 \end{bmatrix} \begin{bmatrix} s(t) \\ x(t) \\ y(t) \end{bmatrix} \ . \tag{3.12}$$

If $\alpha < 1$ (and therefore neither E_1 nor E_+ exist), the eigenvalues appearing on the diagonal of the matrix in (3.12) are all negative. Therefore E_0 is locally asymptotically

stable. If, on the other hand, $\alpha > 1$, then one of the eigenvalues is positive and E_0 is a saddle.

Theorem 3.3.1. *If $\alpha < 1$, then E_0 is globally asymptotically stable with respect to solutions of system (3.6) with initial data in X^0.*

Proof. We use Lyapunov's Direct Method for delay differential equations (see [39], [40]). Consider the following function:

$$\begin{aligned} V(s(t),x(t),y(t)) &= s(t) - 1 - \ln s(t) + \frac{x(t)}{\alpha} \\ &+ \frac{1}{\alpha K \int_0^\infty e^{-u}h(u)\,\mathrm{d}u}\left[y(t) + K\int_0^\infty \int_{-u}^0 x(t+\theta)y(t+\theta)\,\mathrm{d}\theta\, e^{-u}h(u)\,\mathrm{d}u\right] . \end{aligned}$$

By Lemma 3.2.6, the double integral in the definition of V is always positive for solutions of (3.6) with initial data in X^0. On the other hand, by Lemma 3.2.7 follows that there exists $T > 0$ such that $s(t) > 0$, $x(t) > 0$, $y(t) > 0$ for all $t > T$. Note that the domain of V is $C((-\infty,\infty), int\mathbb{R}_+) \cap C((-\infty,\infty),\mathbb{R}_+) \cap C((-\infty,\infty), int\mathbb{R}_+)$ and $V(s(t),x(t),y(t))$ is 0 if and only if $s(t) = 1$, $x(t) = 0$ and $y(t) = 0$ for all $t \in (-\infty,\infty)$. Otherwise, V is positive.

Note that:

$$\begin{aligned} \frac{\mathrm{d}}{\mathrm{d}t}\left(\int_{-v}^0 x(t+\theta)y(t+\theta)\,\mathrm{d}\theta\right) &= \frac{\mathrm{d}}{\mathrm{d}t}\left(\int_{t-v}^t x(u)y(u)\,\mathrm{d}u\right) \\ &= \frac{\mathrm{d}}{\mathrm{d}t}\left(\int_a^t x(u)y(u)\,\mathrm{d}u - \int_a^{t-v} x(u)y(u)\,\mathrm{d}u\right) \\ &= x(t)y(t) - x(t-v)y(t-v) . \end{aligned}$$

Differentiate V with respect to t:

$$\begin{aligned}
\dot{V}(t) &= \left(1-\frac{1}{s(t)}\right)(1-s(t)-s(t)x(t)) + x(t)\left(-\frac{1}{\alpha}+s(t)-\frac{y(t)}{\alpha}\right) \\
&+ \frac{1}{\alpha K\int_0^\infty e^{-u}h(u)\,\mathrm{d}u}\left(-y(t)+K\int_0^\infty x(t-u)y(t-u)e^{-u}h(u)\,\mathrm{d}u\right) \\
&+ \frac{\int_0^\infty (x(t)y(t)-x(t-u)y(t-u))\,e^{-u}h(u)\,\mathrm{d}u}{\alpha\int_0^\infty e^{-u}h(u)\,\mathrm{d}u} \\
&= -\frac{1}{s(t)}(s-1)^2 - s(t)x(t) + x(t) - \frac{x(t)}{\alpha} + s(t)x(t) - \frac{x(t)y(t)}{\alpha} \\
&\quad -\frac{y(t)}{\alpha K\int_0^\infty e^{-u}h(u)\,\mathrm{d}u} + \frac{x(t)y(t)}{\alpha} \\
&= -\frac{1}{s(t)}(s-1)^2 + x(t)\left(1-\frac{1}{\alpha}\right) - \frac{y(t)}{\alpha K\int_0^\infty e^{-u}h(u)\,\mathrm{d}u}\ .
\end{aligned}$$

Since $\alpha < 1$ holds, then $1-\frac{1}{\alpha} < 0$ and therefore $\dot{V}(t) \leq 0$. Note that equality holds only when $s(t) = 1$, $x(t) = 0$ and $y(t) = 0$. Since E_0 is the largest invariant set where $\dot{V}(t) = 0$, then by the LaSalle Extension Theorem for delay equations [41], E_0 is globally asymptotically stable. □

Lemma 3.3.2. *E_0 is globally asymptotically stable with respect to solutions of (3.6) with initial data in X_1.*

Proof. By Lemma 3.2.7 and equation (3.6a) it follows that $x(t) = 0$ for all $t > 0$ and $s(t) \to 1$ as $t \to \infty$.

Consider the case where $L = \infty$. If $\phi_2(\theta)\phi_3(\theta) = 0$ for all $\theta \in (-\infty, 0]$ and therefore $\int_0^\infty \phi_2(-u)\phi_3(-u)e^{-u}h(u)\,\mathrm{d}u = 0$, then since $x(t) = 0$ for all $t > 0$, $\int_0^\infty x(t-u)y(t-u)e^{-u}h(u)\,\mathrm{d}u = 0$ for all $t > 0$. Therefore, $\dot{y}(t) = -y(t)$ for all $t > 0$. It follows that $\lim_{t\to\infty} y(t) = 0$.

If there exists $\theta \in (-\infty, 0]$ such that $\phi_2(\theta)\phi_3(\theta) > 0$ then there exists $T > 0$ such that $\int_0^\infty x(t-u)y(t-u)e^{-u}h(u)\,\mathrm{d}u > 0$ for all $t > T$. On the other hand, $x(t) = 0$ for

all $t > 0$, $\int_0^t x(t-u)y(t-u)e^{-u}h(u)\,\mathrm{d}u = 0$ for all $t > 0$. Therefore,

$$\begin{aligned}\dot{y}(t) &= -y(t) + K\int_0^t x(t-u)y(t-u)e^{-u}h(u)\,\mathrm{d}u + K\int_t^\infty x(t-u)y(t-u)e^{-u}h(u)\,\mathrm{d}u \\ &= -y(t) + K\int_t^\infty x(t-u)y(t-u)e^{-u}h(u)\,\mathrm{d}u\ .\end{aligned}$$

The limit of $K\int_t^\infty x(t-u)y(t-u)e^{-u}h(u)\,\mathrm{d}u$ as $t \to \infty$ is 0. Therefore, $\lim_{t\to\infty}\dot{y}(t) = -y(t)$. The solutions of $\dot{y}(t) = -y(t)$ approach 0 as $t \to \infty$.

Consider the case where $L < \infty$. Since $x(t) = 0$ for $t > 0$, then $K\int_t^\infty x(t-u)y(t-u)e^{-u}h(u)\,\mathrm{d}u = 0$ for all $t > L$. Then $\dot{y}(t) = -y(t)$ for all $t > L$. The solutions of $\dot{y}(t) = -y(t)$ approach 0 as $t \to \infty$. □

Lemma 3.3.3. *If $\alpha < 1$, then E_0 is globally asymptotically stable with respect to solutions of (3.6) with initial data in X_2.*

Proof. By Lemma 3.2.7, $y(t) = 0$ for all $t > 0$. Since $\alpha < 1$, there exists $\epsilon > 0$, such that $\alpha(1+\epsilon) < 1$. Since by Lemma 3.2.3 $\limsup_{t\to\infty} s(t) \le 1$, then there exists $T > 0$ such that $s(t) < 1 + \epsilon$ for all $t > T$. Then $\dot{x}(t) = (\alpha s(t) - 1)x(t) \le (\alpha(1+\epsilon) - 1)x(t)$. The solution of $\dot{z}(t) = (\alpha(1+\epsilon)-1)z(t)$ with non-negative initial conditions approaches 0, as $t \to \infty$. By the Comparison Theorem in [38], $\limsup_{t\to\infty} x(t) \le 0$. Since $x(t) \ge 0$, then $\lim_{t\to\infty} x(t) = 0$. From (3.6a) it follows that $\lim_{t\to\infty} s(t) = 1$. □

3.3.2 Stability at E_1

Linearizing around E_1, (3.11) becomes

$$\begin{bmatrix}\dot{s}(t)\\ \dot{x}(t)\\ \dot{y}(t)\end{bmatrix} = \begin{bmatrix}-\alpha & -\frac{1}{\alpha} & 0\\ \alpha(\alpha-1) & 0 & 1-\alpha\\ 0 & 0 & -1\end{bmatrix}\begin{bmatrix}s(t)\\ x(t)\\ y(t)\end{bmatrix} + \begin{bmatrix}0 & 0 & 0\\ 0 & 0 & 0\\ 0 & 0 & (\alpha-1)K\end{bmatrix}\begin{bmatrix}\int_0^\infty s(t-u)e^{-u}h(u)\,\mathrm{d}u\\ \int_0^\infty x(t-u)e^{-u}h(u)\,\mathrm{d}u\\ \int_0^\infty y(t-u)e^{-u}h(u)\,\mathrm{d}u\end{bmatrix}. \tag{3.13}$$

The corresponding characteristic equation is

$$\left(\lambda + 1 - (\alpha - 1)K \int_0^\infty e^{-u(1+\lambda)} h(u)\,\mathrm{d}u\right)[\lambda(\lambda + \alpha) + \alpha - 1] = 0\ . \tag{3.14}$$

Theorem 3.3.4. *E_1 is locally asymptotically stable if $\alpha > 1$ and $K(\alpha-1)\int_0^\infty e^{-u}h(u)\,\mathrm{d}u < 1$ and unstable if either inequality is reversed.*

Proof. We consider the sign of the real parts of the roots of (3.14). The term in the square brackets of (3.14) has two roots , $\lambda_1 = -(\alpha - 1)$ and $\lambda_2 = -1$, which are both negative, if and only if $\alpha > 1$. Therefore, if $\alpha > 1$ the stability of E_1 is determined by the sign of the real parts of the roots of $m(\lambda) = \lambda+1-K(\alpha-1)\int_0^\infty e^{-u(1+\lambda)}h(u)\,\mathrm{d}u = 0$.

Assume $\alpha > 1$. Substituting $\lambda = \beta + i\gamma$; $\gamma \geq 0$ in $m(\lambda)$ and seperating real and imaginary parts, we obtain

$$L(\beta) = \beta + 1 = K(\alpha - 1)\int_0^\infty e^{-u(1+\beta)}\cos(\gamma u)h(u)\,\mathrm{d}u = R(\beta)\ , \tag{3.15a}$$

$$\gamma = -K(\alpha - 1)\int_0^\infty e^{-u(1+\beta)}\sin(\gamma u)h(u)\,\mathrm{d}u = 0\ . \tag{3.15b}$$

First we show that if $K(\alpha - 1)\int_0^\infty e^{-u}h(u)\,\mathrm{d}u > 1$, then $m(\lambda)$ has a positive real root. Note that if $\gamma = 0$, then (3.15b) is satisfied. In this case, in (3.15a), $L(0) < R(0)$, $R(\beta)$ is a decreasing function of β and $L(\beta)$ is an increasing function of β and $\lim_{\beta\to\infty} L(\beta) = +\infty$. Therefore, $m(\lambda)$ has a positive real root and E_1 is unstable.

On the other hand, if $K(\alpha-1)\int_0^\infty e^{-u}h(u)\,\mathrm{d}u > 1$, $L(0) > R(0)$, $R(\beta)$ is decreasing and $L(\beta)$ is increasing, and (3.15a) can never be satisfied for $\beta > 0$. Hence, E_1 is localy asymptotically stable. □

Theorem 3.3.5. *If $\alpha > 1$ and $(\alpha - 1)K\int_0^\infty e^{-u}h(u)\,\mathrm{d}u < 1$, then E_1 is globally asymptotically stable with respect to solutions of (3.6) with initial data in X^0.*

Proof. We use Lyapunov's Direct Method for delay differential equations (see [39],

[40]). Consider the following function:

$$V(s(t),x(t),y(t)) = s(t) - \frac{1}{\alpha} - \frac{1}{\alpha}\ln \alpha s(t) + \frac{1}{\alpha}\left(x(t) - \alpha + 1 - (\alpha-1)\ln\frac{x(t)}{\alpha-1}\right) + \frac{\alpha-1}{\alpha}\left[y(t) + K\int_0^\infty \int_{-u}^0 x(t+\theta)y(t+\theta)\,\mathrm{d}\theta\, e^{-u}h(u)\,\mathrm{d}u\right] .$$

From Lemma 3.2.6, the double integral in the definition of V is always positive for solutions of (3.6) with initial data in X^0. On the other hand, by Lemma 3.2.7 follows that there exists $T > 0$ such that $s(t) > 0$, $x(t) > 0$, $y(t) > 0$ for all $t > T$. Note that the domain of $V(t)$ is $C((-\infty,\infty), int\mathbb{R}_+) \cap C((-\infty,\infty), int\mathbb{R}_+) \cap C((-\infty,\infty), int\mathbb{R}_+)$ and $V(s(t),x(t),y(t))$ is 0 if and only if $s(t) = \frac{1}{\alpha}$, $x(t) = \alpha - 1$ and $y(t) = 0$ for all $t \in (-\infty,\infty)$. Otherwise, $V(t)$ is positive.

Note that:

$$\begin{aligned}\frac{\mathrm{d}}{\mathrm{d}t}\left(\int_{-v}^0 x(t+\theta)y(t+\theta)\,\mathrm{d}\theta\right) &= \frac{\mathrm{d}}{\mathrm{d}t}\left(\int_{t-v}^t x(u)y(u)\,\mathrm{d}u\right)\\ &= \frac{\mathrm{d}}{\mathrm{d}t}\left(\int_a^t x(u)y(u)\,\mathrm{d}u - \int_a^{t-v} x(u)y(u)\,\mathrm{d}u\right)\\ &= x(t)y(t) - x(t-v)y(t-v)\ .\end{aligned}$$

Differentiate V with respect to t:

$$\begin{aligned}\dot{V}(t) = &\left(1 - \frac{1}{\alpha s(t)}\right)(1 - s(t) - s(t)x(t)) +\\ &x(t)\left(-\frac{1}{\alpha} + s(t) - \frac{y(t)}{\alpha}\right)\left(1 - \frac{\alpha-1}{x(t)}\right) +\\ &\frac{\alpha-1}{\alpha}\left(-y(t) + K\int_0^\infty x(t-u)y(t-u)e^{-u}h(u)\,\mathrm{d}u\right) +\\ &\frac{K(\alpha-1)\int_0^\infty (x(t)y(t) - x(t-u)y(t-u))\,e^{-u}h(u)\,\mathrm{d}u}{\alpha}\ .\end{aligned}$$

$$\begin{aligned}\dot{V}(t) &= 1 - s(t) - s(t)x(t) - \frac{1}{\alpha s(t)} + \frac{1}{\alpha} + \frac{x(t)}{\alpha} - \frac{x(t)}{\alpha} + 1 - \frac{1}{\alpha} \\ &\quad + s(t)x(t) - s(t)(\alpha - 1) - \frac{x(t)y(t)}{\alpha} + \frac{\alpha - 1}{\alpha} y(t) - \frac{\alpha - 1}{\alpha} y(t) \\ &\quad + K\frac{\alpha - 1}{\alpha} x(t)y(t) \int_0^\infty e^{-u} h(u)\, \mathrm{d}u \\ &= -\frac{1}{\alpha s(t)} \left(\alpha s(t) - 1\right)^2 + \frac{x(t)y(t)}{\alpha} \left(K(\alpha - 1) \int_0^\infty e^{-u} h(u)\, \mathrm{d}u - 1 \right) .\end{aligned}$$

Since $\alpha > 1$ and $(\alpha - 1)K \int_0^\infty e^{-u} h(u)\, \mathrm{d}u < 1$, therefore $\dot{V}(t) \leq 0$. Note that the equality holds only when $s(t) = \frac{1}{\alpha}$ and $x(t) = 0$ or $y(t) = 0$. However, the solution set described by $s(t) = \frac{1}{\alpha}$, $x(t) = 0$, $y(t) \geq 0$ is not invariant, as all the solutions with initial conditions in the set converge to E_0. On the other hand, if the set $s(t) = \frac{1}{\alpha}$, $x(t) \geq 0$, $y(t) = 0$ is invariant, then $x(t) = \alpha - 1$. Therefore, E_1 is the largest invariant set where $\dot{V}(t) = 0$. It follows, by the LaSalle Extension Theorem for delay equations [41], E_1 is globally asymptotically stable. □

Lemma 3.3.6. *If $\alpha > 1$, then E_1 is globally asymptotically stable with respect to solutions of (3.6) with initial data in X_2.*

Proof. By Lemma 3.2.7, $y(t) = 0$ for all $t > 0$. System (3.6a-3.6b) reduces to a standard ODE model of growth in the chemostat.

Since $\alpha > 1$, by Lemma 4.1 in [37] it follows that E_1 is globally asymptotically stable with respect to solutions of (3.6) with initial data in X_2.

□

3.4 Properties of the model when E_+ exists

In what follows we investigate the dynamics of system (3.6) when E_+ exists. We assume that the kernel of the delay distribution $h(u)$ has the same properties as the delay kernel $g(s)$ described in Chapter 2.

3.4.1 Local dynamics at E_+

In what follows we investigate the local dynamics at E_+. In particular, we are interested in regions of local asymptotic stability of E_+ with respect to τ. Another aspect of interest is persistence of solutions when E_+ exists.

The characteristic equation for the linearization around $E_+ = (s^*, x^*, y^*)$ is:

$$\begin{gathered} P(\lambda) = \lambda^3 + (2 + x^*)\lambda^2 + \left(1 + x^* + \tfrac{\alpha x^*}{1+x^*}\right)\lambda + \tfrac{\alpha x^*}{1+x^*} \\ +Kx^* \int_0^\infty e^{-u(1+\lambda)} h(u)\,\mathrm{d}u \left(-\lambda^2 + \left(\tfrac{\alpha}{1+x^*} - 2 - x^*\right)\lambda + \alpha - x^* - 1 - \tfrac{\alpha x^*}{1+x^*}\right) \\ = 0 \end{gathered} \tag{3.16}$$

Lemma 3.4.1. *If (3.10) holds and $\tau = 0$, then E_+ is locally asymptotically stable.*

Proof. Since $\tau = 0$, then $h(u) = \delta_0(u)$. Integral $\int_0^\infty e^{-\alpha u} h(u)\,\mathrm{d}u = 1$ and equilibrium E_+ becomes $\left(\frac{K}{K+1}, \frac{1}{K}, \frac{\alpha K}{K+1} - 1\right)$. The characteristic equation becomes:

$$\begin{gathered} \lambda^3 + (2 + x^*)\lambda^2 + \left(1 + x^* + \tfrac{\alpha x^*}{1+x^*}\right)\lambda + \tfrac{\alpha x^*}{1+x^*} \\ +Kx^* \left(-\lambda^2 + \left(\tfrac{\alpha}{1+x^*} - 2 - x^*\right)\lambda + \alpha - x^* - 1 - \tfrac{\alpha x^*}{1+x^*}\right) \\ = 0 \end{gathered} \quad . \tag{3.17}$$

The equation simplifies to the following cubic equation:

$$\lambda^3 + \left(1 + \frac{1}{K}\right)\lambda^2 + (\alpha - 1)\lambda + \alpha - 1 - \frac{1}{K} = 0\ . \tag{3.18}$$

Since one of the roots is $\lambda = -1$, the other two roots satisfy the following quadratic equation:

$$\lambda^2 + \frac{1}{K}\lambda + \alpha - 1 - \frac{1}{K} = 0\ .$$

Since $\alpha - 1 > \frac{1}{K}$, it follows that two remaining roots are either negative or have negative real parts. □

Theorem 3.4.2. *As τ increases from zero, the number of roots of (3.16) with positive real part can change only if a root appears on or crosses the imaginary axis as τ increases from 0.*

Proof. For

$$\begin{aligned} g(\lambda) &= (2+x^*)\lambda^2 + \left(1+x^* + \frac{\alpha x^*}{1+x^*}\right)\lambda + \frac{\alpha x^*}{1+x^*} + \\ & \quad Kx^* \int_0^\infty e^{-u} h(u)\,\mathrm{d}u \left(-\lambda^2 + \left(\frac{\alpha}{1+x^*} - 2 - x^*\right)\lambda + \alpha - x^* - 1 - \frac{\alpha x^*}{1+x^*}\right) \end{aligned}$$

it is easy to see that

$$\limsup_{\lambda\to\infty} |\lambda^{-3} g(\lambda)| = 0 < 1 \ .$$

Therefore, by Theorem 1.4, (in [42], Chapter 3, page 66) no root of (3.16) with positive real part can enter from infinity as τ bifurcates from 0. Since Lemma 3.4.1 holds, the result follows. □

Note that if (3.10) holds, then, by (3.16), $P(0) = \alpha - x^* - 1 > 0$ and therefore $\lambda = 0$ is not a root of (3.16).

In what follows Rouché's Theorem is used to approximate the region of stability of E_+.

Theorem 3.4.3. *If (3.10) holds, then there exists a subset of subspace $x^* - \alpha$ where E_+ is locally asymptotically stable.*

Proof. Note that $\lambda = -1$ is root of (3.16). Therefore, the rest of the roots can be found by solving the following equation:

$$q(\lambda) = \lambda^2 + \lambda(1+x^*) + \frac{\alpha x^*}{1+x^*} - Kx^* \int_0^\infty e^{-u(1+\lambda)} h(u)\,\mathrm{d}u(\lambda - \frac{\alpha}{1+x^*} + x^* + 1) = 0 \ .$$

Define $f(\lambda) = \lambda^2 + \lambda(1+x^*) + \frac{\alpha x^*}{1+x^*}$ and $g(\lambda) = Kx^* \int_0^\infty e^{-u(1+\lambda)} h(u)\,\mathrm{d}u \left(\lambda - \frac{\alpha}{1+x^*} + x^* + 1\right)$. Therefore, $f(\lambda) - g(\lambda) = q(\lambda)$.

Note that $f(0) = \frac{\alpha x^*}{1+x^*}$ and $f(\lambda) > 0$ for $\lambda \geq 0$.

Define $\Gamma_1 = \{\lambda \in \mathbb{C} : \lambda = Re^{\theta i},\ R > 0,\ -\pi/2 \leq \theta \leq \pi/2\}$, $\Gamma_2 = \{\lambda \in \mathbb{C} : \lambda = \beta i,\ -R \leq \beta \leq R,\ R, \beta \in \mathbb{R},\ R > 0\}$ and $\Gamma = \Gamma_1 \cup \Gamma_2$. We show that for all $\lambda \in \Gamma$, as $R \to \infty$ $|f(\lambda)| > |g(\lambda)|$, since then, by Rouché's theorem, it follows that $f(\lambda) + g(\lambda)$ has no root with positive real part.

Consider contour C_1. Note that $|e^{-\lambda u}| = |e^{-Re^{i\theta}s}|$ is maximized at $\theta = \pi/2,\ -\pi/2$ and therefore $|e^{-\lambda u}| \leq 1$. It follows that

$$\begin{aligned} |f(\lambda)| &\geq R^2 - (1+x^*)R^2 - \frac{\alpha x^*}{1+x^*}\ , \\ |g(\lambda)| &\leq Kx^* \int_0^\infty e^{-u} h(u) \mathrm{d}u \left(R + \left| \frac{\alpha}{1+x^*} - x^* - 1 \right| \right) \\ &= R + \left| \frac{\alpha}{1+x^*} - x^* - 1 \right| \ . \end{aligned}$$

For R large enough $|f(\lambda)| > |g(\lambda|)$ for $\lambda \in \Gamma_1$.

Consider contour C_2. Similarly, note that $|e^{-\lambda u}| \leq 1$. Then

$$\begin{aligned} f(\lambda) &= -\beta^2 + i\beta(1+x^*) + \frac{\alpha x^*}{1+x^*}, \\ g(\lambda) &= Kx^* \int_0^\infty e^{-u(1+i\beta)} h(u)\, \mathrm{d}u \left(\beta i - \frac{\alpha}{1+x^*} + x^* + 1 \right) \ . \end{aligned}$$

Therefore,

$$|f(\lambda)|^2 = \left(\frac{\alpha x^*}{1+x^*} - \beta^2 \right)^2 + \left(\beta \left(1 + x^* \right) \right)^2 , \tag{3.19}$$

$$\begin{aligned} |g(\lambda)|^2 &\leq k^2(\lambda) = K^2 (x^*)^2 \left(\int_0^\infty e^{-u} h(u) \mathrm{d}u \right)^2 \left(\left(x^* + 1 - \frac{\alpha}{1+x^*} \right)^2 + \beta^2 \right) \\ &= \left(x^* + 1 - \frac{\alpha}{1+x^*} \right)^2 + \beta^2 \ . \end{aligned} \tag{3.20}$$

Then,

$$|f(\lambda)|^2 - k^2(\lambda) = \beta^4 + \beta^2 b_2 + b_0 = q(y)\ ,$$

where

$$b_2 = -\frac{2\alpha x^*}{1+x^*} + 2x^* + (x^*)^2 \ , \tag{3.21}$$

$$b_0 = \frac{\alpha^2(x^*-1)}{x^*+1} - (x^*+1)^2 + 2\alpha \ . \tag{3.22}$$

Set $w = \beta^2 \geq 0$. We want to know when $q(\beta) = Q(w) = w^2 + wb_2 + b_0$ is positive. $Q(w)$ is quadratic and $\lim_{w\to\infty} = \infty$. Denote the discriminant of $Q(w)$ by Δ and, if $Q(w)$ has two real distinct roots, the larger of the two by w_c. Provided this, there are two ways for $Q(w)$ to remain positive (note we only need to consider right half plane):

(1) Either $\Delta < 0$ and therefore $Q(w)$ has no real roots and remains positive for all, $\beta \in \mathbb{R}, \beta \geq 0$;

(2) or $\Delta \geq 0$ and $w_c < 0$.

If either one of the two conditions hold then $|f(\lambda)| > |g(\lambda)|$ for all $\lambda \in \Gamma_2$. □

While the two above inequalities do not land themselves for theoretic analysis, we can solve them numerically and plot subset of the space $\alpha - x^*$ in which either one of them holds and thus describe the region where E_+ is stable. Therefore, we fixed $K = 2$ and created a mesh of values of α and x^* and checked at each point of the mesh whether one of the two conditions stated above hold. Each such point was marked with blue dot. The code for the approximation can be found in Appendix A.

In the sections to follow we will refine this conservative estimate with some precise results obtained for specific distributions.

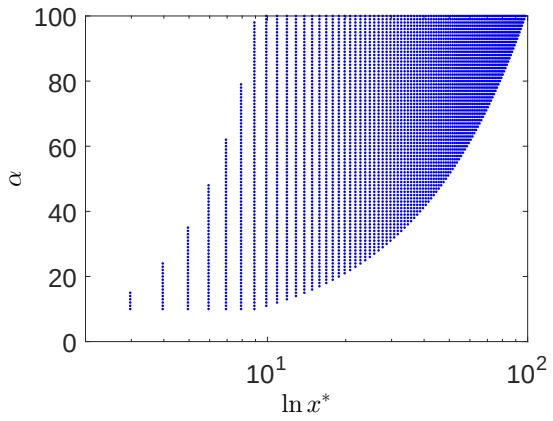

Figure 3.1: System (3.6) with a general distribution for the delay and $K = 2$. Blue region corresponds to a conservative approximation of the set of values of x^* and α at which E_+ is locally asymptotically stable.

Lemma 3.4.4. *If (3.10) holds, then (3.16) has no positive real roots.*

Proof. Observe that $\lambda = -1$ is the root of (3.16). Therefore, the stability of E_+ is determined by the roots of
$m(\lambda) = \lambda^2 + \lambda\,(1 + x^*) + \frac{\alpha x^*}{1+x^*} - Kx^* \int_0^\infty e^{-u(1+\lambda)} h(u)\,\mathrm{d}u\,\big(\lambda - \frac{\alpha}{1+x^*} + x^* + 1\big) = 0$. Set $f(\lambda) = \lambda^2 + \lambda\,(1 + x^*) + \frac{\alpha x^*}{1+x^*}$ and $g(\lambda) = Kx^* \int_0^\infty e^{-u} h(u)\,\mathrm{d}u\,\big(\lambda - \frac{\alpha}{1+x^*} + x^* + 1\big)$. Observe that $f(\lambda) > 0$ for all $\lambda \geq 0$.

Consider the case $\frac{\alpha x^*}{1+x^*} - x^* - 1 \leq 0$. Then for all $\lambda \geq 0$, $g(\lambda) \leq k(\lambda) = \lambda - \frac{\alpha}{1+x^*} + x^* + 1$. It follows that $f(\lambda) - k(\lambda) = \lambda^2 + \lambda x^* + \alpha - x^* - 1 > 0$, since, by (3.10), $\alpha - 1 > x^*$.

Consider the case $\frac{\alpha x^*}{1+x^*} - x^* - 1 > 0$. Then $g(\lambda) \leq 0$ for all $0 \leq \lambda \leq \frac{\alpha x^*}{1+x^*} - x^* - 1$. For all $\lambda > \frac{\alpha x^*}{1+x^*} - x^* - 1$, $g(\lambda) \leq k(\lambda) = \lambda - \frac{\alpha}{1+x^*} + x^* + 1$. It follows that $f(\lambda) - k(\lambda) = \lambda^2 + \lambda x^* + \alpha - x^* - 1 > 0$, since, by (3.10), $\alpha - 1 > x^*$. □

3.4.2 Global dynamics

We begin by considering the case of mean delay $\tau = 0$.

Lemma 3.4.5. *If $K(\alpha - 1) > 1$ and $\tau = 0$, then E_+ is globally asymptotically stable with respect to solutions with $s \geq 0$, $x(0) > 0$ and $y(0) > 0$.*

Proof. Since $\tau = 0$, $h(u) = \delta_0(u)$ and therefore, system (3.6) reduces to its ODE prototype:

$$\dot{s}(t) = 1 - s(t) - s(t)x(t) \ , \tag{3.23a}$$

$$\dot{x}(t) = x(t)(-1 + \alpha s(t) - y(t)) \ , \tag{3.23b}$$

$$\dot{y}(t) = -y(t) + Kx(t)y(t) \ . \tag{3.23c}$$

By Lemma 3.2.6, there exists $T > 0$ such that $s(t) > 0$, $x(t) > 0$ and $y(t) > 0$ for all $t > T$. Set $w(t) = s(t) + \frac{x(t)}{\alpha} + \frac{y(t)}{K\alpha}$ and observe that $\lim_{t\to\infty} w(t) = 1$. Since, by Theorem 3.2.1, $s(t) \geq 0$, $x(t) \geq 0$ and $y(t) \geq 0$, lim sup of each $s(t), x(t), y(t)$ is bounded by 1 and $(s(t), x(t), y(t))$ approaches the simplex $s(t) + \frac{x(t)}{\alpha} + \frac{y(t)}{K\alpha} = 1$. Moreover, the simplex is invariant with respect to solutions of (3.23). For solutions of (3.23) with initial data on the simplex and $x(0) > 0$ and $y(0) > 0$, $s(t) = 1 - \frac{x(t)}{\alpha} - \frac{y(t)}{K\alpha} \geq 0$. Therefore, (3.23) decouples to

$$\dot{x}(t) = x(t)\left(-1 + \alpha\left(1 - \frac{x(t)}{\alpha} - \frac{y(t)}{K\alpha}\right) - y(t)\right) \ , \tag{3.24a}$$

$$\dot{y}(t) = -y(t) + Kx(t)y(t) \ . \tag{3.24b}$$

Observe that system (3.24) can be rescaled to have the same form as system (2.20). Therefore, using similar reasoning as in the proof of Lemma 2.4.5 and the fact that $s(t) = 1 - \frac{x(t)}{\alpha} - \frac{y(t)}{K\alpha}$, it follows that if $K(\alpha - 1) > 1$ and $\tau = 0$, then E_+ is globally asymptotically. □

Lemma 3.4.6. *Consider the solutions of (3.6) with initial data in $X^0 \cup X_2$. If $\alpha > 1$, then there is no positive monotonically increasing sequence $\{t_n\}$, with $t_n \longrightarrow \infty$ as $n \longrightarrow \infty$ such that $(s(t_n), x(t_n), y(t_n))$ converges to E_0.*

Proof. Note that for every solution with initial data in $X^0 \cup X_2$, $x(t) > 0$ for all $t \geq 0$. Proof by contradiction. Assume that there exists a positive monotonically increasing sequence $\{t_n\}$, with $t_n \longrightarrow \infty$ as $n \longrightarrow \infty$ such that $x(t_n) \geq x(t_{n+1})$ and $\dot{x}(t_n) \leq 0$. Set $0 < \epsilon < \alpha - 1$. There exists $T > 0$ such that $y(t_n) < \epsilon$ and $s(t_n) > \frac{1+\epsilon}{\alpha}$ for all $t_n > T$. The last part is true, since $x(t_n)$ can be made arbitrarily small provided sufficiently large n. Then $\dot{x_n}(t) > x(t_n)(-1 + \alpha\frac{1+\epsilon}{\alpha} - \epsilon) > 0$. Therefore, $x(t_n)$ can not approach 0. □

Lemma 3.4.7. *Consider the solutions of (3.6) with initial data in X^0. If (3.10) holds, then no solution with initial data in X_0 converges to E_1.*

The proof of Lemma 3.4.7 is similar to the proof of Lemma 2.4.8.

Denote $\liminf_{t\to\infty} s(t) = s_\infty$, $\liminf_{t\to\infty} x(t) = x_\infty$, $\liminf_{t\to\infty} y(t) = y_\infty$, $\limsup_{t\to\infty} s(t) = s^\infty$, $\limsup_{t\to\infty} x(t) = x^\infty$ and $\limsup_{t\to\infty} y(t) = y^\infty$.

Lemma 3.4.8. *If a solution $(s(t), x(t), y(t))$ of 3.6 has initial data in X and $\alpha > 1$, then $\liminf_{t\to\infty} s(t) \geq \frac{1}{\alpha}$.*

Proof. Recall that by Theorem 3.2.1, $s(t) > 0$ for all $t > 0$ and by Theorem 3.2.5, $\limsup_{t\to\infty} x(t) \leq \alpha - 1$. Then

$$\dot{s}(t) \geq 1 - s(t) - s(t)(\alpha - 1) = 1 - \alpha s(t) \ .$$

For every solution of $\dot{z}(t) = 1 - \alpha z(t)$ and for every $\epsilon > 0$, there exists $T > 0$, such that $\liminf_{t\to\infty} z(t) \geq \frac{1}{\alpha} - \epsilon$. Therefore by the Comparison Theorem in [38], it follows that $\liminf_{t\to\infty} s(t) \geq \frac{1}{\alpha} - \epsilon$. Since it is true for all $\epsilon > 0$, then $\liminf_{t\to\infty} s(t) \geq \frac{1}{\alpha}$. □

Lemma 3.4.9. *Let $(s(t), x(t), y(t))$ to be a solution of (3.6) with initial data in $X^0 \cup X_2$. Then $x^\infty \geq \min\left\{\alpha - 1, \frac{1}{K\int_0^\infty e^{-u}h(u)\,\mathrm{d}u}\right\}$.*

Proof. We proceed using proof by contradiction. Assume $x^\infty < \min\left\{\alpha - 1, \frac{1}{K\int_0^\infty e^{-u}h(u)\,\mathrm{d}u}\right\}$. Using an argument similar to that given in the proof of Lemma 2.4.9 with $g(s) = h(s)$, $d = 1$ and $K = Y$, it follows that

$$\int_0^\infty x(t_n - u)y(t_n - u)e^{-u}h(u)\,\mathrm{d}u \leq (x^\infty + \epsilon)(y^\infty + \epsilon)\int_0^\infty e^{-u}h(u)\,\mathrm{d}u\ ,$$

for sufficiently large n. Then, letting $n \to \infty$ and $\epsilon \to 0+$

$$0 = \dot{y}(t_n) \leq -y(t_n) + Kx^\infty y^\infty \int_0^\infty e^{-u}h(u)\,\mathrm{d}u\ .$$

Since $lim_{n\to\infty} y(t_n) = y^\infty$, then

$$0 \leq -y^\infty + Kx^\infty y^\infty \int_0^\infty e^{-u}h(u)\,\mathrm{d}u\ .$$

Since $x^\infty < \frac{1}{K\int_0^\infty e^{-u}h(u)\,\mathrm{d}u}$, $y^\infty = 0$. Therefore, $\lim_{t\to\infty} y(t) = 0$.

Define $w(t) = \alpha s(t) + x(t)$. Then $\dot{w}(t) = \alpha - \alpha s(t) - x(t) - x(t)y(t) = 1 - w(t) - x(t)y(t)$. Since $x(t)$ is bounded and $\lim_{t\to\infty} y(t) = 0$, therefore $\lim_{t\to\infty} w(t) = \alpha$. By (3.6b), it follows that:

$$\dot{x}(t) = x(t)(-1 + w(t) - x(t) - x(t)y(t)) > x(t)(\alpha - 1 - \epsilon - x(t))\ ,$$

for sufficiently large t. From the Comparison Theorem (in [38]) it follows that $x_\infty \geq \alpha - 1 - \epsilon$. Since this is true for all $\epsilon > 0$, $x_\infty \geq \alpha - 1$, a contradiction. □

Lemma 3.4.10. *Let $(s(t), x(t), y(t))$ be a solution of (3.6) with initial data in $X^0 \cup X_2$. There exists $\epsilon_x > 0$ such that $x_\infty > \epsilon_x$.*

The proof of Lemma 3.4.10 is similar to the proof of Lemma 2.4.10.

Lemma 3.4.11. *Consider solutions of (3.6) with initial data in X^0. If (3.10) holds, then there exists $\epsilon > 0$ such that $y^\infty > \epsilon$.*

Proof. We denote the Laplace transform of a function $f(t)$ as $\widehat{f}(\lambda) = \int_0^\infty e^{-\lambda t} f(t)\, dt$, and note that the Laplace transform of $y(t)$ exists for all $\lambda > 0$, since $y(t)$ is bounded by Lemma 3.2.3. Taking the Laplace transform on both sides of of (3.6c) and simplifying we obtain:

$$\begin{aligned}(\lambda+1)\widehat{y}(\lambda) &= y(0) + K\widehat{xy}(\lambda)\int_0^\infty e^{-\lambda u}e^{-u}h(u)\mathrm{d}u \\ &\quad + K\int_0^\infty e^{-\lambda\theta}\int_\theta^\infty x(\theta-u)y(\theta-u)e^{-u}h(u)\mathrm{d}u\ \mathrm{d}\theta.\end{aligned}$$

There exists $\delta > 0$ such that $x(t) \geq x_\infty - \delta$ for all $t \geq 0$, and so $\widehat{xy}(\lambda) \geq (x_\infty - \delta)\widehat{y}(\lambda)$.

$$(\lambda+1)\widehat{y}(\lambda) \geq K(x_\infty - \delta)\widehat{y}(\lambda)\int_0^\infty e^{-\lambda u}e^{-u}h(u)\mathrm{d}u.$$

By Lemma 3.2.6, $y(t) > 0$ for all sufficiently large t, and hence $\widehat{y}(\lambda) > 0$, we can divide by $\widehat{y}(\lambda)$ to obtain

$$(\lambda+1) \geq K(x_\infty - \delta)\int_0^\infty e^{-\lambda u}e^{-u}h(u)\mathrm{d}u.$$

After a shift of time, if necessary, we can take the limit as $\delta, \lambda \to 0^+$ to obtain $x_\infty \leq \frac{1}{K\int_0^\infty e^{-u}h(u)\mathrm{d}u}$.

Since (3.10) holds then there exist $\epsilon > 0$, such that

$$\alpha - 1 - \epsilon > \frac{1}{K\int_0^\infty e^{-u}h(u)\mathrm{d}u}\ . \tag{3.25}$$

We proceed using proof by contradiction. Assume there is $\phi \in X$ such that $y^\infty < \frac{\epsilon}{4(\alpha-1)(1+\epsilon)}$. Then there exists $T > 0$ such that $y(t) < \frac{\epsilon}{2(\alpha-1)(1+\epsilon)}$, for all $t > T$. Since, by Theorem 3.2.5, $\limsup_{t\to\infty} x(t) \leq \alpha - 1$, assume also, that T is large enough so that $x(t) < (\alpha-1)(1+\epsilon)$, for all $t > T$. Set $w(t) = \alpha s(t) + x(t)$. Differentiating $w(t)$ with respect to t:

$$\dot{w}(t) = \alpha - w(t) - x(t)y(t) > \alpha - \epsilon/2 - w(t),$$

for sufficiently large t. From the Comparison Theorem (in [38]) it follows that $w(t) > \alpha - \epsilon/2$ for all sufficiently large t. Recall, that $\alpha s(t) = w(t) - x(t)$. Then by (3.6b)

follows:

$$\dot{x}(t) = x(t)(-1 + w(t) - x(t) - x(t)y(t)) > x(t)(\alpha - 1 - \epsilon - x(t)) \ ,$$

for sufficiently large t. From the Comparison Theorem (in [38]) it follows that $x_\infty \geq \alpha - 1 - \epsilon$ and therefore, by (3.25), $x_\infty > \frac{1}{K\int_0^\infty e^{-u}h(u)\mathrm{d}u}$, a contradiction. □

Theorem 3.4.12. *If (3.10) holds, then solutions of (3.6) with initial data in X^0 are uniformly persistent, i.e., there exists $\epsilon > 0$ such that $x_\infty > \epsilon$ and $y_\infty > \epsilon$.*

The proof of Theorem 3.4.12 is similar to the proof of Theorem 2.4.12.

To sum up, if E_+ exists, solutions of (3.6) are uniformly persistent. The dynamic in the case is the subject of the discussion to follow.

3.5 Dynamics of the model with gamma distributed delay kernel

In this section we consider system (3.6) with gamma distribution of order $p = 1$, $h(u) = ae^{-ua}$ used as the delay kernel. The coexistence equilibrium becomes $E_+ = \left(\frac{Ka}{(K+1)a+1}, \frac{a+1}{Ka}, \frac{\alpha Ka}{Ka+a+1} - 1\right)$. The condition for the coexistence of both species is

$$\frac{(\alpha - 1)Ka}{a + 1} > 1 \ . \tag{3.26}$$

In this section we investigate conditions for occurrence of Hopf bifurcation at E_+. Consider the characteristic equation at E_+:

$$\begin{aligned} \lambda^4 Ya\left(Ya + a + 1\right) + \lambda^3\left(Ya(a+3)\left(Ya + a + 1\right) + (a+1)\left(Ya + a + 1\right)\right) \\ +\lambda^2\left(Ya\left(a+2\right)\left(Ya + a + 1\right) + (a+1)(a+2)\left(Ya + a + 1\right) + \alpha Ya^2\right) \\ +\lambda\left(Ya(\alpha - 1)(a+1)(Ya + a + 1) + Ya\alpha(a+1)\right) \\ +(a+1)\left(Ya + a + 1\right)\left(\alpha Ya - Ya - a - 1\right) \quad = 0 \end{aligned} \tag{3.27}$$

Hopf bifurcation is indicated by the pure imaginary roots of (3.27), provided that the transversality condition holds. Observe that the equation (3.27) is of the form $g(\lambda) = b_4(a)\lambda^4+b_3(a)\lambda^3+b_2(a)\lambda^2+b_1(a)\lambda+b_0(a)$, where $b_i(a),\ i = 0 \ldots 4$ are polynomial in a defined as:

$$\begin{aligned}
b_4(a) &= Ya\,(Ya + a + 1)\ , \\
b_3(a) &= (Ya(a + 3)\,(Ya + a + 1) + (a + 1)\,(Ya + a + 1))\ , \\
b_2(a) &= \left(Ya\,(a + 2)\,(Ya + a + 1) + (a + 1)(a + 2)\,(Ya + a + 1) + \alpha Ya^2\right)\ , \\
b_1(a) &= (Ya(\alpha - 1)(a + 1)(Ya + a + 1) + Ya\alpha(a + 1))\ , \\
b_0(a) &= (a + 1)\,(Ya + a + 1)\,(\alpha Ya - Ya - a - 1)\ .
\end{aligned}$$

The equation (3.27) is similar to the characteristic equation of system (2.5) with gamma distribution of order $p = 2$ corresponding to E_+. Therefore similar reasoning can be applied. Since all of the coefficients are positive when E_+ exists, we rule out that there is a zero root.

In order for $\lambda = i\omega$ to be the root of $g(\lambda) = 0$, the following condition should hold:

$$b_4(a)b_1(a)^2 - b_1(a)b_2(a)b_3(a) + b_0(a)b_3(a)^2 = 0\ .$$

If the condition holds, then ω is defined by the expression $\omega^2(a) = \frac{b_1(a)}{b_3(a)}$. After simplification and cancellation of terms $a + 1$ and $Ya + a + 1$, the condition for existence of pure imaginary roots becomes

$$\begin{aligned}
n(a) = \quad & Ya(a + 1)(Ya(\alpha - 1)(Ya + a + 1) + Ya\alpha)^2 \\
& -Ya((\alpha - 1)(Ya + a + 1) + \alpha) \\
\times \ & (Ya(a + 2)(Ya + a + 1) + (a + 1)(a + 2)(Ya + a + 1) + \alpha Ya^2) \\
\times \ & (Ya(a + 3) + a + 1) \\
& +(\alpha Ya - Ya - a - 1)(Ya + a + 1)^2(Ya(a + 3) + a + 1)^2 = 0\ . \qquad (3.28)
\end{aligned}$$

It is difficult to analyse $n(a)$, however, certain properties of it can be deduced that illuminate local dynamics at E_+. Note that $n(a)$ is a polynomial in a of degree seven.

The coefficient next to a^7 is $-Y^4\alpha - 2Y^3\alpha - Y^2\alpha$. On the other hand, $n(0) < 0$. Therefore, $n(a)$ has at least one negative real root. Also, $n'(0) = -3K\alpha - 7K - 5 < 0$. This tell us that either there are roots that are also local extrema and the number of roots that are nor local extrema is even, or roots occur in pairs. In other words, if $n(a)$ has local maxima that are located in the right half plane and they are either negative, zero or positive. In the first case, it means that per each maximum there exist two values of a_c such that $n(a_c) = 0$ and $n'(a_c) \neq 0$. In the second case, $n(a_c) = n'(a_c) = 0$. According to the Theorem 2.5.3, only in the first case E_+ undergoes two Hopf bifurcations, while in the second case, no Hopf bifurcation occurs. Observe that, since $n(a)$ is a polynomial, then if its roots a_c occur in pairs and at the consecutive a_c^k and a_c^{k+1} the signs of $\frac{\partial Re(\lambda)}{\partial a}$ are opposite. Therefore, we do not expect nested "bubbles". Moreover, we do not expect more than 3 such "bubbles". In our experiments for the values of parameters that we have considered we witnessed only two Hopf bifurcations.

3.6 Numerical Results

In this section we consider system (3.6) with specific delay distributions: the Dirac delta distribution, the gamma distribution of order $p = 1$ and $p = 2$ and the uniform distribution. We confirm analytic results established in the previous section and conduct further numerical bifurcation analysis using mean delay τ as a primary bifurcation parameter and α as a secondary.

As was done in the previous chapter, we applied the linear chain trick to system (3.6) with the gamma distribution and the uniform distribution.

The diagrams in this section were obtained using similar methods as in Chapter 2. The meaning of the curve colors and markers remains the same.

We start by discussing the ongoing work by Wolkowicz, Humphries and Teslya

with respect to the bifurcation dynamics of system (3.6) with discrete delay using τ as the control parameter. We then proceed to describe our finding for the systems with gamma and uniform distributions. We compare the distributed delay system dynamics to those of the system with the discrete delay.

3.6.1 Discrete delay

In this section we briefly review results given by Fan and Wolkowicz [3] for the predator-prey model in the chemostat with discrete time delay. Following that, we go over new numerical bifurcation results for the same system. This is a part of ongoing work by Wolkowicz, Humphreys and Teslya.

Recall that Fan and Wolkowicz [3] gave the conditions for the existence of a value of τ, at which the system undergoes a Hopf bifurcation. Their numerical bifurcation analysis indicated that if such $\tau = \tau_1$ exists, then there is a second value of τ, τ_2 at which E_+ undergoes second Hopf bifurcation. E_+ loses stability as τ increases from zero to τ_1 and a stable periodic solution appears. As τ increases to τ_2, the stable periodic solution disappears and E_+ regains stability. The authors also showed, that there is a set of parameters such that the characteristic equation can have two pairs of pure imaginary roots. Results of [3] are suggestive of several things:

(1) Existence of Hopf bifurcations depends on the value of a secondary parameter, so that when that parameter passes some critical value, the Hopf bifurcations cannot occur and E_+ is locally asymptotically stable for all values of τ, while it exists;

(2) There is a potential for more than one pair of Hopf bifurcations to occur.

(3) Finally, it is possible that the system can go through one or more double Hopf bifurcations.

Points of interest with respect to the dynamics of the model are:

(1) Does the stable periodic solution born as the result of the first Hopf bifurcation undergo any bifurcations as τ increases?

(2) If more than two Hopf bifurcations appear, what is the order in which pairs of complex eigenvalues cross the imaginary axis? Does this order change as the value of the secondary parameter varies?

In what follows we fixed $K = 2$ and studied the bifurcation dynamics of system (3.6) using τ as a primary bifurcation parameter and α as a secondary. Figure 3.2 captures the findings.

For $1+\frac{1}{K} < \alpha < 7.994$, E_+ remains locally asymptotically stable for the duration of its existence (Figure 3.3a). At $\alpha \approx 7.994$, two supercritical Hopf bifurcations appear. An example of such dynamics at E_+ is depicted on Figure 3.3b. Equilibrium E_+ is stable at $\tau = 0$ and remains so until $\tau \approx 0.0208$ when E_+ goes through the first Hopf bifurcation and a pair of complex eigenvalues crosses the imaginary axis to the right, a stable periodic orbit appears. As τ increases to 0.917, E_+ goes through the second Hopf bifurcation, where the pair of complex eigenvalues crosses the imaginary axis to the left, a stable periodic solution disappears and E_+ restabilizes again. Stable periodic solution does not go through any bifurcations for the duration of its existence. At $\alpha \approx 43.87$ right Hopf bifurcation turns from supercritical to subcritical (Figure 3.3c). As the result an accompanying saddle node of limit cycles appears. At $\alpha \approx 48.69$ second set of Hopf bifurcations appears to the right of the first pair (Figure 3.4a). Both bifurcations are supercritical.

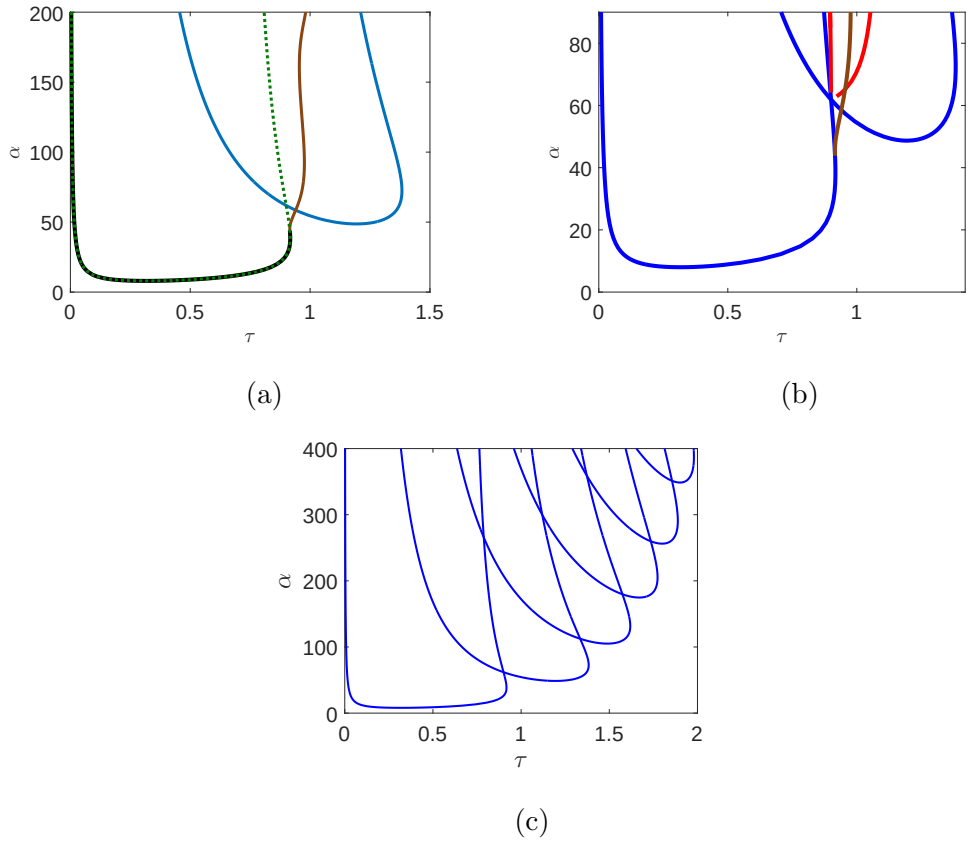

Figure 3.2: Two-parameter bifurcation diagrams for system (3.6) with discrete delay and $K = 2$ showing that as the value of α increases the local dynamics at E_+ becomes richer. Figure (a): black and blue - supercritical Hopf bifurcation, dashed green - subcritical Hopf bifurcation, brown - saddle node of limit cycles bifurcation. Figure (b): blue - Hopf bifurcation, red - torus bifurcation, brown - saddle node of limit cycles bifurcation. Figure (c): Hopf bifurcations only. As the value of α increases additional pairs of Hopf bifurcations appears.

As the value of α increases, second and third Hopf bifurcations move closer, until they collide in a double-Hopf bifurcation at $\alpha \approx 62.15$ and, as the result, torus bifurcation appears for higher values of α. As α continues to increase past double Hopf bifurcation value, second and third bifurcations switch places (Figure 3.4b). Once

the switch happens, the periodic solution born from the second Hopf bifurcation is unstable but restabilizes as τ increases past torus bifurcation of the second periodic solution.

The numerical analysis suggests that, as the value of α increases further, new pairs of Hopf bifurcations appear (Figure 3.2c). From the diagram we see that the pattern observed for the first two pairs of Hopf bifurcations repeats in the following pairs. For example, we expect the fourth Hopf bifurcation to switch its criticality as the value of α increases, and fourth and fifth Hopf bifurcations to move closer and eventually switch places in double Hopf bifurcation, giving birth to two torus bifurcations. So far there is no evidence that there is a critical value of α, α_c such that no new Hopf bifurcations are born for $\alpha > \alpha_s$.

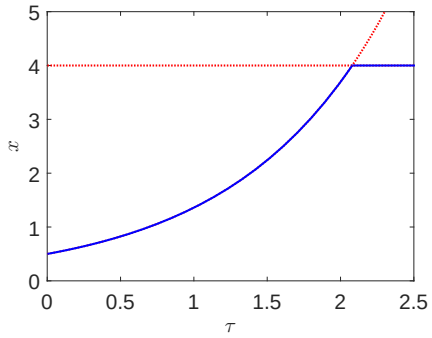

(a) $\alpha = 5$

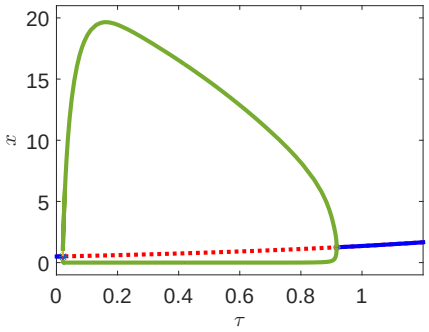

(b) $\alpha = 40$

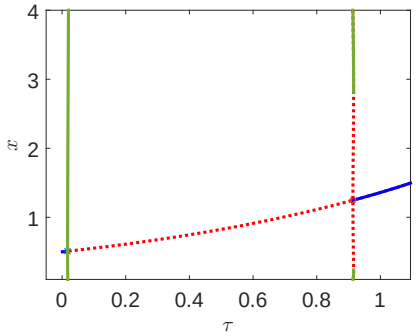

(c) $\alpha = 47$

Figure 3.3: Bifurcation diagram for system (3.6) with discrete delay and $K = 2$ showing the change in bifurcation dynamics as α increases. Figure (a): E_+ is locally asymptotically for the duration of its existence. Figure (b): E_+ loses its stability at the first Hopf bifurcation at $\tau_1 = 0.02086$ and restabilizes at the second Hopf bifurcation at $\tau_2 = 0.0917$. Figure (c): the rightmost Hopf bifurcation goes through a Bautin bifurcation and changes from supercritical to subcritical at $\alpha = 43.87$.

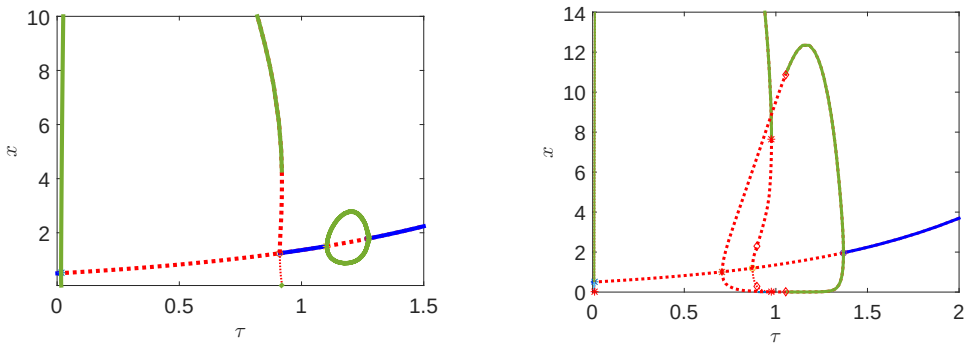

(a) $\alpha = 50$.

(b) $\alpha = 90$.

Figure 3.4: Bifurcation diagram for system (3.6) with discrete delay and $K = 2$ showing the change in bifurcation dynamics as α increases. The diamonds denote torus bifurcations. Figure (a): a second set of supercritical Hopf bifurcations appears. Figure (b): as α increases, the second and third Hopf bifurcations switch places through a double Hopf bifurcation. As a result, the first periodic orbit undergoes a torus bifurcations at $\tau = 0.8964$ and the second periodic orbit undergoes a torus bifurcations at $\tau = 1.052$.

Consider Figure 3.4b. Given $\alpha = 90$, as τ decreases past $\tau = 1.052$, stable periodic solution undergoes torus bifurcation and loses stability. As the result, a stable torus attractor is born. As τ decreases to 0.8964, the torus vanishes. However, our numerical simulations indicate that as τ becomes smaller than 0.9761, periodic solution born from the third on the left Hopf bifurcation restabilizes. Therefore, the system has a state of bi-stability for a range of τ. An example of such dynamics is depicted on the Figure 3.5: depending on the initial data, some solutions converge to the stable periodic solution, while other converge to the torus.

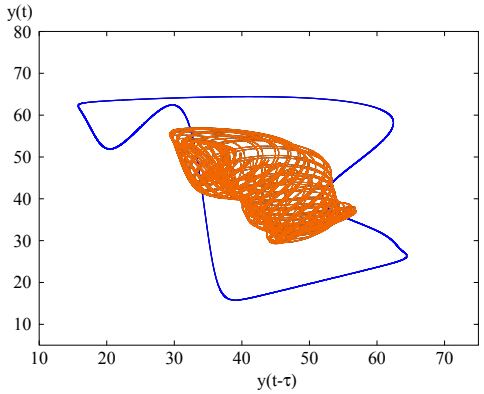

(a)

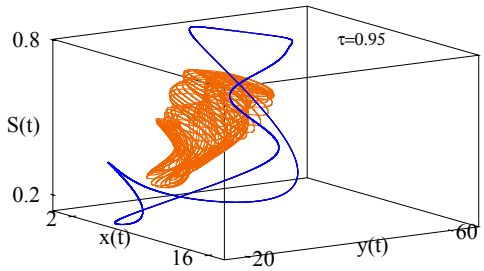

(b)

Figure 3.5: System (3.6) with discrete delay and $K = 2$, $\alpha = 100$ and $\tau = 0.95$ showing bi-stability in the system. Blue denotes a periodic orbit and orange, a torus.

3.6.2 Gamma distribution

To perform numerical bifurcation analysis using XPPAUT we used the linear chain trick (as described in [27]) and converted system (3.6) with the gamma distribution into ordinary differential equations system. Set

$$y_i(t) = \int_0^\infty x(t)y(t)e^{-ds}g_a^i(s)\,\mathrm{d}s\ , i = 1\dots p.$$

Then system (3.6) is equivalent to the following $p+3$-dimensional system:

$$\dot{s}(t) = 1 - s(t) - s(t)x(t)\ , \tag{3.29a}$$

$$\dot{x}(t) = x(t)(-1 + \alpha s(t)) - x(t)y(t)\ , \tag{3.29b}$$

$$\dot{y}(t) = -y(t) + Ky_1(t)\ , \tag{3.29c}$$

$$\dot{y}_1(t) = ax(t)y(t) - (a+d)y_1\ , \tag{3.29d}$$

$$\dot{y}_i(t) = ay_{i-1}(t) - (a+d)y_i(t)\ , i = 2\dots p\ , \tag{3.29e}$$

with initial conditions

$$\begin{aligned} s(0) &= \phi_1(0) \ , \\ x(0) &= \phi_2(0) \ , \\ y(0) &= \phi_3(0) \ , \\ y_i(0) &= \int_0^\infty \phi_2(-u)\phi_3(-u)e^{-u} g_a^i(u)\,\mathrm{d}u \ , \end{aligned}$$

where (ϕ_1, ϕ_2, ϕ_3) are initial data functions for $(s(t), x(t), y(t))$ that map from the interval $(-\infty, 0]$ into $int\mathbb{R}^3_+$.

The coexistence equilibrium becomes: $E_+ = \left(\frac{Ka^p}{Ka^p+(a+1)^p}, \frac{(a+1)^p}{Ka^p}, \frac{\alpha Ka^p}{Ka^p+(a+1)^p} - 1\right)$. The coexistence condition becomes:

$$\frac{K(\alpha-1)a^p}{(a+1)^p} > 1 \ .$$

We calculate the critical value of mean delay τ, τ_c when E_+ seizes to exist:

$$\tau_c = p\left((K(\alpha-1))^{1/p} - 1\right) \ .$$

The expression for τ_c implies that if $\alpha > \frac{1}{K} + 1$, then there is a set of τ, $[0, \tau_c)$ such that E_+ exist.

Consider the system with gamma distribution of order $p = 1$ used as the delay kernel. We graphically describe the stability region of E_+ in $\alpha - \tau$ space. We fixed $K = 2$ and created a mesh of values for α. For each value in the range we solved equation (3.28) for a numerically. Recall that equation (3.28) describes conditions on parameter set $K - \alpha - \tau$ for the existence of pure imaginary roots of the characteristic equation. The result is depicted on the Figure 3.6.

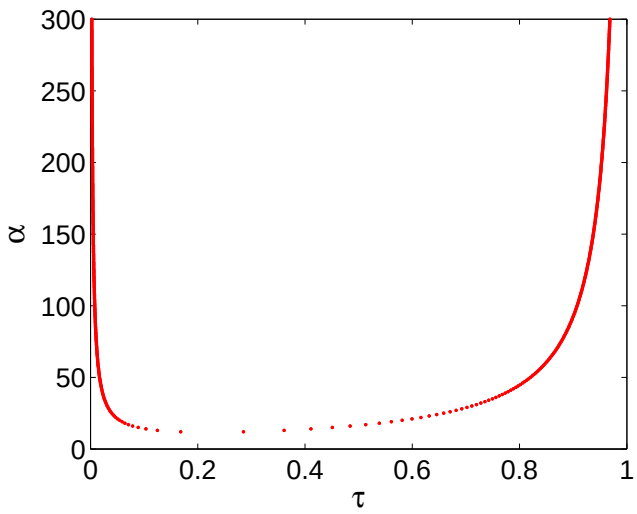

Figure 3.6: Two-parameter bifurcation diagram of Hopf bifurcations in $\alpha - \tau$ space for system (3.6) with $K = 2$ and gamma distribution of order $p = 1$ used as the delay kernel.

For $1 + \frac{1}{K} < \alpha < 13$, E_+ is locally asymptotically stable for the duration of its existence (Figure 3.7a). At $\alpha \approx 13$ two supercritical Hopf bifurcations are born. An example of such dynamics at $\alpha = 15$ is depicted on the Figure 3.7b. Equilibrium E_+ is stable at $\tau = 0$ and remains so until $\tau \approx 0.08907$ when E_+ goes through the first supercritical Hopf bifurcation and a pair of complex eigenvalues crosses the imaginary axis to the right and a stable periodic orbit appears. As τ increases to 0.4509, E_+ goes through the second supercritical Hopf bifurcation, where the pair of complex eigenvalues crosses the imaginary axis to the left, a stable periodic solution disappears and E_+ restabilizes again and remains so until it switches the stability in a transcritical bifurcation. Stable periodic solution does not go through any bifurcations for the duration of its existence.

Observe, that Figure 3.6 indicates that as the value of α increases, the region of instability of E_+ increases as well as the maximum amplitude of the stable periodic

solution (Figure 3.8).

We calculated the Lyapunov first coefficient for every point on the curve depicted on the Figure 3.6 and established that both Hopf bifurcations remain supercritical. Moreover, our numerical experiments indicate that as the value of α increases, the stable periodic solution that was born from the first Hopf bifurcation does not go through any additional bifurcations until it disappears.

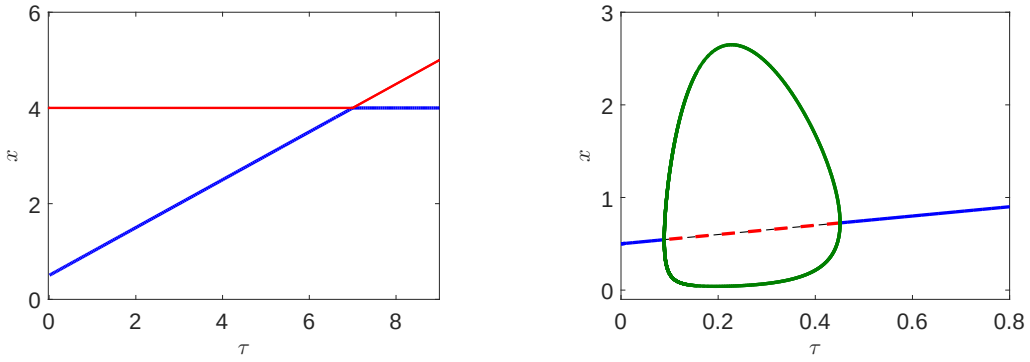

(a) $\alpha = 5$ (b) $\alpha = 15$

Figure 3.7: Bifurcation diagrams for system (3.6) with gamma distribution of order $p = 1$ used as the delay kernel and $K = 2$ showing the change in bifurcation dynamics as α varies its value. Figure (a): E_+ is stable while it exists. Figure (b): equilibrium E_+ is stable at $\tau = 0$ and remains so until $\tau \approx 0.08907$ when a stable periodic orbit appears. As τ increases through 0.4509 the stable periodic solution disappears and E_+ restabilizes and remains stable while it exists.

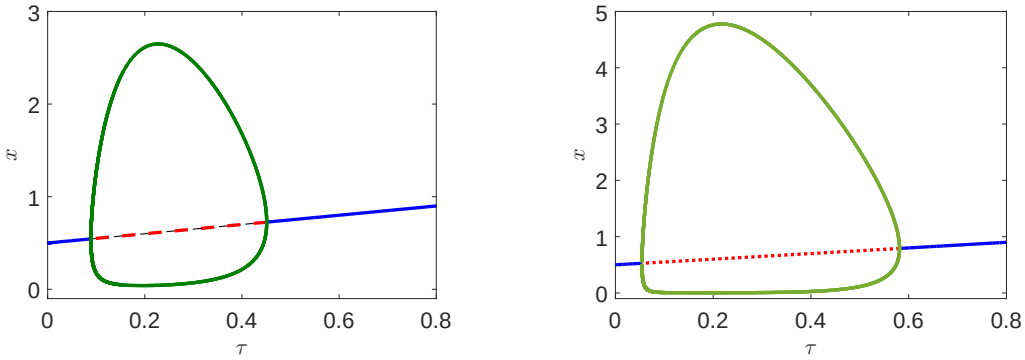

(a) $\alpha = 15$ (b) $\alpha = 25$

Figure 3.8: Bifurcation diagrams for system (3.6) with gamma distribution of order $p = 1$ used as the delay kernel and $K = 2$ showing that an increase in α results in an increase in the maximum amplitude of the amplitude of the stable periodic solution, as well as an increase in the size of region of instability of E_+ with respect to τ.

Next, we consider the system with gamma distribution of order $p = 2$ used as the delay kernel. In other words the kernel is $h(u) = a^2 u e^{-au}$. We used the linear chain trick (as shown in [27]) to turn the distributed delay system (3.6) into 5- dimensional ODE system:

$$\begin{aligned}
\frac{\mathrm{d}s}{\mathrm{d}t} &= 1 - s(t) - s(t)x(t) \ , \\
\frac{\mathrm{d}x}{\mathrm{d}t} &= x(t)(-1 + \alpha s(t)) - x(t)y(t) \ , \\
\frac{\mathrm{d}y}{\mathrm{d}t} &= -y(t) + K y_2(t) \ , \\
\frac{\mathrm{d}y_1}{\mathrm{d}t} &= a x(t) y(t) - (a+1) y_1 \ , \\
\frac{\mathrm{d}y_2}{\mathrm{d}t} &= a y_1(t) - (a+1) y_2(t) \ .
\end{aligned}$$

The characteristic equation corresponding to the linearization of the system at E_+ is of the form $p(\lambda) = b_5\lambda^5 + b_4\lambda^4 + b_3\lambda^3 + b_2\lambda^2 + b_1\lambda + b_0 = 0$, where $b_i,\ i = 0 \ldots 5$ are functions of a and $b_0 \neq 0$. Therefore $\lambda = 0$ is not one of the roots. If the characteristic

equation has pure imaginary root $\lambda = i\omega$ ($\omega > 0$), then ω is the solution of the following system:

$$b_4\omega^4 - b_2\omega^2 + b_0 = 0 \ , \tag{3.31a}$$

$$b_5\omega^4 - b_3\omega^2 + b_0 = 0 \ . \tag{3.31b}$$

We divide the first equation by b_4 and the second by b_5 and then subtract the second equation from the first to obtain:

$$\frac{b_3}{b_5}\omega^2 - \frac{b_2}{b_4}\omega^2 + \frac{b_0}{b_4} - \frac{b_1}{b_5} \ .$$

Solve for ω:

$$\omega^2 = \frac{b_0 b_5 - b_1 b_4}{b_2 b_5 - b_3 b_4} \ .$$

Substitute the expression for ω^2 into (3.31) to obtain the condition on the parameter space $K - \alpha - \tau$ so that the characteristic equation has pure imaginary roots. We fixed $K = 2$, created a mesh of values for α ranging from $1 + \frac{1}{K}$ to 200 and then solved the system for a checking against expression for ω^2 to make sure that it is positive. In this way we calculated two-parameter continuation of two Hopf bifurcations. Having accomplished that for each point on the curve, we calculated the first Lyapunov coefficient (using the method described previously). The code can be found in the Appendix A.

The result of the calculations is captured in Figure 3.9a. The dynamic observed is similar to that of the discrete delay system (Figure 3.9b). For $1 + \frac{1}{K} < \alpha < 7.994$ equilibrium E_+ is locally asymptotically stable while it exists. As α becomes larger two supercritical Hopf bifurcations appear. Equilibrium E_+ loses stability at the first one, and restabilizes at the second and remains stable while it exists. Finally, at $\alpha = 88$, second Hopf bifurcation undergoes Bautin bifurcation and switches from supercritical to subcritical. The subcritical Hopf bifurcation is accompanied by the saddle node of limit cycles bifurcation and therefore, if we denote the value of τ where the subcritical

Hopf bifurcation happens by τ_2, then in the small neighborhood to the left of τ_2 bi-stability of limit cycles takes place.

Similar to the case of gamma distribution of order $p = 1$, our numerical simulation suggest that E_+ goes through at most two Hopf bifurcations for all values of α and stable periodic solution created at the first Hopf bifurcation does not undergo any bifurcations except for these that we have mentioned.

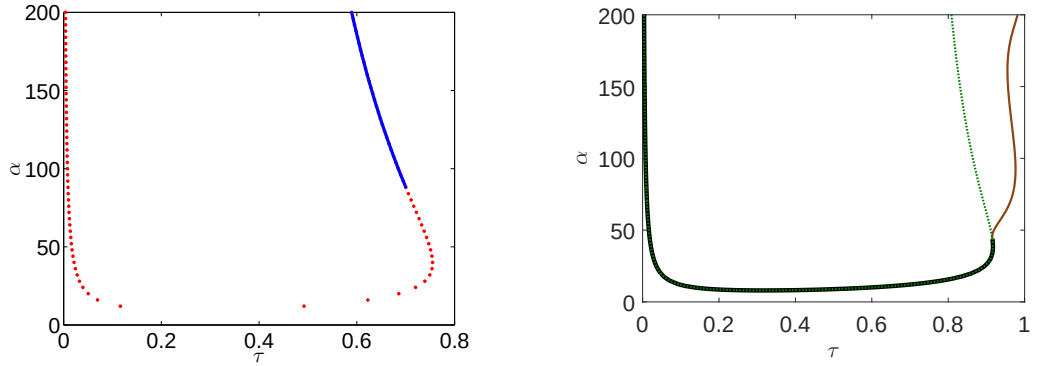

(a) (b)

Figure 3.9: Two-parameter bifurcation diagram in the parameter space $\alpha - \tau$ of system (3.6) with $K = 2$. Figure (a): the delay kernel is given by the gamma distribution of order $p = 2$. Red - supercritical Hopf bifurcation, blue - subcritical Hopf bifurcation. Figure (b): discrete delay, black - supercritical Hopf bifurcation, green - subcritical Hopf bifurcation, brown - saddle node of limit cycles bifurcation.

3.6.3 Uniform distribution

In this section we consider the delay with the uniformly distributed kernel:

$$h(u) = \begin{cases} \frac{\rho}{\tau}, & u \in [\tau(1 - \frac{1}{2\rho}), \tau(1 - \frac{1}{2\rho})], \ \rho > 0 \\ 0, & \text{otherwise.} \end{cases}$$

Therefore, the integral in the equation (3.6c) becomes $\int_{\tau\left(1-\frac{1}{2\rho}\right)}^{\tau\left(1-\frac{1}{2\rho}\right)} x(t-u)y(t-u)e^{-u}\frac{\rho}{\tau}\,\mathrm{d}u$. In order to use numerical bifurcation analysis we applied the linear chain trick to system (3.6).

Set $w(t) = \int_{\tau\left(1-\frac{1}{2\rho}\right)}^{\tau\left(1-\frac{1}{2\rho}\right)} x(t-u)y(t-u)e^{-u}\frac{\rho}{\tau}\,\mathrm{d}u$. Therefore

$$\begin{aligned}\dot{w}(t) &= \int_{\tau\left(1-\frac{1}{2\rho}\right)}^{\tau\left(1-\frac{1}{2\rho}\right)} \frac{\partial}{\partial t}\left(x(t-u)y(t-u)\right)e^{-u}\frac{\rho}{\tau}\,\mathrm{d}u \\ &= -\int_{\tau\left(1-\frac{1}{2\rho}\right)}^{\tau\left(1-\frac{1}{2\rho}\right)} \frac{\partial}{\partial u}\left(x(t-u)y(t-u)\right)e^{-u}\frac{\rho}{\tau}\,\mathrm{d}u\ .\end{aligned}$$

Using integration by parts we obtain

$$\begin{aligned}\dot{w}(t) &= \frac{\rho e^{-\tau}}{\tau}\left(e^{\tau/2\rho}x(t-\tau_1)y(t-\tau_1) - e^{-\tau/2\rho}x(t-\tau_2)y(t-\tau_2)\right) \\ &\quad -\int_{\tau\left(1-\frac{1}{2\rho}\right)}^{\tau\left(1-\frac{1}{2\rho}\right)} x(t-u)y(t-u)e^{-u}\frac{\rho}{\tau}\,\mathrm{d}u\ ,\end{aligned}$$

where

$$\begin{aligned}\tau_1 &= \tau\left(1-\frac{1}{2\rho}\right)\ , \\ \tau_2 &= \tau\left(1+\frac{1}{2\rho}\right)\ .\end{aligned}$$

System (3.6) with the uniform distribution used as the delay kernel becomes

$$\begin{aligned}\frac{\mathrm{d}s}{\mathrm{d}t} &= 1-s(t)-s(t)x(t)\ , \\ \frac{\mathrm{d}x}{\mathrm{d}t} &= x(t)(-1+\alpha s(t)) - x(t)y(t)\ , \\ \frac{\mathrm{d}y}{\mathrm{d}t} &= -y(t)+Kw(t)\ , \\ \frac{\mathrm{d}w}{\mathrm{d}t} &= \frac{\rho e^{-\tau}}{\tau}\left(e^{\tau/2\rho}x(t-\tau_1)y(t-\tau_1) - e^{-\tau/2\rho}x(t-\tau_2)y(t-\tau_2)\right) - w(t)\ ,\end{aligned}$$

where the initial data for s is $s(0)\in\mathbb{R}$, $s(0)\geq 0$, for (x,y), $\phi=(\phi_1,\phi_2)$ is in the Banach space of bounded continuous functions mapping $[-\tau_2,0]$ into $\mathbb{R}^2_+$, equipped with the

uniform norm and $I(0) \in \mathbb{R}$, $I(0) \geq 0$. The complete correspondence to system (3.6) is achieved when $I(0) = \int_0^\infty \phi_1(u)\phi_2(u)e^{-u}h(u)\,\mathrm{d}s$.

The existence condition for E_+ equilibrium is

$$\frac{(\alpha-1)K\rho\left(e^{\tau/2\rho}-e^{-\tau/2\rho}\right)}{\tau e^{\tau}} > 1 \ .$$

While the equation is difficult to solve analytically, from our numerical experiments it follows that, there exists the critical value of α, α_c such that if $\alpha > \alpha_c$, there always exists $\tau_c > 0$ such that E_+ exists and is stable on the interval $(0, \tau_c)$.

We obtained a system with two discrete delays. The system is difficult to analyze theoretically beyond already established results. Therefore, we applied DDE-BIFTOOL to produce numerical bifurcation diagrams using mean delay τ as the bifurcation parameter. In order to facilitate change of τ_1 and τ_2 as τ changes, we used the set up for the state-dependent delay systems. We fixed $K = 2$ and $\rho = 10$. The summary of our findings is depicted on Figure 3.10a.

For the parameter values we selected, the dynamics in the system with the uniformly distributed delay are qualitatively similar to these described in the system with the discrete delay in every respect. For $\alpha_c < \alpha < 8.007$ E_+ is stable while it exists (Figure 3.11a). At $\alpha \approx 8.007$ two supercritical bifurcations appear (an example of such dynamics is captured in Figure 3.11b). Equilibrium E_+ is stable for $0 \leq \tau < 0.03588$, then at $\tau \approx 0.03588$, a pair of complex eigenvalues cross the imaginary axis. As the result, E_+ loses its stability and a stable periodic orbit appears. As τ increases past $\tau \approx 0.8949$ the pair of complex eigenvalues crosses the imaginary axis back, the stable periodic solution disappears and the equilibrium remains stable while it exists. Stable periodic solution while it exists does not undergo any bifurcations.

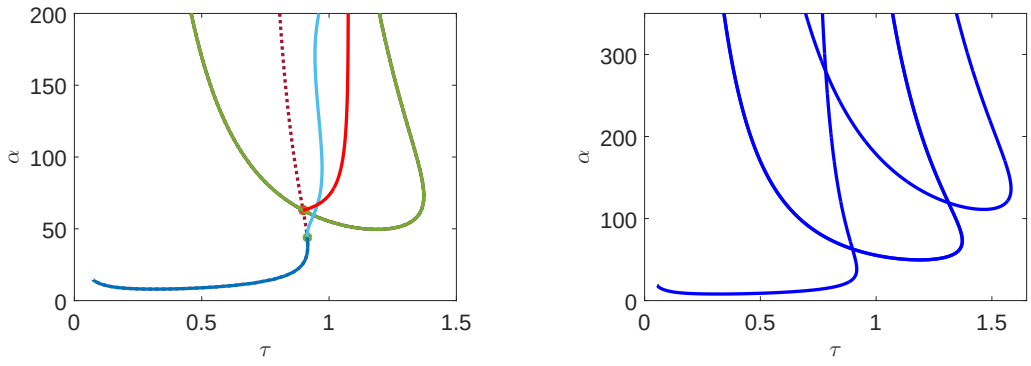

(a) (b)

Figure 3.10: Two-parameter bifurcation diagram in $\tau - \alpha$ space for system (3.6) with the uniform distribution used as the delay kernel with $\rho = 10$ and $K = 2$ showing that as the value of α increases additional pairs of Hopf bifurcations appears. Figure (a): blue and green - supercritical Hopf bifurcations, dotted red - subcritical Hopf bifurcation, blue - saddle node of limit cycles bifurcation, and solid red - torus bifurcation. Figure (b): Hopf bifurcations only.

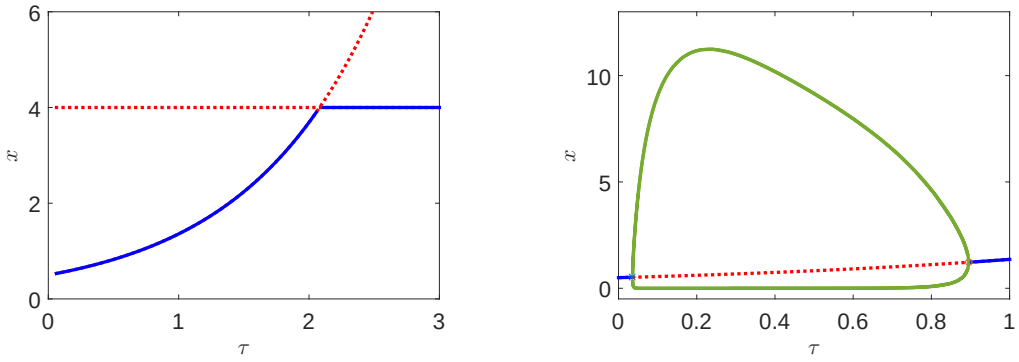

(a) $\alpha = 5$ (b) $\alpha = 25$

Figure 3.11: Bifurcation diagrams for system (3.6) with the uniform distribution used as the delay kernel and $K = 2$, $\rho = 10$ showing the change in bifurcation dynamics as α increases. Figure (a): E_+ is stable while it exists. Figure (b): equilibrium E_+ loses stability at $\tau \approx 0.03588$ and restabilizes at $\tau \approx 0.8949$.

Once α reaches 44.05 the rightmost supercritical Hopf bifurcation goes through a Bautin bifurcation and changes to subcritical and a saddle node of limit cycles bifurcation appears. An example of such dynamics is depicted on the Figure 3.12a.

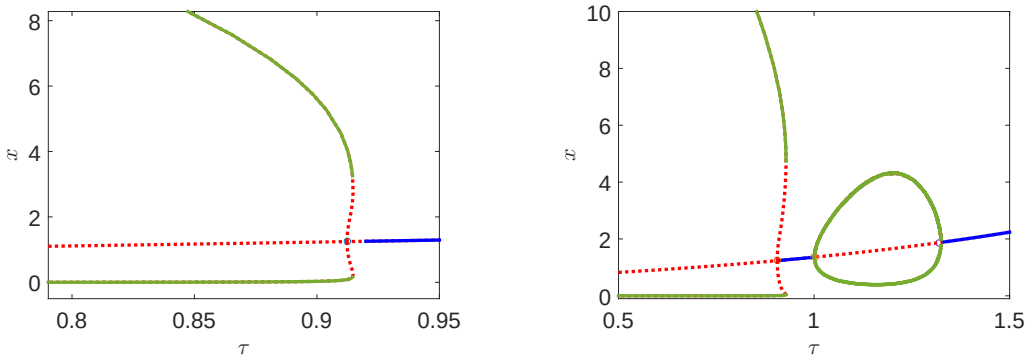

(a) $\alpha = 47$ (b) $\alpha = 55$

Figure 3.12: Bifurcation diagrams for system (3.6) with the uniform distribution used as the delay kernel and $K = 2$, $\rho = 10$ showing the change in bifurcation dynamics as α increases. Figure (a): the rightmost Hopf bifurcation goes through a Bautin bifurcation and changes from supercritical to subcritical at $\alpha \approx 44.05$. Figure (b): a second set of supercritical Hopf bifurcations appears.

At $\alpha = 49.59$ a second pair of supercritical Hopf bifurcations appears to the right of the first pair. For the example of dynamics see Figure 3.12b. As the value of α increases, second and third Hopf bifurcations move closer, until they collide in a double-Hopf bifurcation at $\alpha \approx 62.89$ and, as the result, torus bifurcation appears for higher values of α. As α continues to increase past double Hopf bifurcation value, second and third bifurcations switch places (Figure 3.4b). Once the switch happens, the periodic solution born from the second Hopf bifurcation is unstable but restabilizes as τ increases past torus bifurcation of the second periodic solution at $\tau = 1.062$.

The numerical analysis suggests that as the value of α increases further, new pairs of Hopf bifurcations appear (Figure 3.10b). From the diagram we see that the pattern

observed for the first two pairs of Hopf bifurcations repeats in the following pairs. For example, we expect the fourth Hopf bifurcation to switch its criticality as the value of α increases, and fourth and fifth Hopf bifurcations to move closer and eventually switch places in double Hopf bifurcation, giving birth to a torus bifurcation. So far there is no evidence that there is a critical value of α, α_c such that no new Hopf bifurcations are born for $\alpha > \alpha_s$.

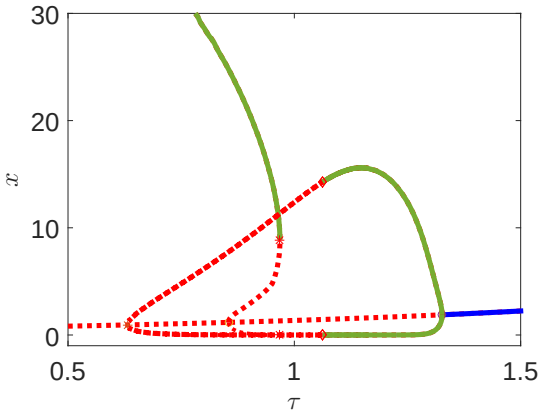

Figure 3.13: Bifurcation diagrams for system (3.6) with the uniform distribution used as the kernel delay and $K = 2$, $\rho = 10$, $\alpha = 110$. Second and third Hopf bifurcations exchange places through a double Hopf bifurcation. As a result, the second periodic orbit undergoes a torus bifurcation at $\tau = 1.063$. The periodic solution born from the second Hopf bifurcation is unstable.

The dynamics we observe in system (3.6) with the uniform distribution is identical to that observed in the discrete delay system. Selecting α as the secondary parameter we observe that the order of appearance of bifurcations of both co-dimension 1 and 2 at E_+ is exactly the same.

3.6.4 Work currently in progress

Now we turn our attention to the latest results concerning the bifurcation dynamics of system (3.6) with discrete delay, for which we have not investigated other systems yet. While the results are not complete, they are strongly suggestive of several interesting phenomena.

We fixed $\alpha = 100$ and produced corresponding bifurcation diagram (Figure 3.14b), using τ as a bifurcation parameter. We discovered, that the unstable periodic solution emanating from third from the left Hopf bifurcation undergoes two period doubling bifurcations as τ decreases.

Consider Figure 3.14a. As α increases from 94.74 we detect two period doubling bifurcations. Our diagram indicates that if α is such that these are possible, then only one torus bifurcation takes place. Therefore, for these values, it is important to investigate the mechanism of birth of torus as τ increases (or equivalently, death of torus as τ decreases).

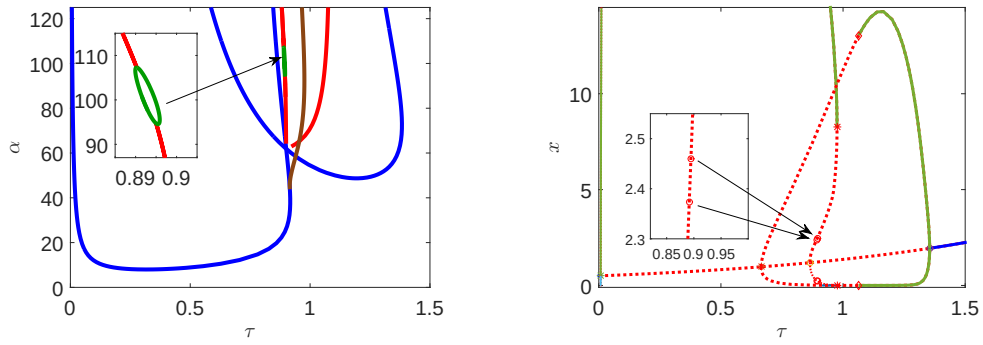

(a) (b)

Figure 3.14: System (3.6) with discrete delay and $K = 2$. Figure (a): two-parameter bifurcation diagram in $\alpha - \tau$ space. Blue - Hopf bifurcation, red - torus bifurcation, green - period doubling bifurcation. Figure (b): bifurcation diagram with $\alpha = 100$. Inset: two period doubling bifurcations.

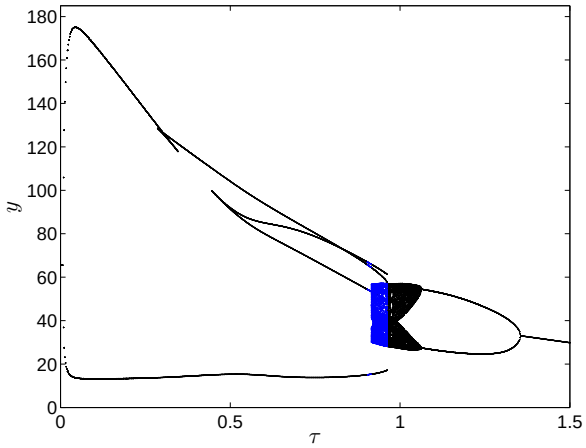

Figure 3.15: Orbit diagram for system (3.6) with discrete delay and $K = 2$, $\alpha = 100$ showing the existence of a range of values of τ with bi-stability in the system. Blue portion of the curve was obtained using different initial data than the black portion of the curve.

Finally, orbit diagram depicted on Figure 3.15 shows that the torus attractor remains stable and exists at the same time as the larger amplitude periodic solution that is born through the saddle node bifurcation.

3.7 Conclusion

In this section we studied the dynamics of predator-prey system in the chemostat with distributed delay. We established properties of the system such as positivity and boundedness, and conditions for global asymptotic stability of some equilibria for the general delay. We confirmed and extended results for the system with discrete delay established by Fan and Wolkowicz [3].

We were particularly interested in the dynamics when E_+ exists. We showed that solutions with positive initial data remain positive for all time. Moreover, we determined the set of initial data such that the solutions eventually become positive and

are uniformly persistent. We established that for each (α, K) there exists a range of values of τ for which E_+ is locally asymptotically stable. We gave a conservative approximation of this region with the help of Rouche's theorem.

We then considered the dynamics of the system using particular types of the delay distribution: Dirac delta, gamma of order $p = 1$ and $p = 2$, and uniform. The bifurcation software available does not accept distributed delay systems. Therefore we used the linear chain trick to convert the gamma distribution systems into ordinary differential equations systems and uniform distribution system into a discrete delay system.

In the system with the Dirac delta distribution, Fan and Wolkowicz recognized that α is a secondary parameter for most bifurcations at E_+. We conducted numerical analysis of the other systems using α in the same role.

We gave the conditions of occurrence of Hopf bifurcations at E_+ for the systems with gamma distribution of order $p = 1$ and $p = 2$. With the help of these conditions, we calculated the precise region of stability of E_+. The bifurcation analysis showed that the lower order gamma distribution systems have several features that distinguish them from the discrete delay system. In the discrete delay system as the secondary parameter α increases, new pairs of Hopf bifurcations can potentially appear as τ changes. Moreover, for sufficiently large α second Hopf bifurcation changes from supercritical to subcritical. In the gamma distribution system we never witnessed E_+ undergo more than two Hopf bifurcations. Since there at most two Hopf bifurcations, we do not expect that a torus bifurcation appears for any value of α. For the gamma distribution of order 1, both Hopf bifurcations remain supercritical for all values of α. For small enough α both of the bifurcations are supercritical. However, as α increases, rightmost Hopf bifurcation changes from supercritical to subcritical and saddle node of limit cycles bifurcation is observed. We hypothesize that for the systems with gamma of order $p = 3$ and higher, Bautin bifurcations will also take place.

On the other hand, the system with the uniform distribution showed bifurcation dynamics identical to the dynamics of the discrete delay system, preserving the order of appearance of every local bifurcation at E_+ of dimension 1 and 2. So far, our investigations lead us to believe that the bifurcation dynamics for the system with uniform distribution will also repeat the dynamics of the discrete delay system.

Our investigations showed that the dynamics for the system with discrete delay are very rich and it is important to investigate the system further.

Chapter 4

Discussion

In this thesis we considered two predator prey models: Gause-type and chemostat. In both models we selected all functional responses to be Holling type I. Without the delay both of the models are known for the absence of the sustained oscillatory dynamics, as all solutions converge to one of the equilibria. We incorporated distributed delay in the models to represent the time that passes between the predator capturing prey and its subsequent conversion to viable predator biomass. We studied the properties of the systems with unspecified delay distributions, as well as compared similarities and differences in the bifurcation dynamics for various kernel delay distributions. The main interest is the possible dynamics when the coexistence equilibrium exists.

Fan and Wolkowicz (in [3], [4]) studied the dynamics of predator-prey models, Gause and in the chemostat, with discrete delay. They established the necessary conditions for stability switches at the coexistence equilibrium E_+. They showed that in the Gause predator-prey model the characteristic equation at E_+ can have at most one pair of pure imaginary roots, while in the chemostat model it is possible to have a set of parameters so that characteristic equation has two pairs of pure imaginary roots. Thus, double Hopf bifurcations are possible.

In their numerical simulations for the Gause-type predator-prey model, they showed that as a secondary control parameter (death rate of the predator) varies, a stable periodic solution can go through a number of subsequent bifurcations.

In our work with the distributed delay we compared the observed dynamics generated by various distributions with dynamics generated using a discrete delay. We also extended the numerical bifurcation analysis for the systems with discrete delay using DDE-BIFTOOL, to be able to systematically describe the development of bifurcation dynamics, as a secondary control parameter changes.

We showed that solutions of the Gause-type model with the distributed delay with non-negative initial data remain non-negative and bounded. Moreover, solutions with positive initial data, remain positive.

We established that in both systems, given a non-specified delay kernel, if equilibrium E_+ exists, then it is stable when the mean delay $\tau = 0$. Stability switches, if they occur, happen through Hopf bifurcations as τ increases. In both models, we approximated region of stability of E_+ when it exists. To get further insight into the system dynamics when E_+ exists, we considered particular types of distributions such as the Dirac delta, gamma and uniform distributions.

For both the Gause predator-prey and the chemostat predator-prey models, for the gamma distribution of lower order ($p = 1, 2$ for Gause-type and $p = 1$ for chemostat), we established analytic conditions necessary for two stability switches at E_+ and thus were able to describe the region of stability of the coexistence equilibrium with respect to parameters d and τ, and α and τ, respectively. Following that, using numerical bifurcation analysis, we discovered that these regions had a similar shape across all distributions for each model.

In the Gause-type predator-prey model we established that rich bifurcation dynamics depends not only on the primary bifurcation parameter, τ but is also subject

to the secondary parameter, d. For all the delay distributions we worked with, it was established that it is possible to select a value of d such that coexistence equilibrium E_+ is stable whenever it exists. On the other hand, for sufficiently small values of d, E_+ undergoes at least two Hopf bifurcations. E_+ loses stability at the first Hopf bifurcation and re-stabilizes at the last Hopf bifurcation. Once the equilibrium restabilizes, it remains stable until the transcritical bifurcation at which it disappears from the positive cone.

Fan and Wolkowicz [4] showed that in the Gause-type system, as d decreases new pairs of Hopf bifurcations appear and they are "nested", i.e. their locus forms non-intersecting "bubbles". Given sufficiently small d, a stable periodic orbit can undergo a number of bifurcations such as a saddle node of limit cycles and a cascade of period doubling bifurcations. Finally, for small enough d, a chaotic attractor is possible.

While local bifurcation dynamics across different distributions had some common motifs, overall, there were a number of differences.

In the Gause-type system with uniform distribution, we observed that the bifurcation dynamics were very similar to the dynamics in the discrete delay system, including period doubling bifurcations and the appearance of a chaotic attractor. For both types of distribution, we observed that as d decreases, new pairs of Hopf bifurcations appear at E_+. There are only two stability switches, and pairs of Hopf bifurcations form concentric "bubbles", thus ruling out the possibility of double Hopf bifurcation.

For the Gause-type system with both the uniform distribution and Dirac delta distribution, the stable periodic solution born from the left-most Hopf bifurcation, undergoes a number of subsequent bifurcations (provided the value of the parameter d is sufficiently small), including two saddle node of limit cycles bifurcations, followed by period doubling bifurcations. When d is sufficiently small, as τ increases there is a cascade of period doubling bifurcations on what appears to be the route to chaos,

followed by a cascade of period halving bifurcations. For sufficiently small d, although varying τ results in a chaotic attractor in both cases, the path from chaos to re-stabilization as τ increases is different. In the discrete delay case, as τ decreases from the rightmost Hopf bifurcation, the stable periodic solution undergoes a cascade of period doubling bifurcations. However, in the case of the uniform distributed delay, as τ decreases, a stable periodic solution undergoes a period doubling bifurcation, followed by a period-halving bifurcation. This is followed by a pair of saddle node of limit cycle bifurcations. Then as τ decreases further there is a cascade of period doubling bifurcations that appears to lead chaos.

Finally, we observed that in the Gause-type system for both the uniform distribution and the Dirac delta distribution for a certain set of parameters, as τ increases from the leftmost Hopf bifurcation, the stable periodic solution born from it undergoes a second pair of period doubling bifurcation so that the stable periodic solution loses the stability at the first and re-stabilizes at the second.

On the other hand, bifurcation analysis of the Gause-type predator-prey system with the gamma distribution (particularly of lower order) showed a number of differences compared to the dynamics of the system with discrete delay. The number of Hopf bifurcations that E_+ can undergo is bounded by $p + 2$. Moreover, in both our numerical experiments and in our two-parameter bifurcations diagrams, we never observed more than two. We also witnessed that for the gamma distribution of order $p = 1$ and $p = 2$, as d decreases, the rightmost Hopf bifurcation undergoes a Bautin bifurcation and changes from supercritical to subcritical. As a result, the stable periodic solution undergoes a saddle-node of limit cycles bifurcation. This is different from the dynamics of the discrete delay and uniform distribution, where both outer Hopf bifurcations are supercritical for all values of d considered. For the gamma distribution with higher orders no Bautin bifurcations were observed.

Aside from the aforementioned saddle node of limit cycle bifurcation, for the gamma

distribution with lower orders, the bifurcation dynamics of the stable periodic solution is uneventful, compared to the discrete delay and uniform distribution systems: the periodic solution is stable when it exists. However, as p increases to 32, the stable periodic solution undergoes two period doubling bifurcations, losing stability at the first one and re-stabilizing at the second. As p increases and d decreases, more period doubling bifurcations occur. These bifurcations are characterized by the Floquet multipliers re-entering the unit circle in the reverse order they left it. Further decrease in d causes the two saddle node of limit cycles bifurcations to occur, prior to the cascade of period doubling bifurcations. This is similar to the dynamics of the discrete delay and uniform distribution systems.

The incorporation of different delay distributions in the chemostat model produced an effect similar to the Gause-type predator-prey model: the uniform distribution produces bifurcation dynamics identical to those of the system with the discrete delay, while the gamma distribution (in particular of low order) causes far simpler dynamics. We used τ as primary bifurcation parameter and α as a secondary parameter.

In general, we observed that as α increases the bifurcation dynamics of the system at E_+ becomes richer. Both uniform distribution and discrete delay system can have infinitely many Hopf bifurcations at the coexistence equilibrium E_+. Systems with the gamma distribution have an upper bound on the possible number of Hopf bifurcations. However, for every type of the distribution that we considered, Hopf bifurcations appear in pairs, which is similar to the Gause-type system. For every delay distribution that we worked with, it is possible to select a small enough value of α such that equilibrium E_+ is stable while it exists. As α increases, two supercritical Hopf bifurcations appear as τ increases from zero. As τ increases from 0, E_+ loses the stability through the first and re-stabilizes through the second. In the cases of discrete and uniform distributions, for an even larger value of α, there is a value of τ at which there is a Bautin bifurcation. Above this value of α, the rightmost Hopf

bifurcation is subcritical instead of supercritical. As well, a saddle node of limit cycles occurs. However, for the gamma distribution systems of order $p = 1$ and $p = 2$, the Hopf bifurcation remains supercritical. Further increase of α, in the discrete delay and uniform distribution systems, causes a second pair of supercritical Hopf bifurcations to appear to the right of the first pair. In the system with the gamma distribution we did not observe new pairs appearing as the response to increase of α increased. Neither did our two-parameter bifurcation diagrams indicate that there is a critical value of α, so that a second pair of Hopf bifurcations appears. We can not say anything for the higher order gamma distributions. However, for $p = 1$ and $p = 2$, the bifurcation analysis did not exhibit any other interesting dynamics.

In the discrete delay and uniform distribution systems, as α increases, two middle Hopf bifurcation get closer, until they switch places in the double Hopf bifurcation, giving birth to the torus bifurcation. As our numerical simulations indicate, further increase of α causes the appearance of new pairs of Hopf bifurcations to the right of the existing ones and subsequent movement towards each other, we anticipate the appearance of new double Hopf bifurcations and corresponding torus bifurcations.

Both Gause-type and chemostat predator-prey systems possess equilibria corresponding to one or more species dying out and one equilibrium corresponding to the coexistence of species. In the absence of the coexistence equilibrium, the solutions tend to one of the remaining equilibria (based on parameter values). This is the dynamic common to all delay distributions, including Dirac delta, and is identical to the dynamics of the ordinary differential equations system in the absence of the coexistence equilibrium.

Once the coexistence equilibrium appears, the dynamics becomes rich. There are a number of differences and similarities in the two models. We have shown that if coexistence equilibrium exists, solutions that eventually become positive, will remain positive for the rest of time and that these solutions are not attracted to the equilibria

corresponding to extinction of at least one species.

In both models, for all types of the delay distribution that were considered, we discovered that the rich bifurcation dynamics is not only subject to change in the mean delay but also depends on the second parameter. It is possible to select a value of the secondary parameter, so that the coexistence equilibrium is locally asymptotically stable while it exists. Another common feature, shared by the local bifurcation dynamics of both models is that Hopf bifurcations when they appear, always appear in pairs corresponding to eigenvalues crossing the imaginary axis in two directions, i.e. as the mean delay becomes sufficiently large, the coexistence equilibrium eventually restabilizes. In both models, for each distribution considered, there is a subset of parameters such that there exists a range of mean delay values, where as τ changes the amplitude of the periodic solutions has negligible changes.

Uniform delay distribution results in the dynamics of the system identical to the discrete delay system. However, for the lower order gamma distribution the bifurcation dynamics is much simpler.

For the delay distributions where E_+ can undergo more than one pair of Hopf bifurcations, the placement of bifurcations is different in the two models. In the standard predator-prey model, the newly appearing Hopf bifurcations appear between the last pair of Hopf bifurcations that appeared prior and give rise to the unstable periodic solution, which never re-stabilizes. The distance between any of the Hopf bifurcations does not decrease as d decreases, thus ruling out the possibility of double Hopf bifurcation and torus bifurcations. This follows from analytic results of Fan and Wolkowicz [4], who showed that the characteristic equation can have at most one pair of pure imaginary roots. Additionally, all of the Hopf bifurcations remain supercritical.

In the chemostat predator-prey model, the Hopf bifurcations occur in pairs and these can overlap, rather than occur in concentric "bubbles", as in the predator-prey

model. Thus, if all other parameters except τ are fixed, the coexistence equilibrium point can re-stabilize and then destabilize again in a subsequent Hopf bifurcation as τ increases. For each pair of Hopf bifurcations, on each branch, as both τ and α increase, the criticality changes from supercritical to subcritical in a Bautin bifurcation, and as well double Hopf bifurcations occur. Thus we also see torus bifurcations.

Overall, local and global dynamics are richer in the chemostat model, due to the possibility of characteristic equation having two pairs of pure imaginary roots, and as a result, the possibility of double Hopf bifurcations and torus bifurcations. Although, in the predator-prey model, for certain distributions, we witnessed that the stable periodic solution goes through a cascade of period doubling bifurcations that can lead to chaos, this was not seen in the chemostat. In the chemostat model, so far we observed the appearance of only two period doubling bifurcations as τ varied. Therefore, it is likely, that the path to chaos (if it happens) will be through the destruction of tori. Similarly, while both models can have a pair of saddle node of limit cycles bifurcation, for similar types of distributions, the location and mechanism through which they appear will be different.

Appendices

Appendix A

Code listing

A.1 Calculation of the stability region of E_+ for the predator-prey model (2.5) with "weak" kernel

In this section we provide the MATLAB script used to produced 3-dimensional following of Hopf bifurcation in $d - Y - \tau$ space in system (2.5).

```
clear all;
i=1;
syms a;
%create mesh of Y values
for y=0.1:0.0025:1
%create mesh of d values such that local extrema of k(a)
%are real and positive
for d=0.0025:0.00125:(y^2+5*(y^3)-(y^2)*sqrt(15*(y^2)+9*y))/(10*(y^2)+y+1)
%check if for a given pair (Y,d(Y)) there is a possibility of two distinct
% values of a that will give rise to pure imaginary roots of
```

```
% charactristic equation
%check whether condition necessary for k(a) to have two positive real
% roots holds
if (-(d/y+5*d-y)+sqrt((d/y+5*d-y)^2
-3*(3*(d^2)/y+5*d^2)))*(6*(3*(d^2)/y+5*d^2)-2*(d/y+5*d-y)^2)/3
+18*(d^3)/y-(d/y+5*d-y)*(3*(d^2)/y+5*d^2)<=0
%Here g stands for k(a)
g=(a^3)/y+(a^2)*(5*d/y+d/(y^2)-1)+a*(3*(d^2)/(y^2)+5*(d^2)/y)+2*(d^3)/y^2;
eqn=g==0;
%solve g=0 to find critical values of a
temp=sort(vpasolve(eqn,a));
if ~isempty(temp)
for j=1:1:length(temp)
if temp(j)>0 && isreal(temp(j))
Res(i,1)=y;
Res(i,2)=d;
%we record tau rather than a for more meaningful plots
Res(i,3)=1/temp(j);
i=i+1;
end
end
end
else % for a given pair (d,Y) E_+ is stable while it exists
Res(i,1)=y;
Res(i,2)=d;
Res(i,3)=NaN;
i=i+1;
end
```

```
end
end
%plot Y vs d vs tau
plot3(Res(:,1),Res(:,2),Res(:,3),'r.');
xlabel('Y');
ylabel('d');
zlabel('\tau');
```

A.2 Two-parameter following of Hopf bifurcations for the predator-prey model (2.5) with discrete delay:

The following script follows the first three pairs of Hopf bifurcations in (τ, d) space in system (2.5). Recall that the outermost bifurcations are the ones where E_+ loses and regains its stability. However, if value of d is sufficiently low we can get additional 'nested bubbles' connecting Hopf bifurcations. This script is written to follow the first 3 pairs of Hopf bifurcations but can be easily extended to follow more bifurcations. We fix $Y = 0.6$.

```
close all; clear all;
k=1;
Y=0.6;
syms tau;
figure;
%for vpa solver we needed to provide a guess to find root furthest from 0
%we provide three guesses for the three pairs of Hopf bifurcations
guess=3000;
```

```
guess2=guess-50;
guess3=guess2-50;
cont=true;
cont2=true
i=1;
%create range of values of d
for d=0.001:0.0005:0.07
%calculate imaginary part of the eigenvalue
omega1=sqrt(0.5*(-(d*exp(d*tau)/Y)^2+sqrt((d*exp(d*tau))^4
+(d^2)*(12*(d^2)*exp(2*d*tau)/(Y^2)-16*d*exp(d*tau)/Y +4))));
%find values of tau where characteristic equation has pure imaginary roots
p=d*(1+exp(d*tau)/Y);
q=-d;
c=d*(1-2*exp(d*tau)/Y);
alpha= (d^2)*exp(d*tau)/Y;
f1=tau*omega1;
xpl=d*exp(d*tau)/Y;
h2=((omega1^2)*(1+d-xpl)-(1-2*xpl)*d*xpl)/(d*((1-2*xpl)^2+omega1^2));
theta1=acos(h2);
eqn=f1==theta1;
temp=vpasolve(eqn,tau);
temp2=vpasolve(eqn,tau,guess)
for j=1:1:length(temp)
if isreal(temp(j))
plot(temp(j),d,'b.');hold on
Res(i,1)=temp(j);
Res(i,2)=d;
i=i+1;
```

```
end
end
for j=1:1:length(temp2)
if isreal(temp2(j))
plot(temp2(j),d,'b.');hold on
Res(i,1)=temp2(j);
Res(i,2)=d;
i=i+1;
end
end
if length(temp2)==1
guess=temp2;
end
%second set of potential Hopf bifurcations
if cont
theta2=theta1+2*pi;
eqn2=f1==theta2;
temp=vpasolve(eqn2,tau);
temp2=vpasolve(eqn2,tau,guess2)

for j=1:1:length(temp)
if isreal(temp(j))
plot(temp(j),d,'g.');hold on
end
end
for j=1:1:length(temp2)
if isreal(temp2(j))
plot(temp2(j),d,'g.');hold on
```

```
end
end
if length(temp2)==1
guess2=temp2;
end
if (length(temp)==0) || (length(temp2)==0)
cont=false;
end
end
%third set of potential Hopf bifurcations
if cont2
theta3=theta2+2*pi;
eqn3=f1==theta3;
temp=vpasolve(eqn3,tau);
temp2=vpasolve(eqn3,tau,guess3)

for j=1:1:length(temp)
if isreal(temp(j))
plot(temp(j),d,'r.');hold on
end
end
for j=1:1:length(temp2)
if isreal(temp2(j))
plot(temp2(j),d,'r.');hold on
end
end
if length(temp2)==1
guess3=temp2;
```

```
end
if (length(temp)==0) || (length(temp2)==0)
cont2=false;
end
end
end
```

A.3 First Lyapunov coefficient calculation for the predator-prey model (2.5) with gamma distributed delay

We used a method for calculation of the Lyapunov first coefficient of the system's normal form at Hopf bifurcation described in [33].

System (2.5) with "weak" kernel delay distribution after application of linear chain trick:

$$\frac{\mathrm{d}x(t)}{\mathrm{d}t} = x(t)(1 - x(t)) - x(t)y(t) \ , \tag{A.1a}$$

$$\frac{\mathrm{d}y(t)}{\mathrm{d}t} = -dy(t) + Yz(t) \ , \tag{A.1b}$$

$$\frac{\mathrm{d}z(t)}{\mathrm{d}t} = ax(t)y(t) - (a+d)z(t) \ . \tag{A.1c}$$

System (A.1) can be represented as $\dot{X} = AX + F(X)$, where $X = [x(t), y(t), z(t)]^T$ and $F(X) = [f_1(X), f_2(X), f_3(X)]^T$.

Denote by τ_c ($\tau = \frac{1}{a}$) the value of τ where the system undergoes Hopf bifurcation. We have earlier shown a_c is the root of

$$k(a) = a^3 + \left(\frac{d}{Y} + 5d - Y\right)a^2 + \left(\frac{3d^2}{Y} + 5d^2\right)a + \frac{2d^3}{Y} = 0 \ . \tag{A.2}$$

The eigenvalue corresponding to the critical value of τ is the root of $\omega^2 = \frac{a_c+2d}{a_c}\frac{d(a_c+d)}{Y}$.

Kuznetsov (see [33], Section 5.4.3) gives the following equation for the first Lyapunov coefficient:

$$\begin{aligned} l_1 &= \frac{1}{2\omega} Re[< p, C(q,q,\bar{q}) > -2 < p, B(q, A^{-1}B(q,\bar{q})) > \\ &\quad + < p, B(\bar{q}, (2iI_n - A)^{-1} B(q,q)) >]. \end{aligned} \tag{A.3}$$

Here, A is the Jacobian matrix of the system evaluated at $E_+ = (x^*, y^*, z^*)$:

$$\begin{bmatrix} -x^* & x^* & 0 \\ 0 & -d & Y \\ ay^* & ax^* & -(a+d) \end{bmatrix},$$

q is the eigenvector of A corresponding to the eigenvalue $i\omega$, p is the adjoint eigenvector (i.e. $A^T p = -i\omega p$), normalized so that scalar product $< p, q >= \sum_{j=1}^{3} \bar{p}_j q_j = 1$, I_3 is a 3×3 identity matrix.

Finally, B and C are multi-linear functions that are defined by

$$B_i(x,y) = \sum_{j,k=1}^{3} \frac{\partial^2 F_i(\xi)}{\partial \xi_j \partial \xi_k}\Big|_{\xi=E_+},$$

$$C_i(x,y) = \sum_{j,k,l=1}^{3} \frac{\partial^3 F_i(\xi)}{\partial \xi_j \partial \xi_k \partial \xi_l}\Big|_{\xi=E_+}.$$

Note that for system (A.1), $F(X)$ is at most quadratic, therefore $C(x,y) = [0,0,0]^T$. On the other hand,

$$B(x,y) = \begin{bmatrix} -2x_1y_1 - x_1y_2 - x_2y_1 \\ 0 \\ ax_1y_2 + ax_2y_1 \end{bmatrix}.$$

We used the following set of functions to calculate the first Lyapunov coefficient for each point of Hopf curve in two-parameter following.

A.3.1 cprod.m

```
function [ res ] = cprod( a,b )
%input: complex vectors and b, assumed of equal dimensions n by 1
%output: dot product of a and b
res=sum(conj(a).*b);
end
```

A.3.2 evalB.m

```
function [B] = evalB(x,y,a)
%input: x,y: 3x1 vectors
%         a: scalar, critical value of bifurcation parameter
%output: B(x,y): 3x1 vector
B(1,1)=-2*x(1)*y(1)-x(1)*y(2)-y(1)*x(2);
B(2,1)=0;
B(3,1)=a*x(1)*y(2)+a*x(2)*y(1);
end
```

A.3.3 Main.m

The script returns two parameter following of Hopf bifurcations with criticality marked, red stands for supercritical, blue for subcritical. We fixed $Y = 0.6$.

```
clear all;
Y=0.6;
syms a;
syms D;
figure;
```

```
l=1;
for d=0.001:0.001:0.0.05
%x-component of the coexistence equilibrium
xstar=d*(d+a)/(Y*a);
%g(a) is the condition on a for the existence of Hopf bifurcation
g=(a^3)/Y+(a^2)*(5*d/Y+d/(Y^2)-1)+a*(3*(d^2)/(Y^2)+5*(d^2)/Y)+2*(d^3)/Y^2;
eqn=g==0;
%find roots of g(a) that could be critical values of a
temp=sort(vpa(vpasolve(eqn,a)));
for j=1:1:length(temp)
if temp(j)>0 && isreal(temp(j))
%record (a,d)-values for the two parameter following
Res(l,1)=double(temp(j));
Res(l,2)=d;
A=Res(l,1);
XSTAR=D*(a+D)/(Y*a);
%Jacobian of the system
J1=[-XSTAR,-XSTAR,0; 0, -D, Y;a*(1-XSTAR),a*XSTAR,-(D+a)];
%calculation of pure imaginary eigenvalue
omega1=sqrt((a+2*D)*D*(a+D)/(Y*a));
%eigenvector of jacobian
q1=[-Y*XSTAR*(XSTAR-omega1*i)/(XSTAR^2+omega1^2);Y;D+omega1*i];
%eigenvector of transposed jacobian corresponding to -omega i
p1=[Y*a*(1-XSTAR)*(XSTAR+omega1*i);
(XSTAR^2+omega1^2)*(a+D-omega1*i);(XSTAR^2+omega1^2)*Y;];
k=1/sum(p1.*conj(q1));
%normalizing p
p1=p1*k;
```

```
J=vpa(subs(J1,[a,D],[A,d]));
p=vpa(subs(p1,[a,D],[A,d]));
q=vpa(subs(q1,[a,D],[A,d]));
omega=vpa(subs(omega1,[a,D],[A,d]));
%for each pait (a,d) we calculate Lyapunov exponent
L1=real(-2*cprod(p,evalB(q,J\evalB(q,conj(q),A),A))+
cprod(p,evalB(conj(q),(2*omega*i*eye(3)-J)\evalB(q,q,A),A)))
/(2*omega);
Res(l,3)=L1;
l=l+1;
end
end
end
%comnvert a to tau
Res(:,1)=1./Res(:,1);
Res=sortrows(double(Res));
subcrind=find(Res(:,3)>0);
plot(Res(:,1),Res(:,2),'.r');
hold on;
plot(Res(subcrind,1),Res(subcrind,2),'b.');
xlabel('$$\tau$$');
ylabel('$$d$$');
```

A.4 Approximation of the region of stability of E_+ for general delay in the predator-prey model in chemostat (3.6)

```
clear all;
close all;
%maximum value of alpha in the mesh
alphamax=100;
alpharange=10:1:alphamax;
%values of x-component of coexistence equilibriun
X=[0:(alphamax-1)/100:alphamax-1];
%create plot matrx x on x-axis, alpha on y axis
[PALPHA,PX]=meshgrid(alpharange,X);
%we create mesh of points, some of which we will mark for plotting
plotmatr=[PX(:) PALPHA(:)];
%matrix that has flag denoting whether E+ is stable
stabilmatr=zeros(length(alpharange),length(X));
% We will populate rows of stabil matr with indication where xstar is
% stable, each row corresponds to the value of alpha
l=1;
for alpha=alpharange
%coefficients of quadratic equation mentioned in the last paragraph
b1=arrayfun(@(x)-2*alpha*x/(1+x)+2*x+x^2,X);
b0=arrayfun(@(x)(alpha^2)*(x-1)/(x+1)-(x+1)^2+2*alpha,X);
%discriminant of quadratic
delta=b1.^2-4*b0;
%largest root of quadratic
```

```
yc2=(-b1+sqrt(delta))*0.5;
%minimum condition for existence of E+
c0=find(X<alpha-1);
%condition one
c1=find(b0>0);
c2=find(delta<=0);
C1=intersect(intersect(c1,c2),c0);
stabilmatr(l,C1)=1;
%OR condition two
c3=find(delta>00);
c4=find(yc2<0);
C2=intersect(intersect(intersect(c1,c3),c4),c0);
stabilmatr(l,C2)=1;

plotmatr(1+(l-1)*length(X):length(X)+(l-1)*length(X),3)=stabilmatr(l,:);
l=l+1;

end
figure(2);
plotind=find(plotmatr(:,3)==1);
plot(plotmatr(plotind,1),plotmatr(plotind,2),'b.')
xlabel('x');
%code for following of Hopf bifurcation in the weak kernel system.
syms a;

i=1;
syms a;
y=2;
```

```
guess= 0.1;
for alpha=1:1:100
b=3+a+(a+1)/(y*a);
c=alpha*(a+1)/(y*a+a+1)+a+2+(a+1)*(a+2)/(y*a);
f= alpha*(a+1)*(y*a+a+2)/(y*a+a+1)-a-1;
h=(a+1)*(alpha*y*a-y*a-a-1)/(y*a);%((a+1)^2)*(y-1)/(y*(y*a+a+1));
g=f^2-c*b*f+h*b^2;
eqn=g==0;
temp=sort(vpasolve(eqn,a));
if ~isempty(temp)
for j=1:1:length(temp)
if temp(j)>0 && isreal(temp(j)) && (1/temp(j)<alpha*y-y-1)

Res(i,1)=alpha;
Res(i,2)=1/temp(j);
Res(i,3)=(temp(j)+1)/(y*temp(j));
i=i+1;
end
end
end

temp2=sort(vpasolve(eqn,a,guess));
if ~isempty(temp2)
for j=1:1:length(temp2)
if temp2(j)>0 && isreal(temp2(j)) && (1/temp2(j)<alpha*y-y-1)
Res(i,1)=alpha;
Res(i,2)=1/temp2(j);
```

```
Res(i,3)=(temp2(j)+1)/(y*temp2(j));
i=i+1;
guess2=1/(5*max(Res(:,1)));
end
end
end
end
hold on;
plot(Res(:,3),Res(:,1),'r.');
ylabel('alpha');
```

A.5 The first Lyapunov coefficient calculation for the predator-prey model in the chemostat with gamma distribution of order $p = 1$

The method is based on the same principles as the method we have previously outlined for the predator-prey model. Function cprod.m is identical to that described in the Section A.3 and therefore, is not reproduced here.

A.5.1 evalB

```
function [B] = evalB(x,y,a,alpha)
%This script evaluates B(x,y), needed for calculation of
%first Lyapounov exponent
%Gamma p=1 Predator prey
%input: x,y: 3x1 vectors
```

```
% a: real positive scalar, critical value of bifurcation parameter
%alpha: real positive scalar
%output: B(x,y): 3x1 vector
B(1,1)=-x(1)*y(2)-x(2)*y(1);
B(2,1)=alpha*(x(1)*y(2)+x(2)*y(1))-x(2)*y(3)-x(3)*y(2);
B(3,1)=0;
B(4,1)=a*(x(2)*y(3)+y(2)*x(3));
end
```

A.5.2 imageigvs.m

This function takes symmetrical matrix A as the input and returns eigenvector q corresponding to the pure imaginary eigenvalue $i\omega$ of A as well as adjunct eigenvector p. Vectors q and p are normalized so that the dot product $< p, q >= 0$.

```
function [q,p] = imageigvs( A )
%This fuction returns eigen vector corresponding to pure imaginary eigenvalue
%as well as its adjoint
% input: A: 3x3 matrix
%output: q - 3x1 eigenvector corresponding to pureimaginary eigenvalue
%p: 3x1 eigenvector of A^T corresponding to -\lambda
%\lambda=omega i, Aq=\lambda q
%A^T p=-\lambda p
%q and p normalised so that their dot product is 1
%warning : sometimesl tolerance needs to be higher
tol=1e-15;
[V1,D1]=eig(A);
eigenvals1=diag(D1);
```

```
pureimag1=find((abs(real(eigenvals1))<tol).*(imag(eigenvals1)>0));
q=V1(:,pureimag1(1));
Atrans=A';
[V2,D2]=eig(Atrans);
eigenvals2=diag(D2);
pureimag2=find((abs(real(eigenvals2))<tol).*(imag(eigenvals2)<0));
p=V2(:,pureimag2(1));
%k=conj(1/dot(conj(p),q));
k=1/sum(p.*conj(q));
p=p*k;
end
```

A.5.3 Main.m

```
close all; clear all;
K=2;
syms a;
figure;
guess=1000;
l=1;
for alpha=12:4:400
x=(1+a)/(K*a);
%calculate coefficients for k(a)
a3=(a*x+x^2+a+4*x+3)/(1+x);
a2=(-K*a*x^2-K*a*x+a*x^2+3*a*x+alpha*x+2*x^2+2*a+5*x+3)/(1+x);
a1=(-K*a*x^3+K*a*alpha*x-3*K*a*x^2-2*K*a*x+a*alpha*x+a*x^2
+2*a*x+2*alpha*x+x^2+a+2*x+1)/(1+x);
a0=(-K*a*x^3+K*a*alpha*x-2*K*a*x^2-K*a*x+a*alpha*x+alpha*x)/(1+x);
```

```
g=a1^2-a1*a2*a3+a0*a3^2;
eqn=g==0;
temp=sort(vpasolve(eqn,a));
temp2=sort(vpasolve(eqn,a,guess));
for j=1:length(temp)
if (isreal(temp(j)) && temp(j)>0) && (temp(j)>1/(alpha*K-K-1))
Res(l,1)=temp(j);
Res(l,2)=alpha;
A=Res(l,1);
ALPHA=alpha;
XSTAR=(1+A)/(K*A);
%Jacobian
J=[-1-XSTAR,-1/(1+XSTAR),0,0;ALPHA*XSTAR,0,-XSTAR,0;0,0,-1,K;
0,A*ALPHA/(1+XSTAR)-A,A*XSTAR,-(1+A)];
%calculation of pure imaginary eigenvalue
omega1=sqrt(subs(a1/a3,a,A));
%eigenvector of jacobian - checked for correctness
[q,p]=imageigvs(J);
L1=real(-2*cprod(p,evalB(q,J\evalB(q,conj(q),A,ALPHA),A,ALPHA))
+cprod(p,evalB(conj(q),(2*omega1*i*eye(4)-J)\evalB(q,q,A,ALPHA),A,ALPHA)))
/(2*omega1);
Res(l,3)=L1;
l=l+1;

end
end
for j=1:length(temp2)
if (isreal(temp2(j)) && temp2(j)>0)&& (temp(j)>1/(alpha*K-K-1))
```

```
Res(l,1)=temp2(j);
Res(l,2)=alpha;
A=Res(l,1);
ALPHA=alpha;
XSTAR=(1+A)/(K*A);
%Jacobian
J=[-1-XSTAR,-1/(1+XSTAR),0,0;ALPHA*XSTAR,0,-XSTAR,0;0,0,-1,K;
0,A*ALPHA/(1+XSTAR)-A,A*XSTAR,-(1+A)];
%calculation of pure imaginary eigenvalue
omega1=sqrt(subs(a1/a3,a,A));
%eigenvector of jacobian
[q,p]=imageigvs(J);
L1=real(-2*cprod(p,evalB(q,J\evalB(q,conj(q),A,ALPHA),A,ALPHA))
+cprod(p,evalB(conj(q),(2*omega1*i*eye(4)-J)\evalB(q,q,A,ALPHA),A,ALPHA)))
/(2*omega1);
Res(l,3)=L1;
l=l+1;
end
end
end
Resd=double(Res);
Resd(:,1)=1./Resd(:,1);
Resd=sortrows(Resd);
subcrind=find(Resd(:,3)>0);
plot(Resd(:,1),Resd(:,2),'.r');
hold on;
plot(Resd(subcrind,1),Resd(subcrind,2),'b.');
```

A.6 Continuation of Hopf bifurcations in $\alpha-\tau$ space in the predator-prey model in the chemostat (3.6) with the gamma distribution of order $p = 2$

This section contains code necessary to calculate Hopf bifurcation extension for the two-parameter continuation of Hopf bifurcation and subsequent evaluation of the first Lyapunov coefficient of each point of the curve. This code is conceptually similar to the one given previously, save for the Jacobian matrix calculation, calculation of continuation of Hopf bifurcation in two dimension and evaluation of the second derivative of the system.

evalB

```
function [B] = evalB(x,y,a,alpha)
%This script is for evaluation of B(x,y), needed for calculation of
%first Lyapounov exponent
%Gamma p=1 Predator prey
%input: x,y: 3x1 vectors
% a: scalar, critical value of bifurcation parameter
%output: B(x,y): 3x1 vector
B(1,1)=-x(1)*y(2)-x(2)*y(1);
B(2,1)=alpha*(x(1)*y(2)+x(2)*y(1))-x(2)*y(3)-x(3)*y(2);
B(3,1)=0;
B(4,1)=a*(x(2)*y(3)+y(2)*x(3));
B(5,1)=0;
end
```

Main.m

```
clear all;
K=2;
syms a;
l=1;
%from running this multiple times I noticed that no roots found for d
%greater than 0.045
figure;
for alpha=12:4:500
x=(a+1)^2/(K*(a^2));
s=1/(1+x);
y=alpha*s-1;
%calculate coefficients of k(a)
a0=K*a^2*alpha*s*x-K*a^2*x^2-K*a^2*x-a^2*alpha*s+a^2*x*y+a^2*x+a^2*y
-2*a*alpha*s+2*a*x*y+a^2+2*a*x+2*a*y-alpha*s+x*y+2*a+x+y+1;
a1=K*a^2*alpha*s*x-K*a^2*x^2-2*K*a^2*x-2*a^2*alpha*s+a^2*x*y+2*a^2*x
+2*a^2*y-6*a*alpha*s+4*a*x*y+3*a^2+6*a*x+6*a*y-4*alpha*s+3*x*y+8*a+4*x+4*y+5;
a2=-K*a^2*x-a^2*alpha*s+a^2*x+a^2*y-6*a*alpha*s+2*a*x*y+3*a^2+6*a*x
+6*a*y-6*alpha*s+3*x*y+12*a+6*x+6*y+10;
a3=-2*a*alpha*s+a^2+2*a*x+2*a*y-4*alpha*s+x*y+8*a+4*x+4*y+10;
a4=-alpha*s+2*a+x+y+5;
%calculate omega^2, such that \lambda=i \omega is a root of char. equation
om=(a1*a4-a0)/(a3*a4-a2);
eqn1=om^2-a3*om+a1==0;
eqn2=om^2-a2*om/a4+a0/a4==0;
temp1=sort(vpasolve(eqn1,a));
temp2=sort(vpasolve(eqn2,a));
```

```
temp=temp1
for j=1:1:length(temp)
%check here for how many roots
if temp(j)>0 && isreal(temp(j)) && subs(om,a,temp(j))>0
Res(l,1)=temp(j);
Res(l,2)=alpha;
Res=double(Res);
A=Res(l,1);
ALPHA=alpha;
XSTAR=(A+1)^2/(K*(A^2));%subs(x,a,A);%
SSTAR=1/(1+XSTAR);%subs(s,a,A);%1/(1+XSTAR);
YSTAR=ALPHA*SSTAR-1;%subs(y,a,A);% %error IS HERE
%Jacobian
J=[ -XSTAR-1,  -SSTAR, 0, 0,  0;
ALPHA*XSTAR,ALPHA*SSTAR-YSTAR-1, -XSTAR, 0, 0;
0,  0,  -1,  0,  K;
0, A*YSTAR, A*XSTAR, -1-A, 0;
0,  0,  0,  A, -1-A];
%calculation of pure imaginary eigenvalue
omega1=sqrt(subs(om,a,A));
%eigenvector of jacobian - checked for correctness
[q,p]=imageigvs(J);
L1=real(-2*cprod(p,evalB(q,J\evalB(q,conj(q),A,ALPHA),A,ALPHA))
+cprod(p,evalB(conj(q),(2*omega1*i*eye(5)-J)\evalB(q,q,A,ALPHA),A,ALPHA)))
/(2*omega1);
Res(l,3)=L1;
l=l+1;
```

```
end
end

end
Resd=double(Res);
Resd(:,1)=2./Resd(:,1);
Resd=sortrows(Resd);
subcrind=find(Resd(:,3)>0);
plot(Resd(:,1),Resd(:,2),'.r');
hold on;
plot(Resd(subcrind,1),Resd(subcrind,2),'b.');
```

Appendix B

Useful theorems and results

Denote by BC^n the Banach space of bounded continuous functions mapping $(-\infty, 0]$ into $\mathbb{R}^n$ equipped with the uniform norm (i.e. if $\Gamma \in BC^n$, then $||\Gamma|| = \sup_{\theta\in(-\infty,0]} |\Gamma(\theta)|$, where $|\cdot|$ is any norm in $\mathbb{R}^n$) and consider the following initial value problem.

$$\begin{aligned} x'(t) &= f(t, x_t),\ t \geq \sigma \\ x_\sigma &= \phi\ , \end{aligned} \tag{B.1}$$

where σ is the initial time and $\phi \in BC^n((-\infty, \sigma], \mathbb{R})$ is the state of the system at the time σ, i.e.

$$x(\sigma + \theta) = \phi(\theta)\ , -\infty \leq \theta \leq 0\ .$$

Also, consider the Lipschitz condition:

For all $a, b \in \mathbb{R}$ and $M > 0$, there is a $K > 0$ such that:

$$|f(t, \phi) - f(t, \psi)| \leq K||\phi - \psi||,\ a \leq t \leq b\ ,\ ||\phi||, ||\psi|| \leq M\ . \tag{B.2}$$

The following is the existence and uniqueness theorem, as stated in [27].

Theorem B.0.1. *Suppose that f is continuous and satisfies the Lipschitz condition (B.2), $\sigma \in \mathbb{R}$, and $M > 0$. There exists $A > 0$, depending only on M such that,*

if $\phi \in BC^n$ satisfies $||\phi|| \leq M$, then there exists a unique solution $x(t) = x(t, \phi)$ of (B.1), defined on $(-\infty, \sigma + A]$. If K in (B.2) can be chosen independent of a, b and M, then we need make no restrictions on A. In this case, the solution exists for all $t \geq \sigma$.

Prior to stating the Comparison Theorem, we establish the necessary notation.

$$
\begin{aligned}
D^+u(t) &= \limsup_{h\to 0+} h^{-1}[u(t+h) - u(t)] \ , \\
D_+u(t) &= \liminf_{h\to 0+} h^{-1}[u(t+h) - u(t)] \ , \\
D^-u(t) &= \limsup_{h\to 0-} h^{-1}[u(t+h) - u(t)] \ , \\
D_-u(t) &= \liminf_{h\to 0-} h^{-1}[u(t+h) - u(t)] \ ,
\end{aligned}
$$

where $u \in \mathbb{C}((t_0, t_0 + a), \mathbb{R})$. Let E be an open set of (t, u) in $\mathbb{R}^2$ and $g \in \mathbb{C}(E, \mathbb{R})$. Consider the scalar initial value differential equation

$$\dot{u}(t) = g(t, u) \ , \ u(t_0) = u_0 \ . \tag{B.3}$$

Definition B.0.2. Let $v(t)$ be a solution of the scalar differential equation (B.3) on $[t_0, t_0 + a)$. Then $v(t)$ is said to be a maximal solution of (B.3) if, for every solution $u(t)$ of (B.3) existing on $[t_0, t_0 + a)$, the inequality

$$u(t) \leq v(t) \ , t \in [t_0, t_0 + a) \tag{B.4}$$

holds. A minimal solution $\omega(t)$ is defined by reversing the inequality (B.4).

Theorem B.0.3 (Comparison Theorem, [38], Theorem 1.4.1, p.15)**.** *Let E be an open set of (t, u) in $\mathbb{R}^2$ and $g \in \mathbb{C}(E, \mathbb{R})$. Suppose that $[t_0, t_0 + a]$ is the largest interval in which the maximal solution $r(t)$ of (B.3) exists, and S is an at-most countable subset of $[t_0, t_0 + a)$. Let $m(t) \in \mathbb{C}[(t_0, t_0 + a), \mathbb{R}]$, $(t, m(t)) \in E$ for $t \in [t_0, t_0 + a)$, $m(t_0) \leq u_0$, and for a fixed Dini derivative, $Dm(t) \leq g(t, m(t))$, $t \in [t_0, t_0 + a)$. Then, $m(t) \leq r(t)$ for $t \in [t_0, t_0 + a)$.*

The following result is called the Fluctuation Lemma. For a proof, see [36] or [44].

Lemma B.0.4. *Let $f : \mathbb{R}^+ \longrightarrow \mathbb{R}$ be a differentiable function. If $\liminf_{t\to\infty} f(t) < \limsup_{t\to\infty} f(t)$, then there are increasing sequences t_n and s_n, such that for all n*

$$\dot{f}(t_n) = 0, \text{ and } f(t_n) \to \limsup_{t\to\infty} f(t) \text{ as } n \to \infty ,$$
$$\dot{f}(s_n) = 0, \text{ and } f(s_n) \to \limsup_{t\to\infty} f(t) \text{ as } n \to \infty .$$

Lemma B.0.5. *Let $a \in (-\infty, \infty)$ and $f : [a, \infty) \longrightarrow \mathbb{R}$ be a differentiable function. If $\lim_{t\to\infty} f(t)$ exists (finite) and the derivative function $\dot{f}(t)$ is uniformly continuous on (a, ∞), then $\lim_{t\to\infty} \dot{f}(t) = 0$.*

Bibliography

[1] C.S. Holling. The functional response of predators to prey density and its role in mimicry and population regulation. *Memoirs of the Entomological Society of Canada*, 97:5–60, 1 1965.

[2] C.S. Holling. Some characteristics of simple types of predation and parasitism. *The Canadian Entomologist*, 91:385–398, 1959.

[3] G. Fan and G.S.K. Wolkowicz. A predator-prey model in the chemostat with time delay. *International Journal of Differential Equations*, 2010.

[4] G. Fan and G.S.K. Wolkowicz. Chaotic dynamics in a simple predator-prey model with discrete delay. *Pre-print.*

[5] B. Liu, Y. Zhang, and L. Chen. Dynamics complexities of a Holling I predator-prey model concerning periodic biological and chemical control. *Chaos, Solitons & Fractals*, 22(1):123 – 134, 2004.

[6] S.M. Moghadas and M.E. Alexander. Dynamics of a generalized Gause-type predator-prey model with a seasonal functional response. *Chaos, Solitons & Fractals*, 23:55–65, 2005.

[7] H. Zhu, S.A. Campbell, and G.S.K. Wolkowicz. Bifurcation analysis of a predator-prey system with nonmonotonic functional response. *SIAM Journal on Applied Mathematics*, 63(2):636–682, 2002.

[8] C.J. Krebs, S. Boutin, and R. Boonstra. *Ecosystem Dynamics of the Boreal Forest: The Kluane Project*. Oxford University Press, New York, 2001.

[9] M. Scheffer, S. Rinaldi, Y.A. Kuznetsov, and E.H. van Nes. Seasonal dynamics of *Daphnia* and algae explained as a periodically forced predator-prey system. *Oikos*, 80(3):pp. 519–532, 1997.

[10] M.L. Rosenzweig and R.H. MacArthur. Graphical representation and stability conditions of predator-prey interactions. *The American Naturalist*, 97(895):209–223, 1963.

[11] J.M. Cushing. Periodic time-dependent predator-prey systems. *SIAM Journal on Applied Mathematics*, 32(1):82–95, 1977.

[12] T. Zhao, Y. Kuang, and H.L. Smith. Global existence of periodic solutions in a class of delayed Gause-type predator-prey systems. *Nonlinear Analysis: Theory, Methods & Applications*, 28(8):1373 – 1394, 1997.

[13] S.B. Hsu and T.W. Huang. Global stability for a class of predator-prey systems. *SIAM J. Appl. Math*, 55:763–783, 1995.

[14] J.K. Hale. *Ordinary Differential Equations*. Wiley-Intersience, New York, 1969.

[15] S.A. Gourley and Y. Kuang. A stage structured predator-prey model and its dependence on maturation delay and death rate. *Journal of Mathematical Biology*, 49(2):188–200, 2004.

[16] M.Y. Li, X. Lin, and H. Wang. Global Hopf branches and multiple limit cycles in a delayed Lotka-Volterra predator-prey model. *Discrete and Continuous Dynamical Systems - Series B*, 19(3):747–760, 2014.

[17] Y. Song and J. Wei. Local Hopf bifurcation and global periodic solutions in a delayed predator-prey system. *Journal of Mathematical Analysis and Applications*, 301(1):1 – 21, 2005.

[18] X.P. Yan and C.H. Zhang. Hopf bifurcation in a delayed Lotka-Volterra predator-prey system. *Nonlinear Analysis: Real World Applications*, 9(1):114 – 127, 2008.

[19] G.S.K. Wolkowicz, H. Xia, and S. Ruan. Competition in the chemostat: A distributed delay model and its global asymptotic behavior. *SIAM J. Appl. Math*, 57:1281–1310, 1997.

[20] G.S.K. Wolkowicz, H. Xia, and J. Wu. Global dynamics of a chemostat competition model with distributed delay. *Journal of Mathematical Biology*, 38(4):285–316, 1999.

[21] A. Thiel, H. Schwegler, and C.W. Eurich. Complex dynamics is abolished in delayed recurrent systems with distributed feedback times. *Complexity*, 8(4):102–108, 2003.

[22] W. Ma and Y. Takeuchi. Stability analysis on a predator-prey system with distributed delays. *Journal of Computational and Applied Mathematics*, 88(1):79 – 94, 1998.

[23] R. Xu, F.A. Davidson, and M.A.J. Chaplain. Persistence and stability for a two-species ratio-dependent predator-prey system with distributed time delay. *Journal of Mathematical Analysis and Applications*, 269(1):256 – 277, 2002.

[24] Z.P. Ma, H.F. Huo, and C.Y. Liu. Stability and Hopf bifurcation analysis on a predator-prey model with discrete and distributed delays. *Nonlinear Analysis: Real World Applications*, 10(2):1160 – 1172, 2009.

[25] C.H. Zhang, X.P. Yan, and G.H. Cui. Hopf bifurcations in a predator-prey system with a discrete delay and a distributed delay. *Nonlinear Analysis: Real World Applications*, 11(5):4141 – 4153, 2010.

[26] C. Celik. Dynamical behavior of a ratio dependent predator-prey system with distributed delay. *Discrete and Continuous Dynamical Systems - Series B*, 16(3):719–738, 2011.

[27] H. Smith. *An Introduction to Delay Differential Equations with Applications to the Life Sciences*. Springer-Verlag, New York, 2011.

[28] S. Bernard, J. Bélair, and M.C. Mackey. Sufficient conditions for stability of linear differential equations with distributed delay. *Discrete And Continuous Dynamical Systems Series B*, 1(2):233–256, 2001.

[29] K.L. Cooke and Z. Grossman. Discrete delay, distributed delay and stability switches. *Journal of Mathematical Analysis and Applications*, 86(2):592 – 627, 1982.

[30] S.A. Campbell and R. Jessop. Approximating the stability region for a differential equation with a distributed delay. *Mathematical Modelling of Natural Phenomena*, 4:1–27, 2009.

[31] Y.Yuan and J. Bélair. Stability and Hopf bifurcation analysis for functional differential equation with distributed delay. *SIAM Journal on Applied Dynamical Systems*, 10(2):551–581, 2011.

[32] N. MacDonald. *Biological Delay Systems: Linear Stability Theory*. Cambridge University Press, 1989.

[33] Y.A. Kuznetsov. *Elements of Applied Bifurcation Theory*. Springer-Verlag, New York, 1995.

[34] S.A. Campbell and J. Bélair. Analytical and symbolically-assisted investigation of Hopf bifurcations in delay-differential equations. *Canadian Applied Mathematics Quarterly*, 3, 1995.

[35] V.G. LeBlanc. A degenerate Hopf bifurcation in retarded functional differential equations, and applications to endemic bubbles. *Journal of Nonlinear Science*, pages 1–25, 2015.

[36] H.L. Smith and P. Waltman. *The Theory of the Chemostat: Dynamics of Microbial Competition*, volume 13. Cambridge university press, 1995.

[37] G. Butler and G.S.K. Wolkowicz. Predator-mediated competition in the chemostat. *Journal of mathematical biology*, 24(2):167–191, 1986.

[38] V. Lakshmikantham and S. Leela. *Differential and Integral Inequalities*, volume 1. New York: Academic Press, 1969.

[39] J.K. Hale and S.M. Verdyun. *Introduction to Functional Differential Equations*. Springer-Verlag, 1993.

[40] V. Kolmanovskii and A. Myshkis. *Introduction to the Theory and Applications of Functional Differential Equations*. Kluwer Academic Publishers, Dordrecht, The Netherlands, 1999.

[41] J.P. LaSalle. *The Stability of Dynamical Systems*. SIAM, Philadelphia, 1976.

[42] Y. Kuang. *Delay Differential Equations With Applications In Population Dynamics*, volume 191. Mathematics in Science and Engineering, Academic Press Inc. Boston, MA, 1993.

[43] J.E. Marsden and M.J. Hoffman. *Basic Complex Analysis*. W.H. Freeman and company, 1999.

[44] W. M. Hirsch, H. Hanisch, and J.-P. Gabriel. Differential equation models of some parasitic infections: methods for the study of asymptotic behavior. *Comm. Pure Appl. Math.*, 38:733–753, 1985.